EPSC2017

OPS4/TP8.2 abstracts

EPSC Abstracts
Vol. 11, EPSC2017-155, 2017
European Planetary Science Congress 2017

Venus Aerosol Properties from Modelling and Akatsuki IR2 Observations

K. McGouldrick
(Laboratory for Atmospheric and Space Physics, University of Colorado Boulder, Boulder, CO, USA
(kevin.mcgouldrick@lasp.colorado.edu))

1. Introduction

The global cloud cover at Venus is perhaps its most obvious attribute upon a first glance at the planet. Despite being analyzed by means of polarimetry, planetary emitted and reflected radiation, and in situ probes and balloons, many properties of the Venusian aerosols remain insufficently characterized. Three modes of particles were observed by in situ probes [4], though internal inconsistencies in the data from various instruments have left the identity and particulars of these three modes uncertain [6]. Analyses of the emitted near infrared radiation from Venus tend to attribute most of the observed variation to changes in the number concentrations of the third and largest mode of sulfuric acid droplets in the Venus clouds, despite that their existence and physical characteristics remain uncertain [1, 3]. Remote observations of the upper hazes have long suggested that the primary constituent is one micron radius spherical particles of a solution of sulfuric acid and water [2]. But the frequent and persistent co-existence of an additional submicron mode of particles in the upper haze is difficult to explain if both modes are composed of sulfuric acid.

2. Plan of Attack

The parameter space of radiative effects of the aerosols tends to be large enough to be difficult to adequately sample by means of a purely radiative transfer analysis. Changes in the peak, width, and shape of the particle size distribution, as well as changes in the composition, and even possible phase changes all can contribute to changes in the radiative properties. Considering all of these parameters at sufficient resolution to confidently characterize the aerosol properties is almost prohibitive unless some limiting assumptions are made. By exploring the phase space of microphysical properties, we can potentially eliminate regions of the phase space of radiative effects.

In this work, we employ the Community Aerosol and Radiation Model for Atmospheres (CARMA), version 2.3 in order to simulate the microphysics of the Venusian aerosols. We investigate the effect of changes in the microphysical properties of the aerosols and changes in the photochemical production rates by comparing the mass loading and particle size distributions of the clouds in a suite of simulations. We then compute the upwelling top of atmosphere radiance that would result from the cloud profiles so generated, and compare these predicted radiance variations with those that have been observed with the IR2 camera on the Akatsuki spacecraft.

3. Preliminary Results

Initial results indicate that temperature dependent coalescence efficiency, such as might be expected from a transition to a glass like phase [5], can lead to rapid changes in the particle size distributions on the timescale of days to weeks. In Figure 1, we show the mass loading and effective radius plotted as a function of time over the four year duration for such a simulation. In this profile, simulating the aerosols between 75° and 90° latitude, we see 50% excursions in mass loading and factor of two changes in effective radius, both occurring on timescales of around 1-3 weeks.

4. Summary and Conclusions

Large changes in the aerosol size distribution are being observed in microphysical simulations of the Venus clouds. One driver of these changes appears to be coagulation efficiency. The observed changes will have significant effects in the emitted near infrared radiance. We will attempt to show whether these simulated variations are consistent with those observed in the Akatsuki IR2 data.

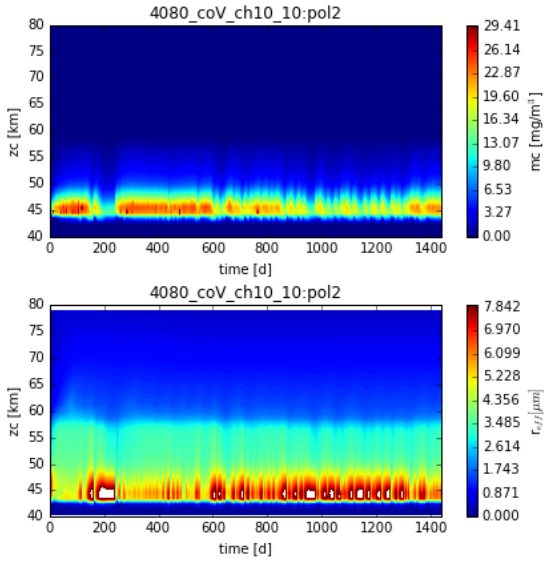

Figure 1: Mass loading (top) and effective radius (bottom) for a simulation in which coagulation efficiency is reduced when temperatures are lower than the nominal freezing point of sulphuric acid.

Acknowledgements

This work was supported by the NASA Venus Climate Orbiter Participating Scientist Program, Grant Number NNX16AC80G and NASA Solar System Workings Program, Grant Number NNH15ZDA001N.

References

[1] Grinspoon, D. H. et al.: Probing Venus's cloud structure with Galileo NIMS, Planetary and Space Science, Vol. 50(7), pp. 515-542, 1993.

[2] Hansen, J., E. and Hovenier, J. W.: Interpretation of the polarization of Venus, Journal of the Atmospheric Sciences, Vol. 31, pp. 1137-1160, 1974.

[3] Haus, R., Kappel, D., and Arnold, G.: Atmospheric thermal structure and cloud features in the southern hemisphere of Venus as retrieved from VIRTIS/VEX radiation measurements, Icarus, Vol. 232, pp. 232-248, 2014.

[4] Knollenberg R. and Hunten, D.: The microphysics of the clouds of Venus: Results of the Pioneer Venus Particle Size Spectrometer Experiment, Journal of Geophysical Research, Vol. 85(A13), pp. 8038-8058, 1980.

[5] McGouldrick, K., Toon, O. B., and Grinspoon, D. H.: Sulfuric acid aerosols in the atmospheres of the terrestrial planets, Planetary and Space Science, Vol. 59(10), pp. 934-941, 2011.

[6] Toon, O. B., et al.: Large, solid particles in the clouds of Venus: Do they exist?, Icarus, Vol. 57(2), pp. 143-160, 1984.

EPSC Abstracts
Vol. 11, EPSC2017-193, 2017
European Planetary Science Congress 2017

DUST PHASE FUNCTION FROM NAVCAM AND HAZCAM IMAGES ON MSL

H. Chen-Chen (hao.chen@ehu.eus), S. Pérez-Hoyos and A. Sánchez-Lavega,
Departamento de Física Aplicada I, ETS Ingenieros de Bilbao, University of the Basque Country (UPV/EHU), Spain

Abstract

The Mars Science Laboratory (MSL) Engineering Cameras were designed for supporting the rover surface operations, but their wide field sky images provide useful information for constraining the aerosol physical properties at Gale Crater. We have developed a DISORT-based radiative transfer model for retrieving such information from the sky brightness measured by these instruments.

1. Introduction

Although not designed for this specific purpose, images taken by the Mars Science Laboratory (MSL) Engineering Cameras can be used for retrieving the dust optical depth and aerosols physical properties at Gale Crater. Dust size distribution and particle shapes can be constrained by evaluating the sky brightness as a function of the scattering angle obtained by MSL cameras [7].

2. MSL Engineering Cameras

The MSL Curiosity rover is equipped with 12 engineering cameras which are built under the same design as the Mars Exploration Rovers (MER) [3]. The goal of these cameras is to support the surface operations of the rover by providing tactical views of the near-field surrounding terrain; in order to detect and avoid hazards, characterize the rover position and orientation, as well as supporting the robotic arm operation [4].

MSL Navigation Cameras (*Navcam*) consist of four mast-mounted cameras with a 45-degree square field of view and a broadband response span of 600 to 850 nm. The Hazard Avoidance Cameras (*Hazcam)* are rover chassis-mounted tactical cameras located in the front and the rear of the vehicle, with a 124-degree square FOV. They have also a broadband coverage of 600-800 nm. Complete technical specifications of the MSL Engineering cameras can be found in [4], while information on the performance of the optics is shown in [3].

3. Observations

The sky radiance as a function of the scattering angle provides useful information for constraining the shape and size distribution of aerosols in the atmosphere. MSL Engineering Camera images were used to determine the scattering properties and phase function of the Martian dust.

Navcam sky surveys cover a wide range of angles from the Sun as they were designed to determine the scattering properties of the atmosphere. In addition to these images, this work has also evaluated the wide FOV images provided by *Hazcam* (see Figure 1)

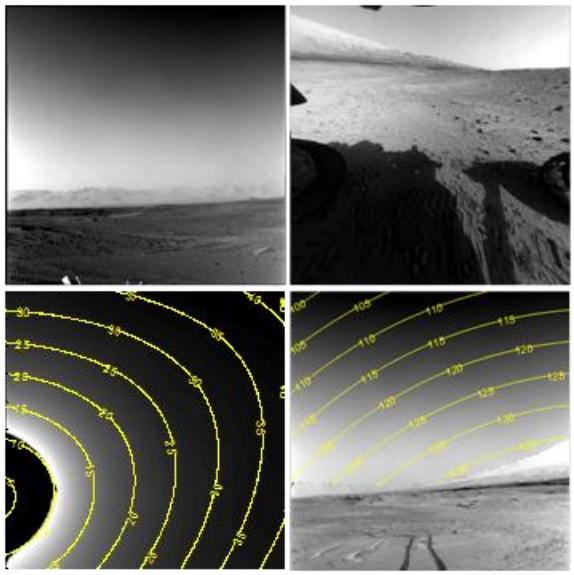

Figure 1: *Navcam* (left) and *Hazcam* (right) surveys. Sample images are shown on top. Scattering angle contours are presented for MSL Sol 669 (bottom)

4. Radiative Transfer model

A radiative transfer model has been developed in order to model the radiation detected by the MSL Engineering Cameras. This model can also be used with other instruments even on-board orbiters.

We use a discrete ordinate method to solve the RT equation (DISORT) [8] in a plane-parallel Martian atmosphere model. The code for setting up the atmosphere and solving the radiative transfer is based on a Python implementation of CDISORT (PyDISORT) [1]. Absorption data for relevant gases are taken from HITRAN [6] and transformed into correlated-k tables. Local and seasonal atmospheric profiles and composition have been retrieved from the Mars Climate Database [2, 5].

The current aerosol model implementation allows to use spherical (Mie approximation) and irregular (T-matrix based) particles.

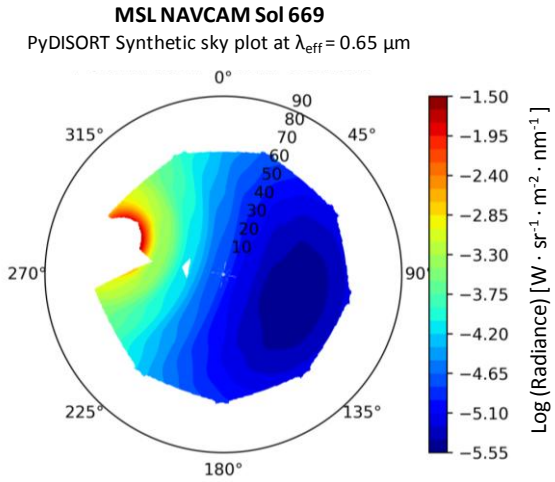

Figure 2: Synthetic sky plot with PyDISORT for MSL-*Navcam* Sol 669 retrieved images at instrument effective wavelength 0.65 µm.

5. Conclusions

We are using the image data sets obtained by the Engineering Cameras (*Navcam* and *Hazcam*) on board the Mars Science Laboratory rover to study the dust characteristics. The sky radiances and dust aerosol phase function are retrieved and processed with a radiative transfer model for constraining the dust physical properties. This is a work in progress report and the latest results for a number of characteristic situations during the Martian year will be presented.

Acknowledgements

This work is supported by the project AYA2015-65041-P with FEDER support, Grupos Gobierno Vasco IT-765-13, Universidad del País Vasco UPV/EHU programme UFI11/55, and Diputación Foral de Bizkaia – Aula EspaZio Gela.

References

[1] Ádámkovics, M., *et al.*: Meridional variation in tropospheric methane on Titan observed with AO spectroscopy at Keck and VLT, Icarus, 270, 376-388. doi:10.1016/j.icarus.2015.05.023 (2016).

[2] Forget, F., *et al* Improved general circulation models of the Martian atmosphere from the surface to above 80 km, J. Geophys. Res., 104(E10), 24155–24175, doi:10.1029/1999JE001025. (1999).

[3] Maki, J. N., *et al.*: Mars Exploration Rover Engineering Cameras, J. Geophys. Res., 108, 8071, doi:10.1029/2003JE002077, E12, (2003).

[4] Maki, J. N., *et al.*: The Mars Science Laboratory engineering cameras, Space Sci. Rev., Vol.170, pp77-93. doi:10.1007/s11214-012-9882-4, (2012).

[5] Millour, E., *et al.*: The Mars Climate Database (MCD version 5.2), EPSC Abstracts, Vol. 10, EPSC2015-248, (2015).

[6] Rothman, L. S., *et al.*: The HITRAN 2012 Molecular Spectroscopic Database, Journal of Quantitative Spectroscopy and Radiative Transfer, Vol.130, 4-50, (2013).

[7] Smith, M. D., and Wolff, M. J.: Dust Aerosol Particle Size and Shape using MER NAVCAM and PANCAM Sky Imaging, 5th Mars Atmosphere Modeling and Observation Workshop. January 13-16, Oxford. Abs. id.2101, (2014).

[8] Stamnes, K. *et al.*: Numerically stable algorithm for discrete-ordinate-method radiative transfer in multiple scattering and emitting layered media, Applied Optics, Vol. 27, No. 12, (1988).

EPSC Abstracts
Vol. 11, EPSC2017-246-1, 2017
European Planetary Science Congress 2017

Modelling cloud microphysics on Uranus

D. Toledo and P. Irwin

Department of Physics, University of Oxford, Parks Rd, Oxford OX1 3PU, UK. (daniel.toledocarrasco@physics.ox.ac.uk)

Abstract

As on Earth, Uranus has a dynamic atmosphere and undergoes a cycle of seasons. Different images of Uranus have revealed the presence of discrete clouds at different locations and time periods [1,2]. Based on the altitude of these clouds and the saturation vapour pressure curves of several possible condensates in Uranus's atmosphere, it has been possible to infer that these clouds were made of methane (CH_4) ice particles. However, more information about the cloud density and size of droplets is required to better understand the different dynamic processes involved in the atmosphere. In addition to methane clouds, previous work based on radiative transfer simulations have suggested the presence of different cloud layers at several levels below the tropopause [3]. However, as a result of the limitation of ground-based telescopes (or observations from telescopes in orbit around the earth) the detection and analysis of the composition and properties of those clouds is a big challenge. According to the gas abundances in Uranus's atmosphere and the T-P profile, a variety of cloud compositions can be found: clouds made of methane (CH_4), hydrogen sulphide (H_2S), ammonia (NH_3), ammonium hydrosulphide (NH_4SH) or water (H_2O) (see **Figure 1**). In this work, we will make use of cloud microphysics to provide key constraints on the density, vertical distribution, size of droplets and time scale of the different clouds that may be present in Uranus's atmosphere.

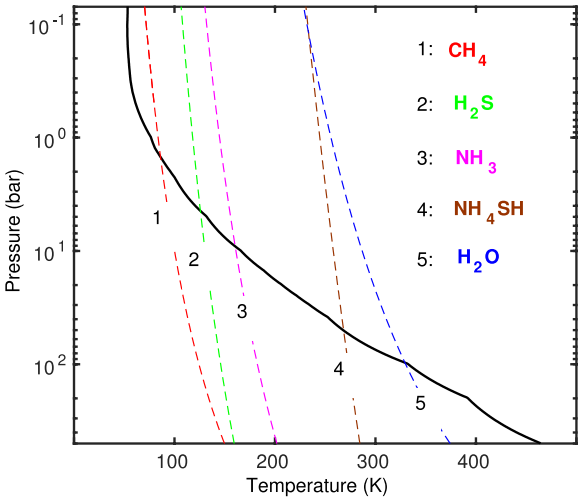

Figure 1: *Vertical temperature profile in the atmosphere of Uranus (continuous black line) and the saturation vapor pressure curves for several possible condensates (dashed lines). The cloud base of each specific condensate is given by the point where the two curves cross.*

References

[1] Karkoschka, E.: Uranus' Apparent Seasonal Variability in 25 HST Filters. Icarus 151, 84-92 (2001).

[2] Irwin, P., et al.: HST/WFC3 observations of Uranus' 2014 storm clouds and comparison with VLT/SINFONI and IRTF/Spex observations. *Icarus* 288, 99-119 (2017).

[3] Sromovsky, L., et al.: Methane on Uranus: The case for a compact CH_4 cloud layer at low latitudes and a severe CH_4 depletion at high-latitudes based on re-analysis of Voyager occultation measurements and STIS spectroscopy. Icarus 215, 292-312 (2011).

EPSC Abstracts
Vol. 11, EPSC2017-250-2, 2017
European Planetary Science Congress 2017

Uranus's cloud and haze properties from VLT observations

D. Toledo (1), P. G. J. Irwin (1), N. A. Teanby (2), A. A. Simon (3), M. H. Wong (4) and G. S. Orton (5)

(1) Department of Physics, University of Oxford, Parks Rd, Oxford OX1 3PU, UK, (2) School of Earth Sciences, University of Bristol, Wills Memorial Building, Queen's Road, Bristol, BS8 1RJ, UK, (3) NASA Goddard Space Flight Center, Solar System Exploration Division (690) Greenbelt, MD 20771, USA, (4) University of California at Berkeley Astronomy Department Berkeley, CA 947200-3411, USA, (5) Jet Propulsion Laboratory, California Institute of Technology, 4800 Oak Grove Drive, Pasadena, CA 91109, USA. (daniel.toledocarrasco@physics.ox.ac.uk)

Abstract

In November 2014, the SINFONI Integral Field Unit Spectrometer on the Very Large Telescope (VLT) mapped Uranus in the 1.46 - 1.70 μm wavelength region. Images at different wavelengths clearly revealed the presence of discrete clouds [1], assumed to be composed of methane ice, and regions with different brightness patterns caused by latitudinal variations in the properties of aerosol. **Figure 1** shows VLT/SINFONI images of Uranus at selected wavelengths in which, for example, a bright region can be identified near the equator. In this work, we analyze through radiative-transfer simulations VLT observations to characterize the vertical distribution and optical properties of clouds and hazes in Uranus's atmosphere. We first tested three different atmospheric models consisting of different cloud and haze layers to choose the cloud model capable of fitting the observations over a wide range of emission angles. Subsequently, properties such as the optical depth, vertical distribution and scattering properties of clouds and hazes were retrieved at key locations to study their latitudinal variations and thus compare them with the bright patterns illustrated in **Figure 1**.

1. Description of the model

For the analysis of images illustrated in **Figure 1** the NEMESIS radiative-transfer and retrieval code [2] was used. We employed three different cloud models whose election of aerosol layers is based on results from previous work (e.g. [1,3]). The first model (M1) consists of a vertically extended haze layer based at the 0.19-bar pressure level, and a deep tropospheric cloud at ~2-bar level. The second model (M2) is similar to M1, but an additional tropospheric haze layer based at ~0.56-bar pressure level is added with a fixed fractional scale height (FSH) set to 0.08. The addition of this haze layer in M2 allows a variation of the haze particles size distribution and refractive index with altitude. The third model (M3) is similar to M2, but the tropospheric haze FSH is treated as a free parameter, thus allowing a vertical extended tropospheric haze. For the three models the pressure base and FSH of the deep cloud are fixed to the values deduced from VLT/SINFONI observations by [1], allowing only the optical depth to vary. The scattering properties of cloud and haze particles are computed using the Mie theory assuming a standard gamma size distribution and where the effective radius (r_{eff}), the effective variance (ν_{eff}) and the imaginary part of the refractive index are retrieved.

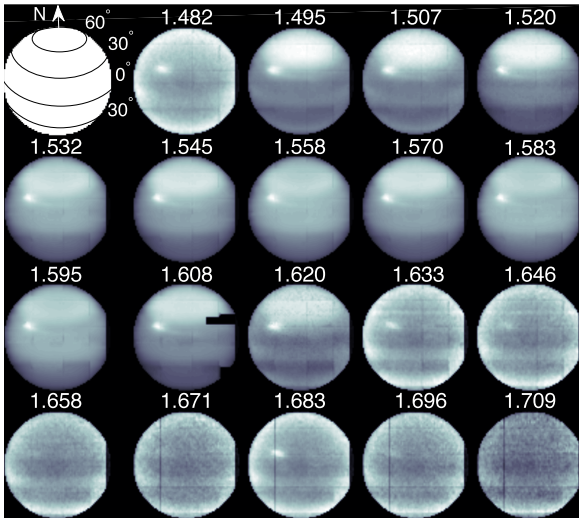

Figure 1: *VLT/SINFONI observations of Uranus at selected wavelengths on 11th November 2014.*

2. Main results

In order to compare the three models over a wide wavelength range and over a range of zenith angles, we conducted a number of limb-darkening analyses at different latitudes. For each latitude selected, six spectra taken at different emission angles (ranging from 20° to 75°) were fitted simultaneously. In terms of χ^2_{red}, we find that M3 provides the best results with values determined to be below 1.0 at most latitudes. For example, **Figure 2** shows a limb darkening analysis carried out at 5°N and for which a χ^2_{red} of 0.96 is obtained by M3.

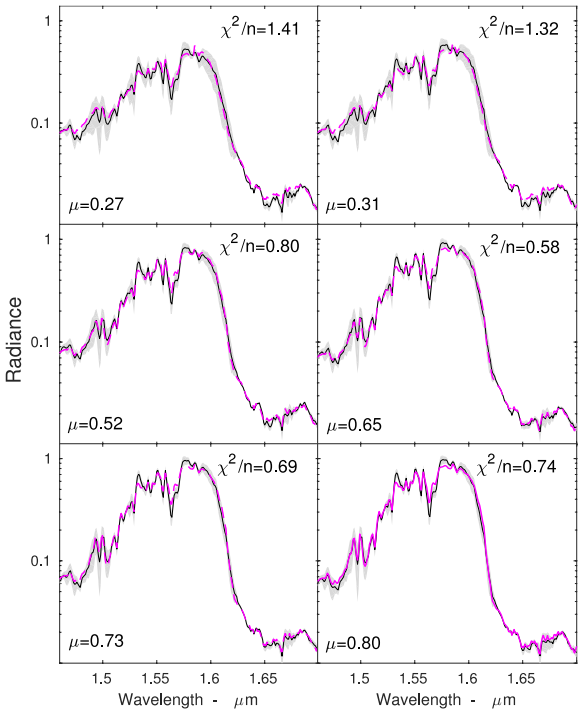

Figure 2: *Comparison of measured VLT/SINFONI spectra at ~5° N with M3 fits. The black solid lines with grey shaded errors are VLT spectra at 5°N with μ (cosine of the emission angle) values of 0.27, 0.31, 0.52, 0.65, 0.73 and 0.80. The shaded errors represent the random errors of the observed radiances and are computed by the VLT/SINFONI pipeline. The six spectra were fitted simultaneously using the M3 model (purple dashed lines) whose χ^2_{red} value is 0.96. The fits performed by M1 and M2 are not as good as for M1 since the χ^2_{red} values achieved by those models are 3.0 and 1.29, respectively.*

Once these different cloud models were tested, we then performed a number of limb-darkening analyses at different latitudes to retrieve the optical and physical properties of the hazes and the tropospheric cloud (size distribution, refractive index and opacity) at different key locations. We will discuss the implication of our observations for Uranus' cloud structure. For example, we find an increase of the stratospheric haze opacity at latitudes near to the equator (see **Figure 3**), region where a bright band can be identified in images illustrated in **Figure 1**.

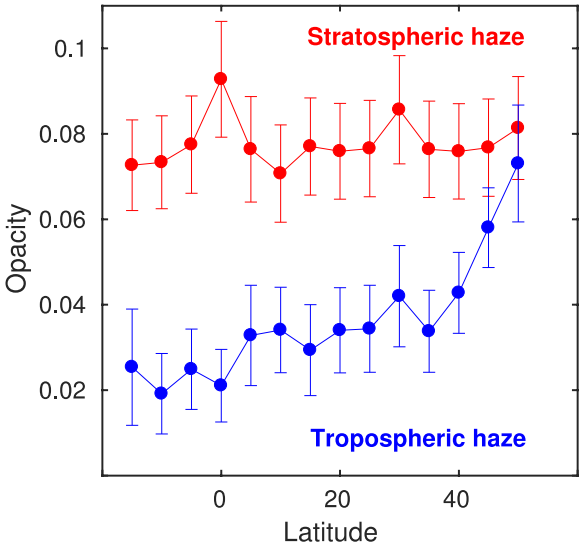

Figure 3: *Latitudinal variation of the stratospheric and tropospheric haze opacities at 1.6 μm.*

References

[1] Irwin, P., et al.: HST/WFC3 observations of Uranus' 2014 storm clouds and comparison with VLT/SINFONI and IRTF/Spex observations. *Icarus* 288, 99-119 (2017).

[2] Irwin, P. et al.: The NEMESIS planetary atmosphere radiative transfer and retrieval tool. *Journal of Quantitative Spectroscopy and Radiative Transfer* 109, 1136-1150 (2008).

[3] Tice, D. et al.: Uranus' cloud particle properties and latitudinal methane variation from IRTF SpeX observations Icarus 223, 684-698 (2013).

EPSC Abstracts
Vol. 11, EPSC2017-254, 2017
European Planetary Science Congress 2017

Martian GCM with complete CO_2 clouds microphysics

J. Audouard (1), A. Määttänen (1), C. Listowski (1), F. Forget (2), E. Millour (2) and A. Spiga (2)
(1) *LATMOS/IPSL, UVSQ Université Paris-Saclay, UPMC Univ. Paris 06, CNRS, Guyancourt, France;* (2) *Laboratoire de Météorologie Dynamique (CNRS/IPSL/UMPC), Paris, France. (joachim.audouard@latmos.ipsl.fr)*

Abstract

Towards understanding Martian CO_2 cloud formation, abundance and features, including their formation and evolution in a Global Climate Model (GCM) is necessary. Their precise radiative impact on the climate throughout the history of the planet is especially of prime importance due to the backscattering of the infrared photons by the CO_2 ice crystals that might have contributed to a greenhouse effect.
The purpose of this work is to include a complete and validated CO_2 cloud scheme (developped by [1,2]) in the GCM of the Laboratoire de Météorologie Dynamique (LMD) [3]. We hereafter present the key steps of this coupling and the first results.

1. Introduction

Numerous observations (e.g. [4,5,6,*7,8]*), theoretical advances and modeling works [1,2,9,10,11,12] have improved our understanding of CO_2 cloud formation and dynamics on Mars. These clouds, less frequently observed than the water ice clouds, form in the troposphere at the poles during winter and at equatorial latitudes in the mesosphere (60 – 110 km). Atmospheric CO_2 condensation requires extremely low temperatures to produce supersaturation. Such low temperatures are reached during the polar night and have been observed at low latitudes in the mesosphere [5, 13, *14]*. These cold pockets are most likely produced by gravity waves propagating to the upper atmosphere [*12]*, at the altitudes of the temperature minima caused by the thermal tides.

Moreover, aerosol particles must be present for the CO_2 to condense on them by the mean of heterogeneous nucleation. At high mesospheric altitudes and such low pressures (typically 0.01 Pa), it is unknown whether dust lifted from the surface or particles coming from above (such as meteoritic smoke particles) prevail. CO_2 clouds are short-lived and do not last long after the favorable conditions vanish (about a dozen of minutes, [*2]*).

2. CO_2 clouds scheme for the GCM

We have adapted the CO_2 cloud microphysics scheme of *[1,2]* for his coupling with the LMD-GCM presented in [3]. The atmosphere is discretized in 32 layers up to about 120 km in the GCM and the timestep is about 7.5 minutes. During one such timestep, the CO_2 cloud scheme is called 50 times (i.e. every 9.5 seconds) and it includes includes heterogeneous nucleation on aerosols (dust, meteoritic smoke particles and water ice clouds), CO_2 ice nucleation and sublimation (as a function of CO_2 partial pressure and temperature) and sedimentation of the particles. For a better nucleation accuracy, the moments of the CO_2 ice particles population are distributed into 100 bin sizes.

3. Results

We have simulated an entire Martian Year, with a resolution of ~7.5 minutes, from the surface to about 120 km. The GCM outputs have been re-binned 15 sols at a time in altitude (13 10-km wide layers) and in local time (30 min resolution). The simulations show frequent CO_2 clouds at low latitude at mesospheric altitudes during the northen hemisphere spring and autumn (Ls 0-45 and Ls 150-190). Overall, nighttime clouds are higher (up to ~ 100 km) and are composed of smaller particles than daytime clouds (down to about ~40km). CO_2 clouds form with respect to the upward propagation of the thermal tide. Clouds are observed at the poles at mesospheric and tropospheric altitudes (even close to the surface) at the poles during their respective winters. Examples can be seen in figures 1,2 and 3.

4. Summary and Conclusions

A complete meteorology of CO_2 clouds inferred from the GCM will be presented and discussed at the conference. The sensibility with regards to various smulation parametrers will also be adressed.

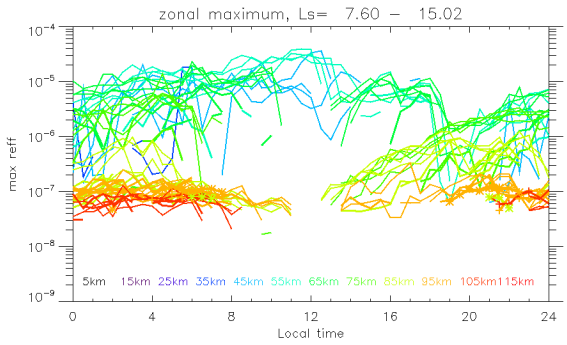

***Fig.1**: Distribution of CO_2 ice clouds particles effective radius as a function of local time and altitude (indicated by different colors). Every line represents a latitude, and the thicker the line, the closer to a pole the latitude is.*

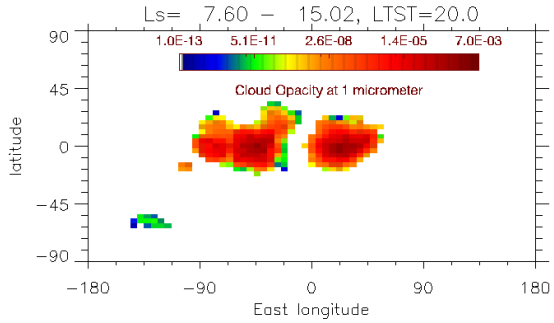

***Fig.2**: Map of maximum CO_2 ice clouds opacity at 1 µm, at a local time of 20 LTST, bewteen 7.6 and 15.02° LS.*

Acknowledgements

J.A. work is funded by the excellence laboratory Exploration Spatiale des Environnements Planétaires, Labex ESEP N 2011-LABX-030.

References

[1] *Listowski, C. et al., 2013, Near-pure vapor condensation in the Martian atmosphere: CO2 ice crystal growth, JGR, 118, 10, 2153-2171 ;* **[2]** *Listowski, C. et al., 2014, Modeling the microphysics of CO2 ice clouds within wave-induced cold pockets in the martian mesosphere, Icarus, 237, 239-261;* ***[3]*** *Forget, F. et al., 1999, Improved general circulation models of the Martian atmosphere from the surface to above 80 km, JGR, 104, E10;* ***[4]*** *Clancy and Sandor, 1998, CO2 ice clouds in the upper atmosphere of Mars, GRL, 25, 4, 489-492 ;***[5]** *Montmessin, F. et al., 2006, Subvisible CO 2 ice clouds detected in the mesosphere of Mars, Icarus, 183, 2, p. 403-410;* ***[6]*** *Montmessin, F. et al., 2007, Hyperspectral imaging of convective CO2 ice clouds in the equatorial mesosphere of Mars, Journal of Geophysical Research, 112, E11;*

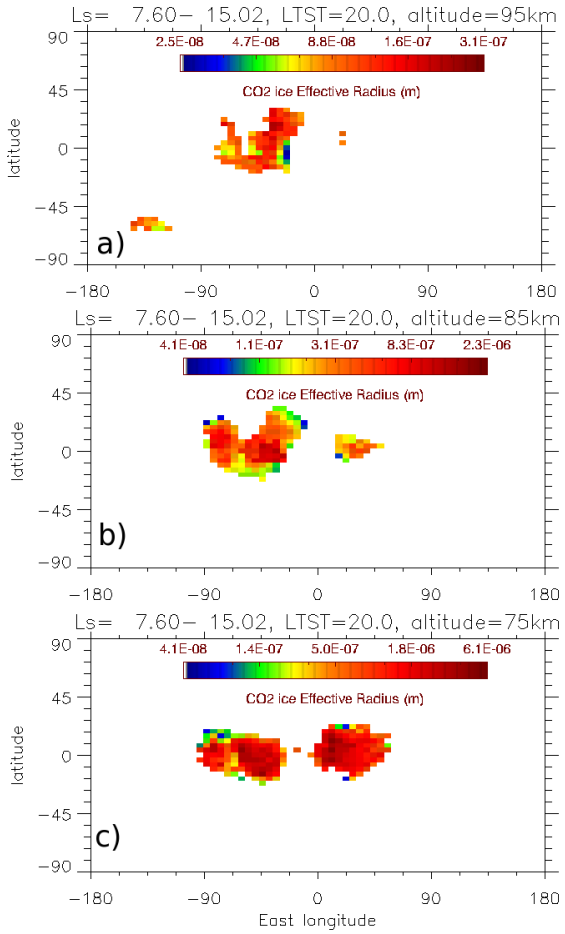

***Fig.3**: Maps of CO_2 clouds ice particles effective Radius. Local time is 20LTST and 3 altitudes are shown: 95km (a), 85km (b) and 75 km(a).*

[7]** Määttänen, A. et al., 2010, Mapping the mesospheric clouds on Mars: MEx/OMEGA and MEx/HRSC observations and challenges for atmospheric models, Icarus, 209, 2, 452-469;* ***[8] *Vincendon, M. et al., 2011, New near-IR observations of mesospheric CO2 and H2O clouds on Mars, JGR, 116;* ***[9]*** *Määttänen, A. et al., 2005, Nucleation studies in the Martian atmosphere, JGR, 110, E2;* ***[10]*** *Määttänen, A. et al., 2007, Two-component heterogeneous nucleation kinetics and an application to Mars, J. of Chemical Physics, 127, 13;* ***[11]*** *Colaprete, A. et al., 2008, CO 2 clouds, CAPE and convection on Mars: Observations and general circulation modeling, PSS, 56, 2;* ***[12]*** *Spiga, A. et al., 2012, Gravity waves, cold pockets and CO2 clouds in the Martian mesosphere, GRL, 39, 2 :* ***[13]*** *Schofield, J. T. et al., 1997, The Mars Pathfinder Atmospheric Structure Investigation/Meteorology, Science, 278, 5344;* ***[14]*** *Forget, F. et al., 2009, Density and temperatures of the upper Martian atmosphere measured by stellar occultations with Mars Express SPICAM, JGR, 114, E1*

EPSC Abstracts
Vol. 11, EPSC2017-261-2, 2017
European Planetary Science Congress 2017

Contrasts in near-IR images of the Venus clouds (VMC/VEx) and their probable causes

O. S. Shalygina[1], E. V. Petrova[2], and W. J. Markiewicz[1]
[1]Max-Planck-Institut für Sonnensystemforschung, Göttingen, Germany (o.s.shalygina@gmail.com), [2]Space Research Institute, Russian Academy of Sciences, Moscow, Russia

1 Introduction

The Venus Monitoring Camera (VMC) onboard the Venus Express (VEx) spacecraft, successfully operated in orbit around Venus since April 2006 until November 2014. It has been imaging Venus in four narrow spectral channels centered at the wavelengths of 0.365 µm (UV), 0.513 µm (VIS), 0.965 µm (NIR1), and 1.010 µm (NIR2) [1]. It took around 350 000 images in four channels covering almost all the latitudes, including night and day sides.

The clouds of Venus scatter radiation in the visible and near infrared wavelengths nearly conservatively and the planet disk has very little contrast. However, many features are observed in UV. The contrast in UV, which is partly caused by SO_2 (in the range between 0.20 and 0.32 µm) and partly by the so-called "unknown UV absorber" (at about 0.365 µm) reach 20 – 30 % [2, 3], while the contrasts in NIR and VIS channels do not exceed 2 – 4 %. Though they are not as numerous and pronounced as the usually considered UV-contrast patterns characteristic of the appearance of the Venus upper cloud deck in UV, their causes remain unclear. So, to study such cases was the aim of the current work.

2 Method

To retrieve the properties of cloud particles from the images of clouds, the phase profiles of brightness obtained from these images taken at small phase angles are used. The shape of the glory feature observed at small phase angles allows the size of scattering particles and, sometimes, their refractive index to be determined. In our previous works it was shown that there is a strong connection between the positions of glory minimum and maximum and particles' sizes [4–7], and ese positions do not change when we compare the single-scattering phase function of particle (red curve in fig. 1), and the phase profiles retrieved for the optically thick layer (see fig. 1).

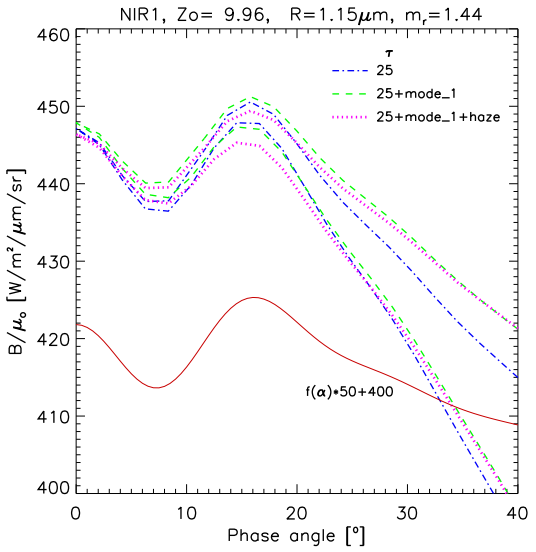

Figure 1: The angular position of glory on the upper deck of the optically thick layer (three sets of the curves) is determined by the single-scattering phase function of the particles f(α) that dominate the scattering in this layer (lower curve; $\lambda = 0.965$ μm, $R_{eff} = 1.15$ μm, $m_r = 1.44$). The brightness coefficient of the plane-parallel layer (the optical thickness $\tau = 25$) with the presence of small submicron particles (mode 1, 95% of the total number of particles in the cloud) and the upper haze of such particles ($\tau_h = 0.05$) was calculated with the radiative transfer code described by [8]. The solar zenith angle is fixed at approximately 10°, while the zenith angleof observations Z_0 is changing, which provides the change in the phase angle α; two branches of the curves correspond to the azimuths 0° and 180°.

Due to the technical reasons, the VEx observations at small phase angles were rare, and such near-IR images, containing contrast features, were obtained in less than a dozen of orbits. The phase profiles of the NIR-dark and NIR-bright features seen in these images are analyzed. They are also compared to the phase profiles obtained from the simultaneously taken UV or visible images (if available). No unambiguous correlation between the brightness of the considered features at different wavelengths has been found: sometimes the contrasts of the same or opposite signs (the feature that is seen as bright (or dark) object in one channel is seen as bright (or dark) in the other one) are observed at the other wavelengths, sometimes not. This may be caused by the fact that different cloud levels are sounded at different wavelengths.

3 Results

The comparison of the measured phase profiles to the single-scattering phase functions of particles with different sizes and refractive indices and the phase profiles of clouds modeled with the radiative-transfer code has shown that

- in most cases, the sizes of particles in the NIR-dark and NIR-bright features are the same;
- in the NIR images (as well as in the visible ones) the higher brightness may be caused by a higher refractive index of particles in the clouds or/and the higher optical depth of the clouds; the effect of the higher refractive index on the UV profiles is opposite due to absorption;
- the presence of small submicron particles in the clouds and, especially, above them produces a considerable effect on brightness in UV and visible, while its influence on the NIR brightness is very weak.

References

[1] W. J. Markiewicz, D. V. Titov, N. I. Ignatiev, et al. In: *Planet. Space Sci.* 55.12 (2007), pp. 1701–1711. DOI: 10.1016/j.pss.2007.01.004.

[2] L. Esposito. In: *J. Geophys. Res.* 85.A13 (1980), pp. 8151–8157. DOI: 10.1029/JA085iA13p08151.

[3] J. Pollack, O. Toon, R. Whitten, et al. In: *J. Geophys. Res.* 85.A13 (1980), pp. 8141–8150. DOI: 10.1029/JA085iA13p08141.

[4] W. J. Markiewicz, E. Petrova, O. Shalygina, et al. In: *Icarus* 234 (2014), pp. 200–203. DOI: 10.1016/j.icarus.2014.01.030.

[5] E. Petrova, O. Shalygina, and W. J. Markiewicz. In: *Planet. Space Sci.* 113-114 (2015), pp. 120–134. DOI: 10.1016/j.pss.2014.11.013.

[6] E. Petrova, O. Shalygina, and W. J. Markiewicz. In: *Icarus* 260 (2015), pp. 190–204. DOI: 10.1016/j.icarus.2015.07.015.

[7] O. Shalygina, E. Petrova, W. J. Markiewicz, et al. In: *Planet. Space Sci.* 113–114 (2015), pp. 135–158. DOI: 10.1016/j.pss.2014.11.012.

[8] M. I. Mishchenko and L. D. Travis. In: *J. Geophys. Res. Atm.* 102.D14 (1997), pp. 16989–17013. DOI: 10.1029/96JD02425.

EPSC Abstracts
Vol. 11, EPSC2017-282, 2017
European Planetary Science Congress 2017

Evidence for an aging process of the haze material on Saturn and Titan

R. Courtin (1), S. J. Kim (2), T. S. Stallard (3), and A. Bar-Nun (4)
(1) LESIA, CNRS/Observatoire de Paris, Meudon, France (regis.courtin@obspm.fr), (2) School of Space Research, Kyung Hee University, Yongin, South Korea (sjkim1@khu.ac.kr), Department of Physics and Astronomy, University of Leicester, Leicester, UK (tss8@leicester.ac.uk), Department of Geosciences, Tel-Aviv University, Tel-Aviv, Israel

Abstract

The 3-µm spectral characteristics of the haze material on Saturn and Titan show marked variations with altitude. We interpret these variations in terms of a chemical alteration during atmospheric motions, a transition between the aromatic and aliphatic spectral types of hydrocarbons, known as aging or annealing.

1. Introduction

From stellar occultation and limb-viewing measurements performed at Saturn by the VIMS experiment on Cassini [1,2], and from solar occultation measurements at Titan [3], we have retrieved the 3-µm spectral properties of the stratospheric haze material in both atmospheres, as well as their variation as a function of altitude [4,5].

2. Results

2.1 Titan

On Titan, our results are relevant to the 250-700 km altitude range at one particular location (71°S). We find a marked change in the relative amplitudes of the 3.3 µm and 3.38 µm features, which are characteristic of aromatic (double C=C chains or rings) or aliphatic (single C–C chains) structural groups, respectively. The "aromatic-to-aliphatic index" η – i.e. the ratio of the 3.33 µm to the 3.38 µm band, uncorrected for the absolute band strengths – varies from 3.3 at 580-700 km to 0.9 at 350-450 km, and 0.5 around 250 km (see Figure 1). The structural change from aromatic to aliphatic type between 580 and 480 km appears to correspond to a spontaneous "aging" of the particles – a transition between unannealed and hardened particles [6,7] – while the further decrease of this index below 480 km may be related to the coating of the core particles by condensates such as heavy alkanes [8].

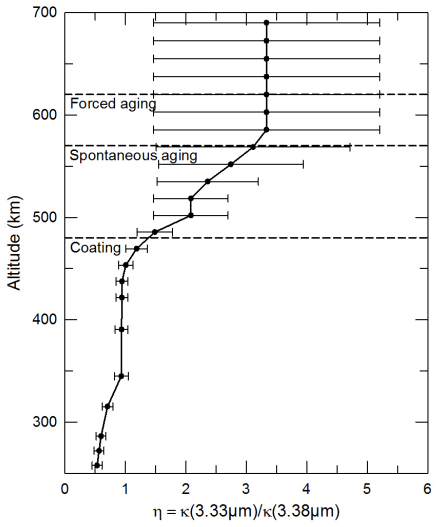

Figure 1: Variation of the aromatic-to-aliphatic index of the haze material, as a function of altitude on Titan.

2.2 Saturn

On Saturn, our results are relevant to the 260-490 km altitude range at 55°N, and to the 375-825 km range at 78°N. The two altitude intervals overlap only by 115 km because of very different viewing conditions. The "aromatic-to-aliphatic index" values are 0.7-0.8 at 55°N, and 1.6-2.2 at 78°N (see Figure 2). In this case, the observed differences in the η values can hardly be interpreted as a consequence of a variation with altitude, since the two profiles differ even in the overlapping zones. Instead, we suggest that in the atmosphere of Saturn, the aging process of the haze material occurs during the latitudinal transport, by advection and/or diffusion, from the polar regions to mid-latitudes, while in the atmosphere of Titan, aging occurs during the vertical precipitation of the haze particles.

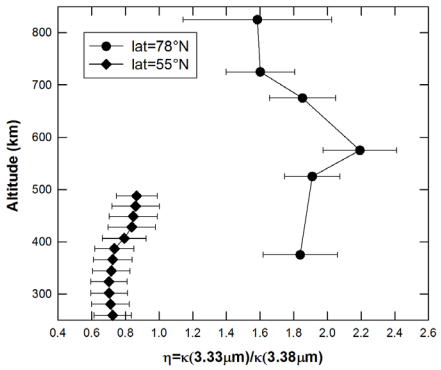

Figure 2: Same as Fig. 1 for Saturn.

3. Summary and Conclusions

In both Saturn and Titan atmospheres, we see evidence for a chemical alteration of the haze material as the particles are transported along with the atmospheric dynamics. On Titan, the change from the aromatic to the aliphatic spectral type of organic compounds occurs around 500 km altitude during the settling down motion, whereas on Saturn, it seems to occur below 400 km during the meridional transport between the polar and mid-latitude regions. These alterations are best interpreted as the consequence of an aging or annealing process, corresponding to the opening up of the triple and double bonds of hydrocarbons under some external effect (e.g., UV photolysis, magnetospheric particles, cosmic rays ionization, etc.).

Acknowledgements

RC acknowledges support from the Centre National d'Etudes Spatiales. SJK acknowledges support from the Brain Korea 21 Plus (BK21+) program through the National Research Foundation of Korea funded by the Ministry of Education, Science and Technology, and from the Korean Astronomy and Space Science Institute. TS acknowledges support from a Research Councils UK Fellowship and from the UK Science and Technology Facilities Council.

References

[1] Nicholson, P.D., Hedman, M.M., Gierasch, P.J., and the Cassini VIMS Team. Probing Saturn's atmosphere with Procyon. 38th AAS/DPS Meeting, October 2006, Pasadena, CA, USA, Bull. Am. Astron. Soc., Vol. 38, p. 555. 2006.

[2] Stallard, T.S., Melin, H., Miller, S., Badman, S.V., Brown, R.H., and Baines, K.H. Peak emission altitude of Saturn's H_3^+ aurora. Geophysical Research Letters, Vol. 39, L15103, 2012.

[3] Bellucci, A., Sicardy, B., Drossart, P., Rannou, P., Nicholson, P.D., Hedman, M., Baines, K.H., Burrati, B. Titan solar occultation observed by Cassini/VIMS: Gas absorption and constraints on aerosol composition. Icarus Vol. 201, pp. 198-216, 2009.

[4] Kim, S.J., Sim, C.K., Lee, D.W., Courtin, R., Moses, J.I., and Minh, Y.C. The three-micron spectral feature of the Saturnian haze: Implications for the haze composition and formation process. Planetary and Space Science, Vol. 65, pp. 122–129, 2012.

[5] Kim, S.J., Jung, A., Sim, C.K, Courtin, R., Bellucci, A., Sicardy, B., Song, I.O., and Minh, Y.C. Retrieval and tentative identification of the 3-μm spectral feature in Titan's haze. Planetary and Space Science, Vol. 59, pp. 699–704, 2011.

[6] Dimitrov, V., and Bar-Nun, A. Aging of Titan's aerosols. Icarus, Vol. 156, pp. 530-538, 2002.

[7] Dimitrov, V., and Bar-Nun, A. Hardening of Titan's aerosols by their charging. Icarus, Vol. 166, pp. 440-443, 2003.

[8] Courtin, R., Kim, S.J., and Bar-Nun, A. Three-micron extinction of the Titan haze in the 250–700 km altitude range: Possible evidence of a particle-aging process. Astronomy & Astrophysics, Vol. 573, A21, 2015.

EPSC Abstracts
Vol. 11, EPSC2017-351, 2017
European Planetary Science Congress 2017

Aerosols and clouds in the atmosphere of HD 189733 b

P. Lavvas (1), T. Koskinen (2)
(1) GSMA, Université Reims Champagne Ardenne, CNRS, France, (2) Lunar and Planetary Lab, University of Arizona, USA (panayotis.lavvas@univ-reims.fr)

Abstract

In the last two decades our view and understanding of planetary atmospheres has significantly expanded as a result of the detection and characterization of numerous exoplanets and of their atmospheres. Apart from the exotic chemical inventories observed in these objects, recent studies suggest that subsequent products of chemical evolution such as hazes (in the form of aerosols or/and clouds) can also exist in these atmospheres. Hazes can strongly influence the thermal structure of the atmosphere, the dynamics, and the photochemistry, as their equivalents in the solar system atmospheres have promptly demonstrated. Our goal is to investigate the processes leading to the formation of aerosols and clouds in exoplanet atmospheres with the use of detailed models of aerosol and cloud formation and evolution coupled with photochemical models of the atmosphere. We apply these models to the case of exoplanet HD 189733 b for which observations indicate the presence of heterogeneous opacities. Our results demonstrate that photochemical haze can have important implications for the interpretation of the available observations.

Methods

We perform our studies using detailed models of atmospheric thermochemistry/photochemistry for the evaluation of the atmospheric composition under different temperature conditions in the atmosphere of HD 189733 b [1]. Based on the composition results we apply models for the simulation of the photochemical aerosols and clouds, which are based on previous studies of relevant processes in Titan's atmosphere [2, 3]. We estimate the production rate of photochemical aerosols from the photolysis rates of major compounds in the upper atmosphere of HD 189733 b, assuming an efficiency for aerosol formation based on previous studies in the solar system and particularly the atmospheres of Titan, Saturn and Jupiter. For the simulation of clouds we consider the formation of silicate condensates, which provide the largest mass flux of condensable species under the assumed temperature conditions. For the latter we evaluate our model results for temperature profiles derived by GCM simulations [4] or the inversion of secondary eclipse observations [5].

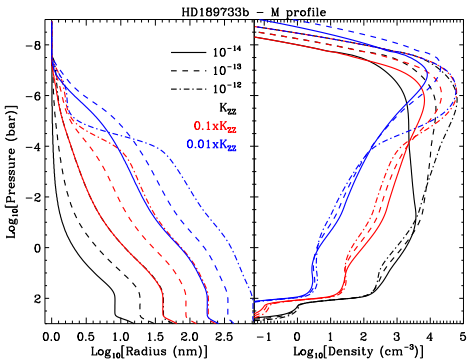

Figure 1: Model results for the average particle size and corresponding density under different assumptions of aerosol mass flux and atmospheric mixing.

Results

Our results suggest that significant mass fluxes of photochemical aerosols can be produced in the upper atmosphere of HD 189733 b (above $\sim 10 \mu$bar). However, the resulting aerosol size and population depend strongly on the assumed atmospheric mixing efficiency (Fig. 1). High mixing values limit the growth of the aerosol particles because particles are transported to the lower atmosphere before having the opportunity to collide with each other and coagulate. However, reduced eddies allow for the formation of large enough particles that reach up to 10 to 100 nm depending on the assumed mass flux and eddy mixing. Using

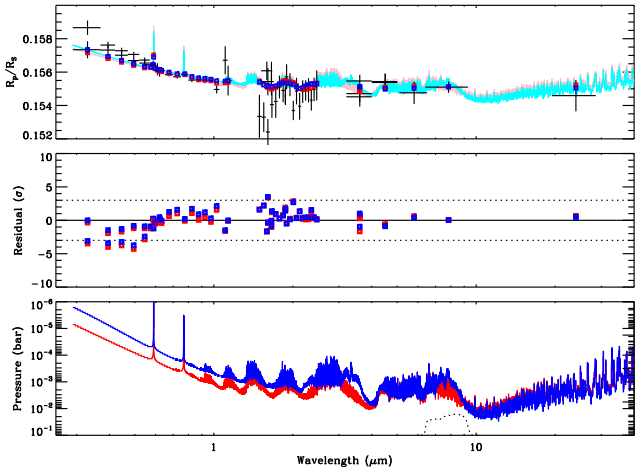

Figure 2: Planetary transit radius for an aerosol mass flux of 5×10^{-13} g cm^{-2}s^{-1} (upper panel). The pink and cyan lines correspond to different temperature profiles, respectively. The red and blue squares present the model mapped on the resolution of the observations. The latter are taken from the compilation of [6]. The simulated spectra are within 3σ of the observations in the whole spectrum (middle panel), although they appear systematically lower than the observed planetary size at UV wavelengths. The two temperature profiles provide a similar transit spectrum, although the reference pressure at the 8μm Spitzer/IRAC band are different (lower panel).

these distributions for the evaluation of the planet radius over transit, we find that mass fluxes of the order to 10^{-13} g cm^{-2}s^{-1} provide a good fit to the observations (Fig. 2), while such mass fluxes are supported by the photochemistry simulations. Our results indicate that in order to match the observed planet size at short wavelengths particles need to be present at pressures lower than 0.1 mbar. Attempting to perform the same fit but assuming only the presence of silicate clouds is a challenge due to the high altitude extend of the cloud layer required. Our simulations indicate that high eddies are required in this case in order to expand the cloud layer to high altitudes, and even in this case the resulting spectral signature is not consistent with the available observations. Thus, our results demonstrate the photochemical hazes are a more likely candidate for the interpretation of the heterogeneous opacity in the atmosphere of HD 189733 b.

Acknowledgements

This project was supported by the Programme National de Planetologie of INSU within the project Atmospheric Molecular Growth (AMG).

References

[1] Lavvas, P., Koskinen, T., Yelle, RV: Electron densities and alkali atoms in exoplanet atmosphere. Ap.J., 796:15.

[2] Lavvas, P., Yelle, RV, Griffith, CA: Titan's vertical aerosol structure at the Huygens landing site: Constraints on particle size, density, charge, and refractive index. Icarus, 210,832-842.

[3] Lavvas, P., Griffith, CA, Yelle, RV: Condensation in Titan's atmosphere at the Huygens landing site. Icarus, 215, 732-750.

[4] Moses et al.: Disequilibrium carbon, oxygen, and nitrogen chemistry in the atmospheres of HD 189733 b and HD 209458 b. Ap.J., 737:15.

[5] Line et al.: A systematic retrieval analysis of secondary eclipse spectra. II. A uniform analysis of nine planets and their C to O ratios. Ap.J. 783:70.

[6] Pont et al.: The prevalence of dust on the exoplanet HD 189733b from Hubble and Spitzer observations. MNRAS, 432, 2917-2944.

EPSC Abstracts
Vol. 11, EPSC2017-353, 2017
European Planetary Science Congress 2017

Benzene formation in Titan's lower atmosphere

J. M. C. Plane (1), K. Douglas (1), M. A. Blitz (1), D. E. Heard (1), P. W. Seakins (1), W. Feng (1,2) and K. Willacy (3)
(1) School of Chemistry, University of Leeds, Leeds, UK, (2) National Centre for Atmospheric Science, UK (3) Jet Propulsion Laboratory, California Institute of Technology, CA, USA (j.m.c.plane@leeds.ac.uk / Fax: +44-113-3436401)

Abstract

The production of benzene (C_6H_6) in Titan's atmosphere is a crucial step to tholin and haze formation. Two pathways which are important below 400 km are considered here. First is the gas-phase route via methylene (CH_2) radical chemistry. We show in a new laboratory study that the more reactive excited singlet state of CH_2, produced by CH_4 photolysis in Titan's atmosphere, is quenched increasingly efficiently at lower temperatures to the less reactive ground state CH_2, rather than reacting with species such as H_2 and CH_4. This has important consequences for the production of ethane and the propargyl (C_3H_3) radical, an important C_6H_6 precursor. The second route to C_6H_6 is the cyclo-trimerization of acetylene (C_2H_2) on cosmic dust analogue particles. The combination of a laboratory study of the heterogeneous chemical kinetics, combined with a new astronomical model of the cosmic dust input to Titan's atmosphere, shows that the production of C_6H_6 *via* uptake of C_2H_2 on the dust, followed by cyclo-trimerization and desorption, is competitive with gas-phase production of C_6H_6 between 80 and 120 km.

1. Introduction

The photolysis of methane by UV photons is the primary source of hydrocarbon radicals in the atmospheres of Titan and the giant planets. The photolysis channels are thought to be:

$$CH_4 + h\nu \rightarrow CH_3 + H \quad \text{(R1a)}$$
$$\rightarrow {}^1CH_2 + H_2 \quad \text{(R1b)}$$
$$\rightarrow {}^3CH_2 + 2H \quad \text{(R1c)}$$
$$\rightarrow CH + H_2 + H \quad \text{(R1d)}$$

Methylene, CH_2, is an important product and can be produced in either the triplet groundstate ($^3CH_2$) or the first excited singlet state ($^1CH_2$). Although the energy gap between the ground and first excited states is small (37.7 kJ mol^{-1}), the chemistry of the two species are quite different. $^1CH_2$ rapidly inserts into bonds followed by dissociation of the chemically activated intermediate, e.g.:

$$^1CH_2 + C_2H_2 \rightarrow C_3H_4^* \rightarrow C_3H_3 + H \quad \text{(R2)}$$

The formation of the propargyl radical, C_3H_3, has been proposed as an important radical route to C_6H_6 formation on Titan [1]:

$$C_3H_3 + C_3H_3 \rightarrow C_6H_6 \quad \text{(R3)}$$

with benzene being the first step in the formation of the layer of tholin aerosols at 300-400 km which surround Titan [2]. In contrast, $^3CH_2$ is relatively unreactive with closed shell molecules and its major loss processes are reactions with radical species such as H and CH_3, yielding (after several steps) C_2H_2. Both methylene species are therefore important in different aspects of Titan's complex photochemistry. For the reactions of $^1CH_2$ there is a parallel relaxation process in which collisions with C_2H_2, CH_4, H_2, and other molecular species lead to ground state $^3CH_2$. It is therefore important to quantify the competition between reaction and relaxation of $^1CH_2$ over the temperature range relevant to Titan's stratosphere.

Another route to C_6H_6 formation is via heterogeneous chemistry involving the cyclo-trimerization of acetylene:

$$3\,C_2H_2 \rightarrow C_6H_6 \quad \text{(R4)}$$

on cosmic dust or meteoric smoke particles (MSPs), which form through the recondensation of metallic vapours produced by meteoric ablation [3]. Contributions to the flux of cosmic dust entering Titan's atmosphere originate from several sources including Edgeworth-Kuiper Belt (EKB) objects and various cometary families (e.g., Jupiter family and Halley type comets) [4]. Data collected from the Pioneer 10 meteoroid detector and from the Student Dust Counter (SDC) on the New Horizons mission has been used to constrain the overall mass production rate from the EKB and the differential mass production distribution into the Saturnian system, including Saturn's satellites and planetary rings [5].

2. Experimental Results

The kinetics of the reactions of $^1CH_2$ with He, N_2, O_2, H_2 and CH_4 were measured over the temperature range 43 – 160 K by pulsed laser photolysis, monitoring $^1CH_2$ removal by laser induced fluorescence. Low temperatures were obtained with either a pulsed Laval expansion (43 – 134 K) or a low temperature, slow flow reaction cell (160 K). The rate coefficients for the reactions with N_2, O_2, H_2 and CH_4 all showed a strong negative temperature dependence. For the reactions of $^1CH_2$ with H_2 and CH_4, the branching ratio for quenching to $^3CH_2$ increases significantly between 160 and 73 K.

A low-temperature flow tube and ultra-high vacuum apparatus were used to explore the uptake and heterogeneous chemistry of C_2H_2 on cosmic dust analogues. The uptake coefficient of C_2H_2 on a variety of olivinic particles is $(1.5 – 1.9) \times 10^{-4}$ at 181 K, and the rate of cyclo-trimerization to C_6H_6 is $2.6 \times 10^{-5} \exp(-741/T)$ s^{-1}.

3. Atmospheric implications

The Leeds Chemical Ablation Model was used to show that the bulk of cosmic dust particles (radius 0.02 - 10 μm) entering Titan's atmosphere do not ablate because of the slow entry velocity (< 29 km s^{-1}) and large atmospheric scale height. Particles smaller than 10 μm sediment very slowly in the troposphere, thereby providing a significant surface for heterogeneous chemistry below 150 km. A 1D atmospheric model of dust sedimentation, C_2H_2 uptake, cyclo-trimerization and desorption of C_6H_6 shows that the peak production of C_6H_6 occurs between 80 and 120 km [6].

The implications of the measured rate coefficients and branching ratios for $^1CH_2$ were examined in a 1D transport model of Titan's atmosphere from Caltech/JPL [7], with chemistry from Moses et al. [8]. The most striking difference with the results from the present study is seen in the profile of C_2H_6, where concentrations decrease by 44% between 1550 and 800 km because of reduced CH_3 production. In contrast, the profiles for the unsaturated hydrocarbons C_2H_2 and C_2H_4 both show significant increases of 15 % and 30 %, respectively, at 50 km, moving both profiles into better agreement with the Composite Infrared Spectrometer (CIRS) limb and nadir observations. Despite this, observed concentrations of C_2H_2 below 250 km are still twice the modelled concentrations, while C_2H_4 observations are almost an order of magnitude higher. Below 500 km, an increase in C_6H_6 by up to 30% is observed, largely as a result of the increased C_2H_2.

4. Summary and Conclusions

The influence of cosmic dust on the atmospheric chemistry of Titan has been examined for the first time. The production of C_6H_6 from the cyclo-trimerization of C_2H_2 on cosmic dust analogues is shown to be efficient and competitive with gas-phase chemistry. The CH_2 radical plays a crucial role in Titan's photochemistry; this study explored the kinetics and quenching of the reactive singlet state with a range of abundant molecules such as CH_4. These reactions have unexpected temperature dependences, with significant effects on C_2H_6, C_2H_2 and C_6H_6, demonstrating the importance of carrying out laboratory measurements over the temperature range appropriate to Titan's atmosphere.

Acknowledgements

This work was supported by the Leverhulme Trust (grant F/00122/BB–PETALS), the European Research Council (project number 291332 –CODITA) and the Science and Technology Facilities Council (grant ST/L000628/1).

References

[1] Wilson, E. H., Atreya, S. K.: Chemical sources of haze formation in Titan's atmosphere. Planet Space Sci., 51, 1017-1033, 2003.

[2] Lorenz, R. D.: Titan: Interior, surface, atmosphere, and space environment. Meteorit Planet Sci, 49, 1139-1140, 2014.

[3] Saunders, R. W., Plane, J. M. C.: A photo-chemical method for the production of olivine nanoparticles as cosmic dust analogues. Icarus, 212, 373-382, 2011.

[4] Poppe, A. R.: An improved model for interplanetary dust fluxes in the outer Solar System. Icarus, 264, 369-386, 2016.

[5] Poppe, A. R., Horanyi, M.: On the Edgeworth-Kuiper Belt dust flux to Saturn. Geophys Res Lett, 39, art. no.: L15104, 2012.

[6] Frankland, V. L. *et al.*: Uptake of acetylene on cosmic dust and production of benzene in Titan's atmosphere. Icarus, 278, 88-99, 2016.

[7] Li, C. *et al.*: A non-monotonic eddy diffusivity profile of Titan's atmosphere revealed by Cassini observations. Planet Space Sci., 104, 48-58, 2014.

[8] Moses, J. I. *et al.*: Photochemistry and diffusion in Jupiter's stratosphere: Constraints from ISO observations and comparisons with other giant planets. J. Geophys. Res.-Planets, 110, 2005.

EPSC Abstracts
Vol. 11, EPSC2017-369, 2017
European Planetary Science Congress 2017

Conditions and dynamics in the active region of a regional Mars dust storm

S. Rafkin (1), J. Pla-Garcia (2) and C. Leung (3)
(1) Southwest Research Institute, Colorado, USA, (2) Centro de Astrobiologia, Torrejon de Ardoz, Spain, Lunar and Planetary Laboratory, University of Arizona, Tucson, USA (rafkin.swri@gmail.com)

Abstract

The conditions within and nearby the active lifting region of a dust storm have never been observed in situ. The unobserved conditions are modeled with the Mars Regional Atmospheric Modeling System using a fully interactive dust cycle. The storm is found to be extremely dynamic, with deep and vigorous vertical plumes of dust that exhibit a life cycle and mesoscale organization.

1. Introduction

The active regions of Mars dust storms may present some of the most challenging operational environments for human and robotic exploration. Visibility is likely to be substantially reduced. Winds, although lacking meaningful momentum, can pick up large quantities of dust causing it to abrade or enter mechanical elements. The large amount of dust may also induce strong electric fields, possibly sufficient to induce breakdown (i.e., lightning) or arching within electronics. The thermal environment is likely to also change dramatically. But all of these conditions are hypothesized; there have never been in situ observations at or near the active lifting center of a regional or larger dust storm on Mars. Landed meteorological packages have recorded the atmospheric environment during large and global dust storms, but only at a distance from the presumed active areas.

2. Numerical Experiment

In support of the Mars 2020 Rover mission (hereafter M2020), mesoscale modeling of 11 landing sites with high science potential have been modeled to characterize and identify possible hazardous atmospheric conditions during entry, descent and landing (EDL) operations. Substantial effort has gone into simulating both nominal (non-dust storm) conditions as well as those conditions that might be expected in a dust storm. For the purposes of this study, the results of dust storm scenarios in the vicinity of the landing sites at Syrtis (lat/lon) and Jezero Crater (lat/lon) are presented.

One method to investigate dust storm conditions is to utilize a fully interactive dust cycle. In this scenario, surface winds are allowed to lift dust, the lifted dust is permitted to radiatively perturb the thermal structure of the atmosphere, and the dynamics (the winds) evolve and transport the lifted dust according to the radiative forcing. The Mars Regional Atmospheric Modeling System (MRAMS [1]) is configured with a fully interactive dust cycle that evolves according to the model-predicted winds and diffusion. Dust also undergoes sedimentation. The simulation has five grids, and dust lifting is permitted only on grids two through four.

Results

During the afternoon on the sol 2, the first day of dust lifting, two primary areas of lifting develop (Fig. 1). The first area is in the northeast region of the grid, and is already organized into a linear feature that becomes more disorganized through the day. The second area is on the southeast rim of the Syrtis impact basin. The Syrtis area organizes into a linear feature roughly aligning with the daytime upslope flow.

A cross-section showing different atmospheric fields at x=85 and ~1400 local is displayed in Fig. 2. The dust mixing ratio shows a deep (> 6 km) plume just to the north of the Isidis crater rim. The mixing ratio peaks near the surface and drops off with height. This dust profile is consistently seen in active lifting regions. The surface maximum is partly due to the surface being the source of dust, with entrainment of less dusty air as the plume rises. However, it is also because the mixing ratio can be dominated by a few large dust aerosol, since the mass is proportional to the cubed of the radius.

In the plume near the surface, the air temperature is as much as 20K colder than nearby areas. This is due to solar absorption higher in the dust column limiting direct heating deeper into the atmosphere. Overall, within the plume, there is an inversion, and although the top of the plume is warmer than below, it is near neutral buoyancy compared to the less dusty air on either side. Apparently, adiabatic cooling nearly offsets the expected positive heating perturbation at the top of the dusty plume.

Turbulent kinetic energy is confined to a much shallower layer near the surface in and around the dust plume. This structure is consistent with the thermal structure—an inversion—that will tend to suppress buoyancy of generation of turbulence. In contrast, near the middle of the grid where a more traditional steep lapse rate is present, deep convective, but non-dusty plumes are present.

Finally, a very strong (>60 m/s) low level jet forms in the vicinity of the dusty plume. This structure results entirely from the dust storm distribution, which can be seen by examining the model solution when lifted dust (foreground dust) is not radiatively active (Fig. 3).

3. Figures

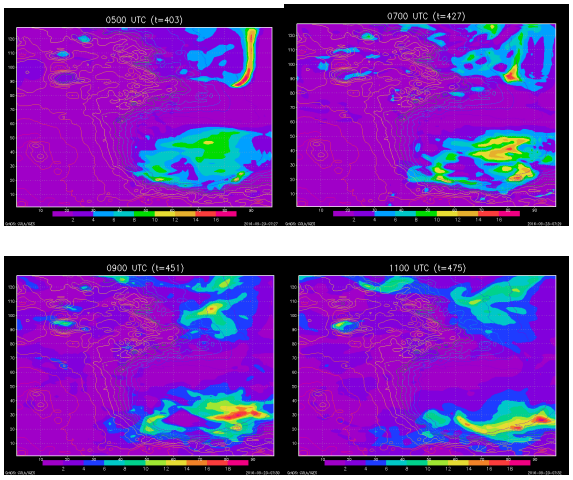

Figure 1. Column visible dust opacity (shaded) and topography (contours) on grid 3 during the afternoon. Times are given in Mars UTC. Add ~5 hours for local time. Axes are labelled by grid point (~27 km spacing).

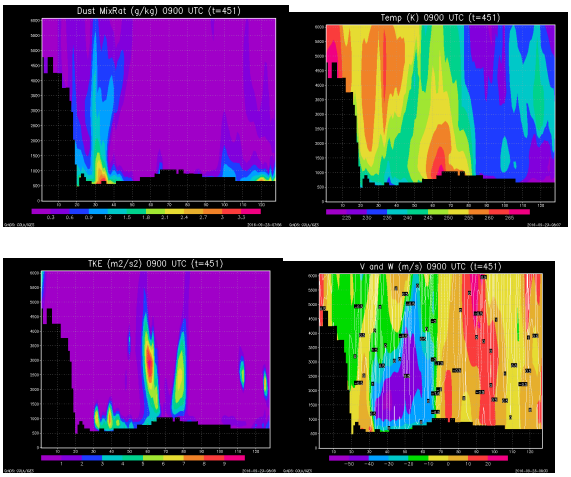

Figure 2. Dust mixing ratio (top left), temperature (top right), Turbulent kinetic energy (bottom left) and v (shaded) and w (contoured) wind (bottom right) on grid 3 at x=85 during the afternoon.

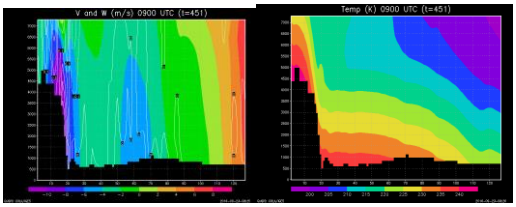

Figure 3. Temperature (left) and winds (right) for the same cross-section as in Figure 2, but for the case of radiatively passive dust.

Acknowledgements

The initial work presented here was sup-ported by a contract under the Mars Critic Data Program. Follow on work as supported by the NASA SSW Program.

References

[1] Rafkin, S. C., Haberle, R. M., & Michaels, T. I. (2001). The Mars regional atmospheric modeling system: Model description and selected simulations. Icarus, 151(2), 228-256.

EPSC Abstracts
Vol. 11, EPSC2017-423, 2017
European Planetary Science Congress 2017

Laboratory investigation of nitrile ices of Titan's stratospheric clouds

D. Nna-Mvondo (1, 2), C. M. Anderson (1), J. L. McLain (1, 3), R. E. Samuelson (1, 3)

(1) NASA GSFC, Greenbelt, MD, USA, (2) Universities Space Research Association (USRA), Columbia, MD, USA, (3) University of Maryland, College Park, MD, USA (delphine.nnamvondo@nasa.gov / Fax: +1-301-6146522)

Abstract

Titan's mid to lower stratosphere contains complex cloud systems of numerous organic ice particles comprised of both hydrocarbon and nitrile compounds. Most of these stratospheric ice clouds form as a result of vapor condensation formation processes. However, there are additional ice emission features such as dicyanoacetylene (C_4N_2) and the 220 cm^{-1} ice emission feature (the "Haystack") that are difficult to explain since there are no observed vapor emission features associated with these ices. In our laboratory, using a high-vacuum chamber coupled to a FTIR spectrometer, we are engaged in a dedicated investigation of Titan's stratospheric ices to interpret and constrain Cassini Composite InfraRed Spectrometer (CIRS) far-IR data. We will present laboratory transmittance spectra obtained for propionitrile (CH_3CH_2CN), cyanogen (C_2N_2) and hydrogen cyanide (HCN) ices, as well as various combinations of their mixtures, to better understand the cloud chemistry occurring in Titan's stratosphere.

1. Introduction

In Titan's stratosphere, at altitudes spanning 60 to ~200 km, and temperatures between about 70K and ~150K, condensed nitriles (and hydrocarbons) constitute a second type of Titan cloud system; this is in addition to the tropospheric convective methane clouds. Stratospheric ice clouds of cyanoacetylene (HC_3N) and dicyanoacetylene (C_4N_2) are observed in CIRS far-infrared spectra at high latitudes during the northern winter [1], as sharp emission features peaking at 506 cm^{-1} and 478 cm^{-1}, respectively. Spectrally broad ice emission features in Titan's stratosphere are also observed in CIRS spectra [2], peaking at 220 cm^{-1} (termed the "Haystack") and at 160 cm^{-1}, the latter feature identified as a nitrile composite ice. Whereas HC_3N vapor in the far-IR is observed at 499 cm^{-1}, and explains the formation of its condensate at 506 cm^{-1}, the presence of C_4N_2 ice and the Haystack remain puzzling since there are no associated vapor emission features to explain these ices to form from vapor condensation processes [3]. Anderson *et al.* [3] have postulated that Titan's stratospheric C_4N_2 and the Haystack ices may form through solid-state (photo)chemistry, in a similar way to the formation of nitric acid trihydrate in the terrestrial polar stratosphere. For the 160 cm^{-1} nitrile composite ice emission feature, Anderson and Samuelson [2] showed that it may arise from lattice/libration vibrations of a combination of nitrile ices, notably that of HCN and HC_3N, with possible contributions from additional trace nitrile ices. Here we present our laboratory efforts so far towards the identification of the chemical composition of Titan's Haystack and nitrile composite ices features.

2. Laboratory experiments

All experiments are conducted in the Spectroscopy for Planetary Ices Environments (SPICE) laboratory at NASA GSFC. Transmission spectroscopy is performed with the SPECtroscopy of Titan-Related ice AnaLogs (SPECTRAL) high-vacuum chamber (Fig. 1) in order to measure the near- to far-infrared spectroscopic and optical properties of thin films of pure and mixed ices of propionitrile, cyanogen and hydrogen cyanide. Transmittance spectra of thin ice films (≤10 µm thick) are acquired from 50 cm^{-1} to 11700 cm^{-1} at low dosing temperatures ranging from 30K to 160K. HCN and C_2N_2 were previously synthesized by thermal reaction of potassium cyanide with stearic acid and by thermal

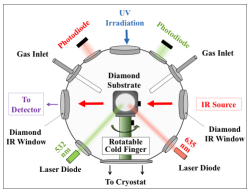

Figure 1: Schematic illustration of the SPECTRAL high-vacuum spherical sample chamber used for the experiments.

decomposition of silver cyanide, respectively. Propionitrile was provided commercially. The samples were purified by several cycles of freeze-pump-thaw under a cooling bath of ethanol and liquid nitrogen (-116˚C).

3. Results

3.1. Pure nitrile ices

For pure HCN and C_2N_2 ices, there is a clear transition in ice phase from amorphous to crystalline. This is evidenced by an increase of the band intensity of the lattice mode libration at 166 cm^{-1} for HCN and the C-C≡N asymmetric bend (ν_5) at 237 cm^{-1} for C_2N_2. Both nitriles show a peak wavenumber shift and also there is a split of the C_2N_2 absorption band (Fig. 2).

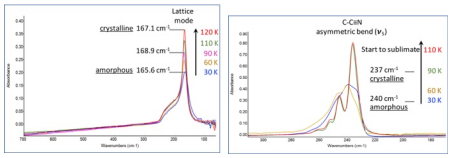

Figure 2: Far-IR spectra of pure HCN ice (2 µm film) dosed at 30K, 60K, 90K, 110K, 120K (left) and pure C_2N_2 ice (3 µm film) dosed at 30K, 60K, 90K, 110K (right).

On the other hand, for propionitrile ice, we observe peculiar temperature-driven ice phases compared to that of C_2N_2 and HCN ices (Fig. 3). The presence in the methyl molecule (-CH_3) and methylene (-CH_2) groups, which have low barriers to rotation around single bonds, produces several orientations and reordering of these groups in the solid phase ice structure. Consequently, several phase transitions are observed in the far-IR spectra at different temperatures, until the final stable crystalline phase is achieved.

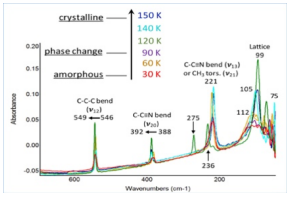

Figure 3: Far-IR spectrum of pure CH_3CH_2CN ice (3-10 µm film) dosed at 30K, 60K, 90K, 120K, 140K, 150K.

3.2. Mixed nitrile ices

For the HCN/C_2N_2 ice mixture, we observe that the HCN libration mode (168 cm^{-1} at 110K) disappears when C_2N_2 prevails in the ice mixture (Fig. 4). We note that for the HCN/CH_3CH_2CN ice mixture, this libration mode significantly broadens when CH_3CH_2CN prevails in the mixture (Fig. 4).

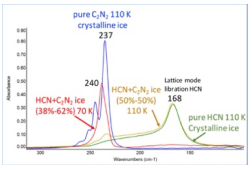

Figure 4: Far-IR spectra of HCN/C_2N_2 (top) and HCN/CH_3CH_2CN (bottom) ice mixtures compared to spectra of pure HCN, C_2N_2 and CH_3CH_2CN ices.

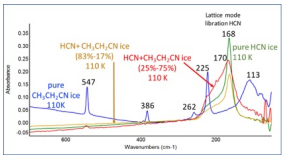

4. Conclusion

We have demonstrated our first attempts of many to ultimately reproduce and identify the CIRS Titan far-IR stratospheric ice observations. In our initial attempts of just a few compounds, we find that the spectral feature of the HCN libration mode (166 – 169 cm^{-1}) can be drastically altered by the surrounding molecule when mixing occurs. These nominal results indicate that the HCN/C_2N_2 ice mixture does not match the spectral shape and wavenumber peak position of the Haystack emission feature, or that of the nitrile composite ice. This is also true of the HCN/CH_3CH_2CN ice mixture even though it shows a broad absorption band at 170 cm^{-1}, which better resembles the Haystack than the previous mixture.

Acknowledgements

This research is supported by an appointment to the NASA Postdoctoral Program at NASA Goddard Space Flight Center, administered by the Universities Space Research Association through a contract with NASA.

References

[1] Anderson, C.M., Samuelson, R.E., Bjoraker, G.L., Achterberg, R.K.: Particle size and abundance of HC_3N ice in Titan's lower stratosphere at high northern latitudes, Icarus, Vol. 207, pp. 914-922, 2010.

[2] Anderson, C.M., Samuelson, R.E.: Titan's aerosol and stratospheric ice opacities between 18 and 500 µm: Vertical and spectral characteristics from Cassini CIRS, Icarus, Vol. 212, pp. 762-778, 2011.

[3] Anderson, C., et al.: Solid-state photochemistry as a formation mechanism for Titan's stratospheric C_4N_2 ice clouds, Geophys. Res. Lett., Vol. 43, pp. 3088-3094, 2016.

EPSC Abstracts
Vol. 11, EPSC2017-428-2, 2017
European Planetary Science Congress 2017

Original deep convection in the atmosphere of Mars driven by the radiative impact of dust and water-ice particles

A. Spiga[1], J.-B. Madeleine[1], D. Hinson[2], T. Navarro[1], E. Millour[1], F. Forget[1], A. Määttänen[3], F. Montmessin[3], [aymeric.spiga@upmc.fr] [1] LMD (UPMC/CNRS), Paris, France [2] SETI Institute / Stanford University, California, USA [3] LATMOS (CNRS/UVSQ), Guyancourt, France

Background and motivation Recent spacecraft observations have shed a new light on "mesoscale" meteorological phenomena in planetary atmospheres, developing at spatial scales smaller than the Rossby radius of deformation: Mars' regional dust storms[1], Venus' cloud layer plumes[2], Titan's methane storms[3], gas giants' convective storms[4,5]. Not only those processes have a crucial influence on the whole climate, but they also unveil key characteristics of planetary environments, and fundamental atmospheric fluid dynamics. Some of the above-mentioned mesoscale phenomena (e.g. convective storms on Titan and gas giants) share similarities with moist convective motions on the Earth: convective instability is triggered by the release of latent heat by condensing species such as water, methane, ammonia. By contrast, Mars was thought to be devoid of deep convection: water-ice clouds do form because the atmosphere is close to saturation, but the associated release of latent heat is negligible given the low quantity of water involved[6]. Here, using dedicated mesoscale modeling and Large-Eddy Simulations[7], using an interactive dust scheme[8] and a complete radiative + scavenging model for water-ice clouds[9,10], we unveil two examples of deep convection on Mars – in dust storms[11] and water-ice clouds[12] – to demonstrate that the radiative effect of aerosols and clouds can lead to powerful convective motions just as much as the release of latent heat in moist convection.

Convection in dust storms Dust storms are often considered as indicative of regional and global winds, and having an impact on global circulation. Mesoscale modeling could draw a slightly different picture[13]. Our simulations with a dust transport scheme showed that deep convective motions, implying a fast and efficient upward transport of dust particles, occur in Martian local and regional dust storms, a phenomena we named "rocket dust storms"[11]. The supply of convective energy is provided by the absorption of incoming sunlight by dust particles (positive buoyancy, Fig 1), rather than by latent heating as in moist convection on Earth and other environments. A potentially strong implication is the formation of detached layers of aerosols[14], which needs to be parameterized in Global Climate Models. This new view on local dust storms might also help to understand how a large regional storms becomes a planet-encircling dust storm, with mechanisms possibly analogous to Mesoscale Convective Systems[15] and convective self-aggregation on the Earth.

Convection in water-ice clouds Nighttime mixing layers were unveiled in the troposphere of Mars by radio-occultations on board Mars Global Surveyor and Mars Reconnaissance Orbiter[16] (they went unnoticed for about a decade because the existing temperature data were never displayed as potential temperature which clearly emphasizes the presence of mixed layers as zero-slope signatures along the vertical axis). We were able to show with mesoscale simulations that the observed deep mixing layers can be reproduced by modeling, and that the radiative effect in nighttime water-ice clouds cause those layers to occur through convective destabilization by the radiative cooling (negative buoyancy, Fig 2) exerted by water-ice particles within the cloud[12]. It was shown that water ice clouds play a key role through their radiative effect in the large-scale thermal structure and dynamics of the Martian atmosphere[9], but their impact on the mesoscale dimensions have not been addressed until now. Large-Eddy Simulations of the atmospheric flow within and below water-ice clouds demonstrate that this deep mixing result from powerful convective plumes, which also cause virga-like phenomena to occur when water-ice particles are transported in a downward plume. We proposed to name those phenomena Martian "convective snowstorms" or "ice microbursts"; they provide explanation for not only the observed nighttime mixing layers, but also the precipitating signatures identified by the Phoenix LIDAR in polar regions on Mars.

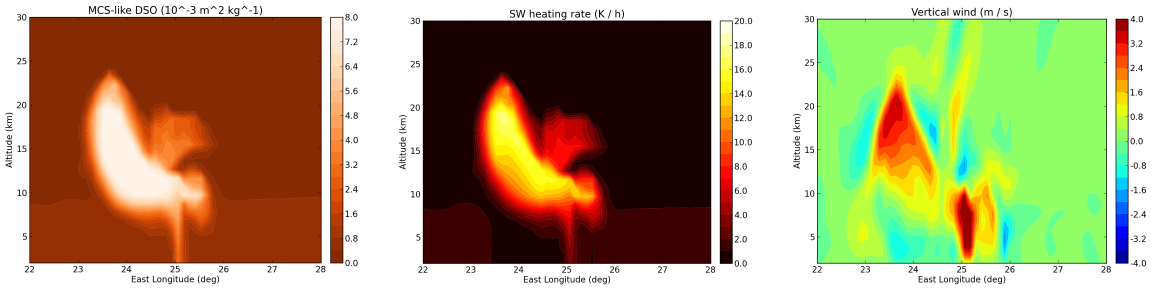

Figure 1: *Mesoscale simulation of a Martian rocket dust storm*[11]*. Longitude-altitude sections obtained at local time* 1500 *and latitude* $2.5°S$*. From left to right: (a) density-scaled optical depth at* 21.6 μm *in* 10^{-3} m^2 kg^{-1}*; (b) vertical wind in m* s^{-1} *(maximum is about* 10 m s^{-1}*); (c) shortwave heating rate in K per Martian hour (maximum is about* 24 *K/h).*

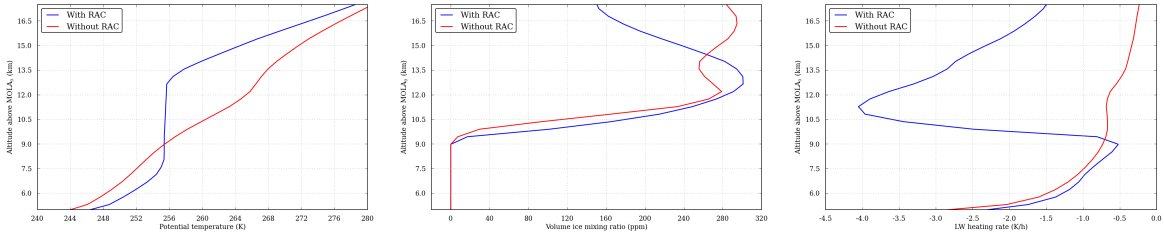

Figure 2: *Mesoscale simulation of a Martian convective snowstorm. Typical vertical profiles of (from top to bottom) potential temperature, water ice mixing ratio, total longwave radiative net heating rate, extracted from mesoscale simulations with (blue curves) and without (red curves) the radiative effects of water-ice clouds included. Profiles were extracted at longitude* $-120°E$*, latitude* $8°N$*, local time* 1000 *PM.*

Perspectives Those two original examples of aerosol-induced deep convection in the Martian atmosphere broaden the knowledge of both aerosols-atmosphere interactions and mechanisms underlying convection in planetary atmospheres, as well as the impact of convection in the regional and global scale (e.g. emission of gravity waves), with possible comparative planetology approaches where the convective dynamics of Martian water-ice clouds could be compared to Venusian sulfuric-acid clouds[17].

Bibliography

[1] A. Määttänen, T. Fouchet, et al. A study of the properties of a local dust storm with Mars Express OMEGA and PFS data. *Icarus*, 201(2):504–516, 2009.

[2] D. V. Markiewicz, W. J. andTitov, S. S. Limaye, et al. Morphology and dynamics of the upper cloud layer of Venus. *Nature*, 450:633–636, 2007.

[3] E.L. Barth and S.C.R. Rafkin. TRAMS: A new dynamic cloud model for Titan's methane clouds. *Geophys. Res. Lett.*, 34:L03203, 2007.

[4] U. A. Dyudina, A. P. Ingersoll, et al. Lightning storms on Saturn observed by Cassini ISS and RPWS during 2004 2006. *Icarus*, 190:545–555, 2007.

[5] A. Sánchez-Lavega, T. del Río-Gaztelurrutia, et al. Deep winds beneath Saturn's upper clouds from a seasonal long-lived planetary-scale storm. *Nature*, 475:71–74, 2011.

[6] H. Savijärvi and A. Määttänen. Boundary-layer simulations for the Mars Phoenix lander site. *Quarterly Journal of the Royal Meteorological Society*, 136:1497–1505, 2010.

[7] A. Spiga and F. Forget. A new model to simulate the Martian mesoscale and microscale atmospheric circulation: Validation and first results. *Journal of Geophysical Research (Planets)*, 114:E02009, 2009.

[8] J.-B. Madeleine, F. Forget, et al. Revisiting the radiative impact of dust on Mars using the LMD Global Climate Model. *Journal of Geophysical Research (Planets)*, 116:11010, November 2011.

[9] J.-B. Madeleine, F. Forget, et al. The influence of radiatively active water ice clouds on the Martian climate. *Geophys. Res. Lett.*, 39:23202, 2012.

[10] T. Navarro, J.-B. Madeleine, et al. Global Climate Modeling of the Martian water cycle with improved microphysics and radiatively active water ice clouds. *Journal of Geophysical Research (Planets)*, 2014.

[11] A. Spiga, J. Faure, et al. Rocket dust storms and detached dust layers in the Martian atmosphere. *Journal of Geophysical Research (Planets)*, 118:746–767, April 2013.

[12] A. Spiga, D.P. Hinson, et al. Snow precipitation on Mars driven by cloud-induced nighttime convection. *Nature Geoscience* (in revision), 2017.

[13] S. C. R. Rafkin. A positive radiative-dynamic feedback mechanism for the maintenance and growth of Martian dust storms. *Journal of Geophysical Research (Planets)*, 114(E13):1009–+, 2009.

[14] N. G. Heavens, M. I. Richardson, et al. Vertical distribution of dust in the Martian atmosphere during northern spring and summer: High-altitude tropical dust maximum at northern summer solstice. *Journal of Geophysical Research (Planets)*, 116(E15):E01007, 2011.

[15] S. E. Yuter and R. A. Houze. Three-Dimensional Kinematic and Microphysical Evolution of Florida Cumulonimbus. Part III: Vertical Mass Transport, Maw Divergence, and Synthesis. *Monthly Weather Review*, 123:1964–+, 1995.

[16] D. P. Hinson, S. W. Asmar, et al. Initial results from radio occultation measurements with the Mars Reconnaissance Orbiter: A nocturnal mixed layer in the tropics and comparisons with polar profiles from the Mars Climate Sounder. *Icarus*, 243:91–103, 2014.

[17] M. Lefèvre, A. Spiga, and S. Lebonnois. Three-dimensional turbulence-resolving modeling of the venusian cloud layer and induced gravity waves. *Journal of Geophysical Research: Planets*, page 2016JE005146, 2017.

EPSC Abstracts
Vol. 11, EPSC2017-445, 2017
European Planetary Science Congress 2017

The microphysical formation process of mesospheric clouds on Earth and Mars

M. Nachbar (1), D. Duft (2) and T. Leisner (1, 2)

(1) Institute of Environmental Physics, University of Heidelberg, Heidelberg, Germany
(2) Institute of Meteorology and Climate Research, Karlsruhe Institute of Technology – KIT, Karlsruhe, Germany
(Mario.nachbar@kit.edu)

Abstract

Mesospheric water ice clouds are a phenomenon frequently occurring on Earth at mid to high latitudes during summer. Surprisingly, similar clouds consisting of CO_2 ice were also detected at low latitudes in the mesosphere of Mars. Both types of clouds are believed to form by heterogeneous nucleation on nanometer size Meteoric Smoke Particles (MSPs). However, describing cloud formation is still flawed by high uncertainties due to a lack of experimental data regarding the nucleation process. We present measurements on heterogeneous nucleation and subsequent growth of H_2O and CO_2 on sub 3nm silica, iron oxide and mixed iron silicates as analogues for MSPs. The experiments were performed at conditions which are relevant to the mesosphere of Earth and Mars. We show measured desorption energies and critical saturations of H_2O and CO_2 for the different particle materials. Using Classical Nucleation Theory (CNT), we infer the contact parameter resulting in a full parameterization of the nucleation process. We conclude that the same parameterization may also be valid for Martian Dust Particles [MDPs] and predict conditions at which H_2O and CO_2 clouds form in the mesospheres of Earth and Mars. The results are discussed in comparison with atmospheric observations.

1. Introduction

Mesospheric water ice clouds, often referred to as Noctilucent Clouds (NLCs), are a phenomenon frequently occurring on Earth at mid to high latitudes during summer [e.g. 5, 10]. Similar clouds were also detected at low latitudes in the mesosphere of Mars. These clouds mainly occur during post- and pre-aphelion season [e.g. 2, 7, 8]. In contrast to Earth, the majority of the martian mesospheric clouds consist of CO_2 ice. Both types of clouds have in common that they are believed to form by heterogeneous nucleation on nanometer size Meteoric Smoke Particles (MSPs) during gravity wave induced supersaturated conditions [e.g. 1, 4, 11]. If the conditions needed for cloud formation would be well known, cloud observations could be used as a tracer for the thermodynamic conditions of the observed region. Unfortunately, predictions for cloud formation still struggle with high uncertainties due to a lack of experimental data regarding the nucleation process at realistic mesospheric conditions of Earth and Mars and regarding realistic nuclei materials.

Recently, we introduced a novel experimental setup [3, 6] specifically designed for the investigation of adsorption, nucleation and subsequent depositional growth of H_2O and CO_2 on nanoparticles with MSP material compositions. With the new setup we are able to determine the desorption energy and contact parameter which are key parameters describing the nucleation ability of the aerosol particles at realistic mesospheric conditions of Earth and Mars [3, 9].

2. Experimental Method

Singly charged nanometer size MSP analogues are produced in a microwave plasma particle source. The particles enter into the TRAPS vacuum system [6] in which we are able to select particles with radii between 1 and 3 nm. The size selected particles are then accumulated in the novel MICE-ion trap [3]. In MICE, the particles are exposed to realistic mesospheric conditions in terms of background pressure and temperature as well as CO_2 and H_2O vapor concentrations. From MICE we extract a small amount of the trapped particle population at periodic time steps and analyze their mass distribution with a time-of-flight mass spectrometer. As a result, we observe the adsorption process of CO_2 and H_2O on the MSP analogues. Depending on the conditions in MICE, adsorption is followed by nucleation and subsequent growth of CO_2 and H_2O ice particles.

3. Results and Discussion

Figure 1 shows an exemplary series of H_2O deposition on 2.6nm Silica particles. Here, the H_2O concentration has been kept constant to 5E15 m^{-3} and the particle mass is shown as a function of trapping time for 4 different particle temperatures.

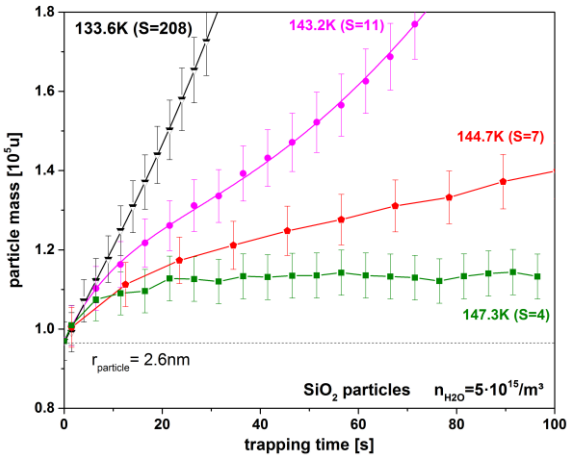

Figure 1: Exemplary dataset of an H_2O deposition experiment on 2.6nm SiO_2 particles used for desorption energy (green curve), critical saturation (red curve) and growth rate (black curve) analysis.

The green curve at a particle temperature of 147.3K and a Saturation of S=4 represents a typical measurement below the nucleation threshold. The increase in mass reflects the adsorption/desorption equilibrium process of H_2O molecules on the surface of the particles under these conditions. From measurements like this we determine the desorption energies for the investigated vapors and nuclei materials. By decreasing the particle temperature and thereby increasing S we reach conditions at which nucleation and further mass aggregation takes place (red curve, T=144.7, S=7). By observing this transition, we are able to experimentally determine the critical saturations needed for cloud formation. Fitting nucleation theory to the determined critical saturations gives us the contact parameter of the particle material. In addition, measurements at high S values (black curve T=133.6K, S=208) allow us to investigate particle growth rates.

Overall, we present a full parameterization of the nucleation process of CO_2 ice between 64K and 74K and of H_2O ice between 128K and 155K on pure iron oxide, silica and mixed iron silicates as analogues for MSPs. We will discuss the differences in the nucleation ability of the materials in respect to CO_2 and H_2O ice and will show that the same parameterization may also be valid for the nucleation on Martian Dust Particles. Using this parameterization we will deduce the Saturations at which H_2O and CO_2 cloud formation is activated at conditions relevant to the mesosphere of Earth and Mars and compare the results to observations.

Acknowledgements

The authors thank the German Federal Ministry of Education and Research (BMBF, grant number 05K13VH3) and the German Research Foundation (DFG, grant number LE 834/4-1) for financial support of this work.

References

[1] Berger, U. and von Zahn, U: The two-level structure of the mesopause: A model study. J. Geophys. Res, Vol. 104(D18), 1999.

[2] Clancy, R. T., Wolff, B. A., Whitney, B.A., et. al.: Mars equatorial mesospheric clouds: Global occurrence and physical properties from Mars Global Surveyor […], J. Geophys. Res.-Planets, Vol. 112(E4), 2007.

[3] Duft, D., Nachbar, M., Eritt, M. and Leisner, T.: A linear ion trap for studying the interaction of nanoparticles with supersaturated vapors. Aerosol. Sci. technol., 2015

[4] Gonzalez-Galindo, F., Määttänen, A., Forget, F. and Spiga, A.: The Martian mesosphere as revealed by CO_2 cloud observations and General Circulation Modeling, Icarus, Vol. 216(1), pp. 10-22, 2011.

[5] Gumbel, J. and Megner, L.: Charged meteoric smoke as ice nuclei in the mesosphere: Part 1-A review of basic concepts, Journal of Atmospheric and Solar-Terrestrial Physics, Vol. 71(12), pp. 1225-1235, 2009.

[6] Meinen, J., Khasmiskaya, S., Rühl, E., Baumann, W. and Leisner, T.: The TRAPS Apparatus: Enhancing Target Density of Nanoparticle Beams in Vacuum for X-ray and Optical Spectroscopy, Aerosol. Sci. Technol., Vol. 44(4), pp. 316-328, 2010.

[7] Montmessin, F., Gondet, B., Bibring, J.P., et al.: Hyperspectral imaging of convective CO_2 ice clouds in the equatorial mesosphere of Mars, J. Geophys. Res. - Planets, Vol. 112, pp. E11S90, 2007.

[8] Montmessin, F., et al.: Subvisible CO_2 ice clouds detected in the mesosphere of Mars, Icarus, Vol. 183(2), pp. 403-410, 2006.

[9] Nachbar, M., Duft, D., Mangan, T.P., et al.: Laboratory measurements of heterogeneous CO_2 ice nucleation on nanoparticles under conditions relevant to the Martian mesosphere, J. Geophys. Res. Planets, Vol. 121, 2016

[10] Rapp, M. and Thomas, G. E.: Modeling the microphysics of mesospheric ice particles: Assessment of current capabilities and basic sensitivities, Journal of Atmospheric and Solar-Terrestrial Physics, Vol. 68(7), pp. 715-744, 2006.

[11] Spiga, A., Gonzalez-Galindo, F., Lopez-Valverde, M. A. and Forget, F.: Gravity waves, cold pockets and CO_2 clouds in the Martian mesosphere, Geophys. Res. Lett., Vol. 39, pp. L02201, 2012.

EPSC Abstracts
Vol. 11, EPSC2017-493-2, 2017
European Planetary Science Congress 2017

Aerosols seasonal variations in Titan's upper atmosphere

B. Seignovert (1), P. Rannou (1), P. Lavvas (1), and R.A. West (2)
(1) GSMA, UMR CNRS 6089, Université Reims Champagne-Ardenne, France, (2) JPL, California Institute of Technology, Pasadena, California, USA (research@seignovert.fr)

Abstract

Cassini repetitive flybys over Titan provide a unique opportunity to monitor the evolution of the aerosol content in its upper atmosphere. Here we will present a complete analysis of the aerosol vertical extinction profiles between 600 to 300 km retrieved by a limb multiple scattering model covering the entire UV3 dataset from the beginning of the mission in 2004 (after the winter solstice in the northern hemisphere) to the end of the mission in 2017 (after the summer solstice). The complexity of these seasonal variations will provide further constrains for GCM and aerosol microphysics models.

1. Introduction

First noticed in 1981 [1] during the Voyager 1 flyby of Saturn, Titan haze layers were analyzed in detail in 1983 by Rages and Pollack [2] after the Voyager 2 flyby. The ISS images showed the presence of an aerosol opaque thick layer around 350 km above the surface and detached from the main haze. Since 2005, the new ISS (wide and narrow) cameras onboard Cassini image Titan at irregular intervals with mean time between intervals of 45 days. In 2011, West et al. [3] confirm the persistence in time of the detached haze layer at the equator but with an important altitude variability. Observed at the equator around 500 km in 2007, the detached haze layer collapsed to 380 km in 2010 and disappeared in 2011 after the equinox. As predicted by 2D and 3D Global Circulation Models (GCM) [4, 5, 6], the detached haze layer reappeared in 2016, but we will see that its behavior did not follow the model predictions.

2. Model description

To get accurate navigation of Cassini ISS images, we search for bright visible stars in the field of view (Fig. 1). With at least two stars we can perform a pointing correction by comparing the star locations with the GAIA catalogue. Otherwise, we fit a circle of Titan's main haze. Both methods provide high precision navigation of the images.

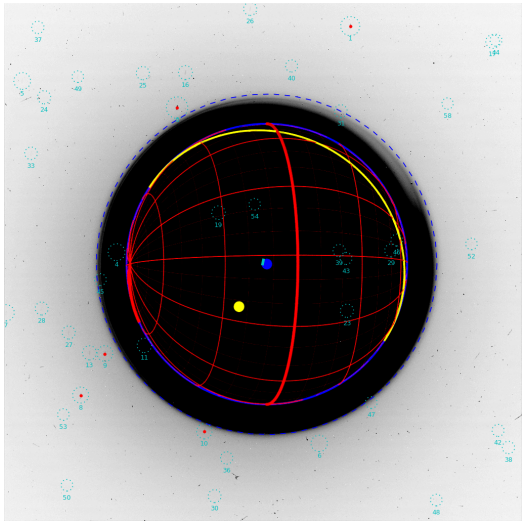

Figure 1: Star locations (red dots) in CL1-UV3 ISS NAC image N1521213736_1 (I/F inverted) compare with the GAIA catalogue (cyan dashed cercles). The red, blue and yellow sketch the solar limb and latitude/longitude grid for the solid body. The blue and yellow dots are the sub-Cassini and sub-solar points.

Based on previous scattering analyses [7, 8], we considered that Titan's detached haze layer is composed of large fractal aggregates with hundreds of monomers of 60 nm [9]. Then, we compute for each altitude between 300 to 600 km a synthetic I_n/F with a spherical limb radiative transfer model inspired from Rages and Pollack 1983 [2]:

$$\frac{I_n}{F} = \sum_{i=1}^{2n} \int_{z_{i-1}}^{z_i} \frac{\langle \omega_0 P(\theta) \rangle_j}{4} \exp\left(-\tau_{0i}(z) - \tau_i(z)\right) \beta_j R_m^j \mathrm{d}z \tag{1}$$

where I is the scattered intensity and $\pi \cdot F$ is the incident solar flux. $\langle \omega_0 P(\theta) \rangle_j$ corresponds to the product of the single scattering albedo and the phase function for a scattering angle θ = 180° - phase. τ_{0i} and τ_i rep-

resent the local incoming and outgoing optical depth. β_j is the extinction coefficient in the layer that we want to invert (Fig. 2). We modeled the local multiple scattering input by R_m^j. This correction factor is an estimation of the ratio between the total and the single single scattered intensity calculated in each layer with a local plane-parallel solver (*SHDOMPP*).

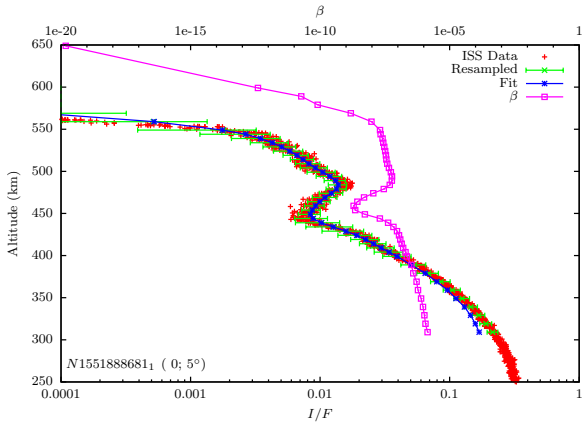

Figure 2: Inverted extinction profile (β) around the photometric equator in N1551888681_1.

3. Results

We carried out a systematic survey of all the illuminated latitudes between 2004 to 2017 (Fig. 3). Between 2004 and 2007 the detached haze layer appears as a continuous layer at 500 km from the south pole to the north polar hood. Around the equinox in 2009, the depletion below the detached layer dropped down to 300 km. We noticed that this drop was quicker in the southern hemisphere. Between 2011 and 2015, the detached haze disappeared but some sporadic depletions are locally observed. In early 2016, the detached haze reappeared as a continuous layer in the northern hemisphere down to the south pole. However, in the most recent images of 2017, we found that the detached layer no longer exists at the equator but is split into two different layers at 525 km in the southern hemisphere and 475 km in the northern hemisphere. All these seasonal variations will be presented in detail to provide further constraints for GCM and aerosol microphysics models.

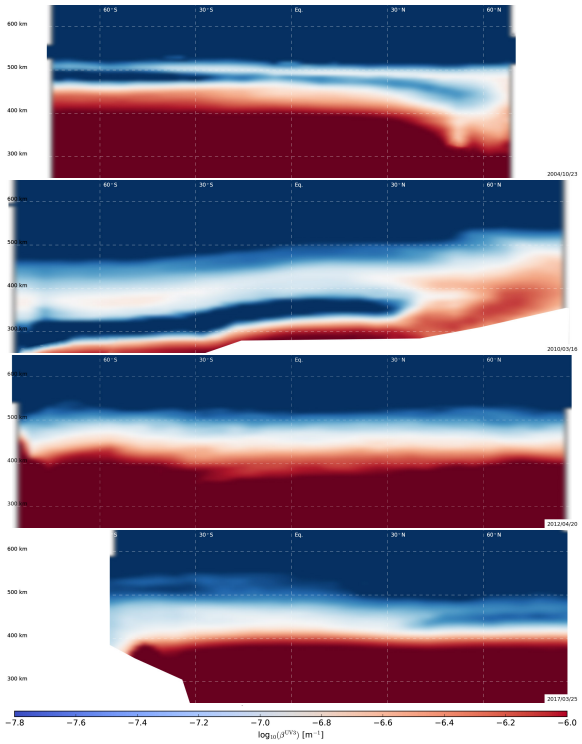

Figure 3: Top to bottom, example of aerosol haze extinction profiles of N1521213736_1 (2004), N1647460435_1 (2010), N1713617586_2 (2013), N1869102271_1 (2017).

References

[1] Smith, B.A., et al., (1981). Encounter with Saturn: Voyager 1 Imaging Science Results. Science 212, 163–191. doi:10.1126/science.212.4491.163

[2] Rages, K., & Pollack, J. B. (1983). Vertical distribution of scattering hazes in Titan's upper atmosphere. Icarus, 55, 50–62. doi:10.1016/0019-1035(83)90049-0

[3] West, R. a., Balloch, J., Dumont, P., Lavvas, P., Lorenz, R., Rannou, P., Trina, R., & Turtle, E. P. (2011). The evolution of Titan's detached haze layer near equinox in 2009. Geophysical Research Letters, 38(6), 2–5. doi:10.1029/2011GL046843

[4] Rannou, P., Hourdin, F., McKay, C.P., (2002). A wind origin for Titan's haze structure. Nature 418, 853–856. doi:10.1038/nature00961

[5] Lebonnois, S., Burgalat, J., Rannou, P., Charnay, B., (2012). Titan global climate model: A new 3-dimensional version of the IPSL Titan GCM. Icarus 218, 707–722. doi:10.1016/j.icarus.2011.11.032

[6] Larson, E.J.L., Toon, O.B., West, R.A., Friedson, A.J., (2015). Microphysical modeling of Titan's detached haze layer in a 3D GCM. Icarus 254, 122–134. doi:10.1016/j.icarus.2015.03.010

[7] Rannou, P., Ferrari, C., Rages, K., Roos-Serote, M., Cabane, M., (2000). Characterization of Aerosols in the Detached Haze Layer of Titan. Icarus 147, 267–281. doi:10.1006/icar.2000.6416

[8] Lavvas, P., Yelle, R. V., & Vuitton, V. (2009). The detached haze layer in Titan's mesosphere. Icarus, 201(2), 626–633. doi:10.1016/j.icarus.2009.01.004

[9] Seignovert, B., Rannou, P., Lavvas, P., Cours, T., West, R.A., (2017). Aerosols optical properties in Titan's detached haze layer before the equinox. Icarus 292, 13–21. doi:10.1016/j.icarus.2017.03.026

EPSC Abstracts
Vol. 11, EPSC2017-495, 2017
European Planetary Science Congress 2017

Observation at 2 µm of Titan's the limb.

P. Rannou (1), B. Seignovert (1), M. Rey (1) , L. Maltagliati, (2) and S. Lemouelic (3)
(1) GSMA, Université de Reims Champagne-Ardenne, FRANCE, (2) Nature Publishing Group, London, UK (3)LPGN, Université de Nantes, FRANCE - (contact : pascal.rannou@univ-reims.fr)

Abstract

The study of Titan properties with remote sensing relies on a good knowledge of the atmosphere properties. The in-situ observations made by Huygens combined with recent advances in the definition of methane properties enable to model and interpret observations with a very good accuracy. However, the amount of opacity in the 2 µm window remains ambiguous and the cut-off setup to use in order to fit peculiar window is significantly different from what is needed in other windows. Our scope in this work is to study the methane lines cut-off and to get information about Titan's surface spectrum.

1. Results

To study the haze layer and more generally the source of opacities in the stratosphere, we use some observation made at the limb of Titan by the VIMS instrument onboard Cassini. We used a model in spherical geometry and in single scattering, and we accounted for the multiple scattering with a parallel plane model that evaluate the multiple scattering source function at the plane of the limb.

Our scope is to retrieve informations about the vertical distribution of the haze, its spectral properties, but also to obtain details about the shape of the methane windows to disantangle the role of the methane and of the aerosols. We study the latitude of 45°N, with an image taken in 2006 with a relatively high spatial resolution (for VIMS) **(Figure 1 - left)**.

We find that the vertical profile of the haze layershows three distinct scale heights with transitions around 250 km and 350 km.

We also find that the shape of the 2 µm depends on the continuum absorption of the methane window (controlled by the setup of line profile cut-off) and on another absorption centered around 2.05 µm which clearly shows up in data. Our tests show that it is possible to use the same cut-off parameters at 2 µm than elsewhere provided we include an absorption feature around 2.05 µm. The different way to treat this absorption produces similar fit of the atmosphere intensity **(Figure 1 - right)**, but, on the other and, the retrieved surface reflectivity can differ a lot **(Figure 2)**.

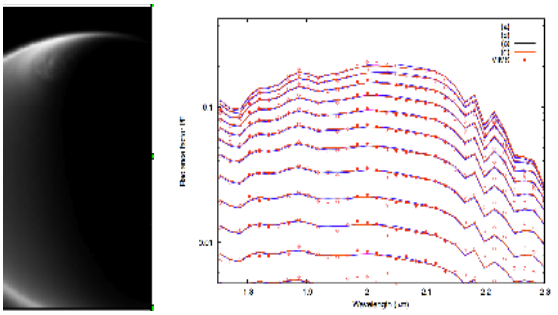

Figure 1: *(**Left**) Image of Titan northern polar region with a extended polar cloud. We a vertical profile composed with the-pixels inside the white rectangle.(**Right**) Spectral variation of I/F in in the 2- µm windows at several altitudes between 100 and 400 km. Lines from (a) to (d) are correspond to models.*

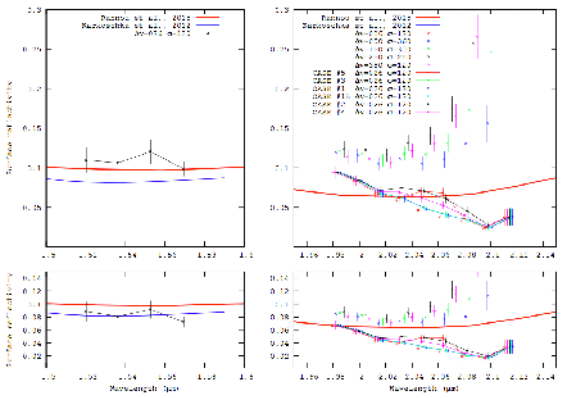

Figure 2: *Surface reflectivities retrieved with our model at 1.6 µm and 2 µm, with different setup of the model. Different setup of the cut-off of the line profiles and different absorption at 2.03 µm are assumed.*

EPSC Abstracts
Vol. 11, EPSC2017-514-2, 2017
European Planetary Science Congress 2017

Refractive indices of Early Earth organic aerosol analogs

L. Gavilan* (1), N. Carrasco (1), B. Fleury (2) and L. Vettier (1)
(1) LATMOS, Université Versailles St Quentin, UPMC Université Paris 06, CNRS, F-78280 Guyancourt, France
(2) Jet Propulsion Laboratory, California Institute of Technology, Pasadena, CA 91109, USA
*lisseth.gavilan@latmos.ipsl.fr

Abstract

Organic aerosols in the early Earth atmosphere are hypothesized to provide additional shielding to solar radiation. We simulate the conditions of this primitive atmosphere by adding CO_2 to a N_2:CH_4 plasma mixture. We produce aerosol analogs (named *tholins*) in plasmas with CO_2 / CH_4 = 1 and 4. For the latter ratio, the production of tholins decreases significantly. We measured the thin organic films via ellipsometry and modeled this data to obtain the thickness, optical band gap, and refractive indices from 1 to 5.5 eV. These absorption coefficients vary with the inclusion of CO_2, where the maximum blueshifts as the CO_2 concentration is increased. Such measurements reveal how organic aerosols in the early Earth atmosphere preferentially absorb photons of shorter wavelengths than typical Titan tholins, suggesting a coolant role in the early Earth. The refractive indices of such materials can further improve climate models of the early Earth.

1. Introduction

CO_2 is considered to be the dominant greenhouse gas offsetting the early Sun that could have kept the early Earth unfrozen. The partial pressure of CO_2 is expected to be more abundant in the Archean eon than in the modern Earth, and even more abundant in the Hadean. Modeling work expects CO_2 abundances of 3% to sustain a global average surface temperature of 273 K in the Late Archean and 10% to sustain a temperature of 288 K in the Early Archean [1, 6]. However, CO_2 can be removed by the flow of carbon into the mantle via the subduction of carbonatized seafloor [4], diminishing the atmospheric reservoir and decreasing its warming effect on the Archean climate. In addition, photochemistry of CO_2 in the early atmosphere could lead to formation of hazes which, depending on their optical properties, could induce early atmospheric warming or cooling. The aim of this work is to experimentally simulate the hypothetical composition of the early and late Archean, and to understand the impact of CO_2 in the production and optical properties of organic hazes.

2. Methods

Tholins, complex amorphous organic solids, were produced using the PAMPRE setup, a low pressure (0.95 mbar) radiofrequency (R.F.) plasma reactor [5]. This setup allows the simulation of the complex organic chemistry initiated by VUV solar photons in the ionosphere of the early Earth and Titan [2]. A 13.56 MHz R.F. power source tuned at 30 W generates a capacitively coupled plasma (CCP) fed by a gas mixture. Two different gas mixtures were used N_2:CH_4:CO_2 at 90:2:8 and 90:5:5 ratios N_2:CH_4 at 95:5 ratios. The plasma was produced within a vertical cylindrical cage. Bare silicon substrates were placed on the bottom electrode. The plasma is turned on until a thin film is deposited on the substrates.

Table 1: Early Earth tholins.

N_2:CH_4:CO_2	CO_2/CH_4	Yield [nm / hour]
90:2:8	4	8 ± 3
90:5:5	1	180 ± 8
95:5:0	0	425 ± 15

3. Analysis

Ellipsometric measurements were performed for the three different tholin samples produced with and without CO_2. The measured Ψ and Δ parameters result from the interaction between the light with both the organic film and the Si substrate. We model a multilayer system consisting of the substrate, the organic material and a roughness layer, combining the optical constants of the organic layer and air. The tholin is modeled via a Tauc-Lorentz oscillator, applicable to amorphous organic films [3]. From these models, we note that the

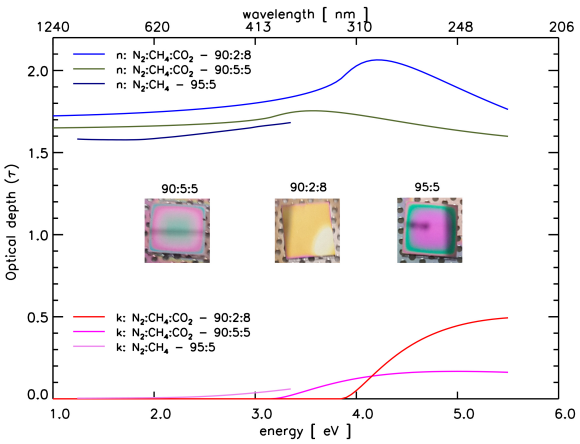

Figure 1: Refractive indices modeled for tholins prepared with different mixtures of N_2:CH_4:CO_2.

center of the main ultraviolet band is blueshifted for CO_2 / CH_4 = 4 with respect to CO_2 / CH_4 = 1, suggesting that the presence of CO_2 leads to organics absorbing UV photons at higher energies.

4. Conclusions

Our experiments show that even at high concentrations of CO_2/CH_4, organic aerosols can still be produced. This suggests that even if the atmosphere of the primitive Earth was oxidized, photochemical organic aerosols could still be produced. However, as the CO_2 concentration increases, the aerosol yield significantly decreases due to the intermediate plasma production of H_2O, among other reactants [2], consequently implying a reduced aerosol yield in the Hadean and early Archean.

We modeled the refractive indices of these tholins from 1 to 5.5 eV (225 - 1000 nm). The far UV shielding properties of the most oxidized tholins (with a maximum absorption peak at 318 nm) makes this organic haze essentially a coolant, particularly if considering the blueshifted spectrum of a young Sun. As the amount of CO_2/CH_4 decreases, the production of organic aerosols is more efficient, but they are optically less absorbing than those produced at higher CO_2 partial pressures, absorbing UV photons shortward of 413 nm. When CO_2 is removed, as in the case of Titan's reducing atmosphere, the tholin production yield is greatest, absorbing UV photons shortward of 518 nm.

Acknowledgements

We thank Dr. Bulkin and Dr. Roca i Cabarrocas for access to the ellipsometer at LPICM (Ecole Polytechnique). We thank Dr. Borondics for access to the infrared spectromicroscope of the SMIS beam line. N.C. and L.G. thank the European Research Council for funding via the ERC *PrimChem* project (grant agreement No. 636829.)

References

[1] Feulner, G. Reviews of Geophysics, 50, RG2006, 2012.

[2] Fleury, B., Carrasco, N., Marcq, E., et al. The Astrophysical Journal Letters, 807, 2, 2015.

[3] Mahjoub, A., Carrasco, N., Dahoo, P.-R., et al. Icarus, 221, 670, 2012.

[4] Sleep, N. H. & Zahnle, K. Journal of Geophysical Research, 106, 1373, 2001.

[5] Szopa, C., Cernogora, G., Boufendi, L., et al. Planetary and Space Science, 54, 394, 2006.

[6] von Paris, P., Rauer, H., Lee Grenfell, J., et al. Planetary and Space Science, 56, 1244, 2008.

EPSC Abstracts
Vol. 11, EPSC2017-527, 2017
European Planetary Science Congress 2017

Properties of a Martian local dust storm in Atlantis Chaos by means of OMEGA/MEX data analysis

F. Oliva, A. Geminale, E. D'Aversa, F. Altieri, G. Bellucci, F.G. Carrozzo, G. Sindoni.

INAF-IAPS, Rome, Italy (fabrizio.oliva@iaps.inaf.it)

Abstract

In this study we present the analysis of the dust properties of a local storm imaged in the Atlantis Chaos region on Mars by the OMEGA imaging spectrometer on March 2nd 2005. We use the radiative transfer model MITRA to study the dust properties at solar wavelengths between 0.5 μm and 2.5 μm and infer the connection between the local storm dynamics and the topography. We retrieve maps of effective grain radius (r_{eff}), optical depth at 9.3 μm ($\tau_{9.3}$) and top altitude (*ta*) of the dust layer. Moreover, we discuss about the region where the storm originated. Finally, we deduce that the 5 μm transmission window can be reliably used to sound the temperature of the surface only for $\tau_{9.3} < 1$.

1. Introduction

The study of suspended dust on Mars is fundamental to understand the planet's thermal structure and climate [6]. Martian aerosols are mainly made up of micron-sized particles, probably produced by soil weathering [11], and are composed by nanophase ferric oxide particles [10].
Different dust phenomena happen on Mars, including dust devils (localized), local dust storms (regional) and global dust storms (global-scale) [3]. In the solar spectral range, where solar light reflection prevails the thermal emission, a dust storm usually appears bright and can mask the underlying low-albedo terrains (e.g. [14]).
The top altitude of local storms varies significantly, ranging from a few hundreds of meters to more than 10-20 km above the surface [7].
In this work, we study a local dust storm observed on Atlantis Chaos region during Martian Year (MY27) by the OMEGA spectrometer [2] on board the Mars Express (MEx) spacecraft. Section 2 describes the analyzed observations. The method of the analysis is presented in Section 3. Finally, our results and conclusions are given in Section 4.

2. Observations

We analyze orbit 1441_5 registered by OMEGA in March 2005 (Ls = 168.619°). In the observation the storm is cut at west and is centered at longitude = 176.5° W and latitude = 33.5° S. In the solar part of the spectrum at about 1.2 μm the storm appears as a bright cloud and is characterized by more than twice the signal of surrounding regions. Reflectance factor spectra taken on and off the storm show changes in the spectral shape between around 0.7 and 1.4 μm. This happens since the surface mafic absorption signature is absent on the storm but becomes important by moving from the storm center to its boundaries and to regions outside the storm itself. Hence, an independent knowledge of the spectral albedo of the surface underneath the cloud is required in order to analyze the storm properties with a radiative transfer (RT) model.
In order to retrieve the surface albedo spectra (Section 3), we analyze OMEGA orbit 3262_5, since it is characterized by a low dust optical depth [9] and covers almost the same region where the storm is observed in orbit 1441_5.

3. Method and Model

In this study, we consider a part of the intersection between orbits 1441_5 and 3262_5, extending between longitudes 176.5° W and 177.5° W and latitudes 32.0° S and 35.7° S, covering regions both on and off the storm.
To derive the surface albedo spectra of this region we apply the Surface Atmosphere Separation (SAS) method [5] to the pixels of orbit 3262_5.
To retrieve the dust cloud effective radius (r_{eff}), top altitude (*ta*) and optical depth at 9.3 μm ($\tau_{9.3}$) we adopt the RT model and inversion algorithm described in [12] and [13].
The atmospheric temperature-pressure profiles and gases mixing ratios are derived from the Mars Climate Database (MCD, [8]).

To account for the dust composition, we adopt the optical constants by [14] and assumed a lognormal particles size distribution with 0.5 effective variance (MCD).

4. Results and conclusions.

We obtained spatial maps of the retrieved parameters, showing that larger particles (r_{eff} = 1.6 μm) are gathered at the center of the storm, where $\tau_{9.3} > 7$ and the dust cloud extends to more than 18 km. On the other hand, outside the storm, the dust appears confined down to the surface with smaller particles ($r_{eff} < 0.9$ μm) and $\tau_{9.3} < 0.2$ (in agreement with the estimates from [9]). By analyzing the thermal inertia of the region [4] we deduce that the dust making the storm comes from a region at west/north-west of Atlantis Chaos, characterized by low thermal inertia values. Once lifted, the dust is then confined within the north-east ridge of Atlantis Chaos by the combination of the horizontal and vertical wind profiles (MCD), in agreement with the results from our retrieval.
Finally, by comparing the retrieved dust optical depths with the data in the thermal range, we deduced that when $\tau_{9.3} > 1$, the 5 μm transmission window, usually adopted to sound surface temperatures (e.g. [1]), cannot be reliably used. A paper describing this study has been submitted to Icarus.

Acknowledgements

This study has been performed within the UPWARDS project and funded in the context of the European Union's Horizon 2020 Programme (H2020-Compet-08-2014), grant agreement UPWARDS-633127. Moreover, the study has been co-funded within the PRIN INAF 2014. We would like to thank the whole OMEGA team for the support in this work.

References

[1] Bellucci, G., et al., 2007. Evidence for enhanced hydration on the northern flank of Olympus Mons, Mars, Icarus, 192, 2, p. 361-377.

[2] Bibring, J.P., et al., 2004. Omega: Observatoire pour la minéralogie, l'eau, les glaces et l'activité. ESA SP-1240: Mars Express: The Scientific Payload. ESA Publications Division, Estec, Noordwijk, The Netherlands, pp. 37–49.

[3] Briggs, G.A., et al., 1979. Viking Orbiter imaging observations of dust in the martian atmosphere. J. Geophys. Res. 84, 2795–2820.

[4] Christensen, P. R. and H. J. Moore (1992). The Martian surface layer, in Mars, edited by H. H. Kieffer, et al., pp. 686-729, University of Arizona Press, Tucson, AZ.

[5] Geminale, A., et al., 2015. Removal of atmospheric features in near infrared spectra by means of principal component analysis and target transformation on Mars: I. Method. Icarus, Volume 253, p. 51-65.

[6] Kahre, M.A., et al., 2008. Investigations of the variability of dust particle sizes in the martian at-mosphere using the NASA Ames General Circulation Model. Icarus 195, 576-597.

[7] Määttänen, A., et al., 2009. A study of the properties of a local dust storm with Mars Express OMEGA and PFS data. Icarus 201, 504-516.

[8] Millour, E., et al., 2015. The Mars Climate Database (MCD version 5.2). European Planetary Science Congress 2015, held 27 September - 2 October, 2015 in Nantes, France.

[9] Montabone, L., et al., 2015. Eight-year climatology of dust optical depth on Mars. Icarus, Volume 251, p. 65-95, doi: 10.1016/j.icarus.2014.12.034.

[10] Morris, R.V., et al. 2006. Mössbauer mineralogy of rock, soil, and dust at Gusev Crater, Mars: Spirit's journey through weakly altered olivine basalt on the plains and pervasively altered basalt in the Columbia Hills, J. Geophys. Res., 111, E02S13.

[11] Pollack, J., et al., 1979. Properties and effects of dust particles suspended in the Martian atmosphere. J. Geophys. Res., 84, 2929 – 2945.

[12] Oliva, F., et al., 2016. Clouds and hazes vertical structure of a Saturn's giant vortex from Cassini/VIMS-V data analysis. Icarus, Volume 278, p. 215-237.

[13] Sindoni, G., et al., 2013. Development of a Monte-Carlo Radiative Transfer Code for the Juno/JIRAM Limb Measurements. European Planetary Science Congress 2013, held 8-13 September in London, UK.

[14] Wolff, M.J., et al., 2009. Wavelength dependence of dust aerosol single scattering albedo as observed by the Compact Reconnaissance Imaging Spectrometer. Journal of Geophysical Research, Volume 114, Issue E9, CiteID E00D04.

EPSC Abstracts
Vol. 11, EPSC2017-531, 2017
European Planetary Science Congress 2017

Earth as an exoplanet: VIRTIS-M/Venus Express data analysis.

F. Oliva, G. Piccioni, E. D'Aversa, G.Bellucci, G. Sindoni, G. Filacchione, and F. Capaccioni.

INAF-IAPS, Rome, Italy (fabrizio.oliva@iaps.inaf.it)

Abstract

The VIRTIS spectrometer on board the Venus Express spacecraft observed Earth several times. A subset of 48 observations has been taken from a distance at which our planet is imaged as sub-pixel size. We study this full subset to understand which spectral signatures, related to different surfaces and cloud types, can be identified from the integrated planet spectrum. As expected, we find that the cloud coverage has a key role in the identification of surface features. To investigate this finding we built a simple tool capable to simulate observations of an Earth-like planet as seen from a VIRTIS-like spectrometer, in order to infer the percentages that are required to identify each surface and cloud type when all the spectral information is integrated into a single pixel.

1. Introduction

One of the main objectives of exoplanets science is to find and characterize habitable planets. To this extent, a major role will be played by the direct imaging technique (first direct images of an exoplanet published in 2008 by [5]), taking advantage of a generation of adaptive optics assisted telescopes like ESO/VLT-SPHERE [1] and Gemini Planet Imager (GPI, [6]).
Radial velocity and transit searches indicate that Earth analogs are common. However, an extreme contrast at very small angular separations must be achieved in order to image them [7].
Disk averaged spectra of planets detected with this technique will allow the characterization of these worlds' atmospheres and, hopefully, their surfaces.
Sensitivity studies focused on what we can expect to detect on Earth-like planets have already been done by analyzing synthetic spectra consistent with ground based and satellite observations [9,3].
In this work we perform a sensitivity study, focused on the detectability of different surface and cloud spectral endmembers (Section 2), based on the use of data registered by the VIRTIS spectrometer [2,8] on board both the Rosetta and Venus Express (VEx) spacecrafts.

2. The planet simulator

We selected Earth spectral endmembers from an Earth observation registered by the Rosetta/VIRTIS-M spectrometer during the third flyby of the spacecraft around our planet, occurred in November 2009. From the observation, relative to a region at the north-west of Africa, we obtained endmembers for vegetation, ocean, desert, liquid water clouds and water ice clouds. Then, we mixed these endmembers with a randomization algorithm to generate planets observed by a VIRTIS-like spectrometer from user defined distances and observing geometries. At the first order, the Lommel correction has been applied to photometrically correct the selected endmembers.
We fixed the observing geometry to reproduce a secondary eclipse condition, with the emission angle equal to 0° at the center of the planet and the azimuth of the stellar boresight at 45° with respect to the center of the planet. Then, we investigated all possible combinations of percentages for the different endmembers to obtain the threshold values needed to detect each spectral class when the planet is observed as a single pixel. From this analysis, it results that clouds have a major impact on the detectability of the surface, confirming previous studies by other authors, based on models [9]. Our results suggest that, when the total cloud coverage is larger than 40%, surface features are undetectable.

3. Investigation of VEx data

We performed the same sensitivity analysis directly on VEx/VIRTIS data. It results that surface is never detectable in these observations and the signal from clouds is dominating the spectral information of the integrated spectrum. To verify this result, we studied the daily cloud coverage from MODIS spectrometer [4] data, available at the Nasa Earth Observations

website. The average cloud coverage relative to VEx Earth observations is always larger than 40%, confirming the results we obtained with the tool described in Section 2.

4. Summary and Conclusions

The results from our simple planet simulator show that, when the planet is observed as a single pixel, the surface endmembers can be detected only when the total cloud coverage is less than 40% in the instrument field of view (Section 2). The analysis of VEx Earth sub-pixel observations shows that only clouds can be detected, in agreement with our results and with the computed daily Earth cloud coverage (Section 3).
We will update out planet simulator by refining the endmembers photometric correction. Then, we will investigate different viewing and illumination angles to check the dependence of the endmembers detection thresholds with the observing geometry. Moreover, we will investigate other possible spectral conditions to exploit more the wavelengths of VIRTIS-M infrared channel.

Acknowledgements

We thank the Agenzia Spaziale Italiana (ASI), the Centre National Spatiales (CNES), DLR (Deutsche Zentrum für Luft und Raumfahrt) and ESA (European Space Agency) for the support to the VIRTIS, Venus Express and Rosetta programs. This work has been supported by the "Progetto Premiale WOW (Way to Other Worlds)" of INAF (Istituto Nazionale di Astrofisica).

References

[1] Beuzit, J.L., et al., 2010. SPHERE: a planet imager for the VLT. Proceedings of the conference In the Spirit of Lyot 2010, Univeristy of Paris Diderot, Paris, France.

[2] Coradini, A., et al., 1998. VIRTIS: An Imaging Spectrometer for the Rosetta Mission. Planet. Space Sci. 46 (9/10), 1291–1304.

[3] Irwin, P.G.J., et al., 2014. The transit spectra of Earth and Jupiter. Icarus, 242, pp. 172-187.

[4] Justice, C.O., et al., 1998. The Moderate Resolution Imaging Spectroradiometer (MODIS): Land Remote Sensing for Global Change Research. IEEE Transactions on Geoscience and Remote Sensing, vol. 36, no. 4.

[5] Kalas, P., et al., 2008. Optical Images of an Exosolar Planet 25 Light-Years from Earth. Science, Vol. 322, Issue 5906, pp. 1345-1348.

[6] Macintosh, B., et al., 2006. The Gemini Planet Imager. Advances in Adaptive Optics II. Edited by Ellerbroek, Brent L.; Bonaccini Calia, Domenico. Proceedings of the SPIE, Volume 6272.

[7] Males, J.R., et al., 2014. Direct imaging of exoplanets in the habitable zone with adaptive optics. Proc. SPIE 9148, Adaptive Optics Systems IV, 914820.

[8] Piccioni, G., et al., 2007. VIRTIS: The Visible and Infrared Thermal Imaging Spectrometer. ESA Special Publication, SP-1295, 1-27.

[9] Tinetti, G., et al., 2005. Disk-averaged Spectra & light-curves of Earth. Eprint arXiv:astro-ph/0502238.

EPSC Abstracts
Vol. 11, EPSC2017-571, 2017
European Planetary Science Congress 2017

Microphysical modelling of the Venusian clouds with the IPSL Venus GCM

S. Guilbon[1], A. Määttänen[1], F. Montmessin[1], J. Burgalat[2], S. Lebonnois[3], K. McGouldrick[4], A. Stolzenbach[1], F. Lefèvre[1]
[1]*UVSQ ; Sorbonne Universités, UPMC Université Paris 06 ; CNRS/INSU, LATMOS-IPSL, France.*
[2]*GSMA UMR CNRS 7331, Université de Reims Champagne-Ardenne, Reims, France.*
[3]*Laboratoire de Météorologie Dynamique (LMD), France.*
[4]*University of Colorado-Boulder, Laboratory for Atmospheric and Space Physics, USA.*
(sabrina.guilbon@latmos.ipsl.fr)

Abstract

To understand the Venus atmosphere, LMD and LATMOS laboratories have developed a 3D IPSL Venus Global Climate Model (Lebonnois et al. 2010). In this GCM, the cloud description is simplified. As clouds play a crucial role in radiative transfer, dynamics and generally the climate of Venus, it is necessary to improve the VGCM with a microphysical representation.

1. Introduction

Venus is a terrestrial planet enshrouded by a 20 km-thick layer of clouds. The clouds are thin, like cirrus on Earth but they are stratified and create a large opacity. The cloud layers are surrounded by haze above and below. Moreover, this cloud system is divided by properties of particle size distribution into three layers: the upper cloud deck (57 to 68 km), the middle cloud deck (51 to 57 km) and the lower cloud deck (48 to 51 km) [1]. The droplets that constitute the clouds are composed of a H_2SO_4-H_2O solution. The crystalline phase of the cloud particles is still debated [1,2]. There is only one complete in-situ profile on cloud droplet properties measured by Pioneer Venus during its descent [1].

The upper cloud deck and the upper haze were studied by several missions, for example recently by Venus Express [3]. The droplet size distribution is divided in several size modes. The mode 1 (mean radius $r_m \approx 0.2\mu m$) is the smallest but has the largest number concentrations. Modes 2 ($r_m \approx 1.0\mu m$) and 3 ($r_m \approx 3.5\mu m$) hold most of the condensed mass [1]. The division in modes 2 and 3 of the largest particles and the existence of mode 0 and 2' are still debated [1,4,5]. The cloud top and base altitude change with latitude, and the particle size has a latitudinal dependence [4,6].

In addition, an unknown UV absorber is present in the cloud layers and may be related to clouds. At last, the clouds affect the radiative balance, the sulfur chemical cycle, the dynamics and the atmospheric structure of Venus.

2. Modelling

In order to understand the observations and the atmospheric processes on Venus, it is crucial to develop a climate model like the IPSL Venus GCM.

2.1 The IPSL Venus GCM

The Venus Global Climate Model has been developed at the LMD [7]. The characteristics of this model include radiative transfer, dynamics, atmospheric chemistry, diurnal cycle and a full topography defined by Magellan mission's data. With this full GCM, the Venusian atmosphere is simulated between 0 and 150 km. However, the description of the cloud layers is simplified. [7] have pointed out some problems with the prediction of the temperature profile. These problems may be due to the too simple representation of clouds. Thus, to achieve better simulations of the Venus climate, the GCM needs a microphysical model.

2.2 MAD-VenLA and the moments

To this end, we develop a microphysical bi-modal model based on Modal Aerosol Dynamics of Venus Liquid Aerosol cloud model (MAD-VenLA). This model uses an implicit moment scheme to describe the particle size distribution and the microphysical processes in 0D. The moment method is a statistical method to describe a distribution function with few parameters called moments. Each moment is associated with meaningful parameters of the aerosol size distribution. In our case the particle size distribution is described by its first moments: total particle number (zeroth moment) and total particle volume (third moment) of the size distribution [8]. Moreover, with this representation, the form of the size distribution is assumed to be a log-normal function. MAD-VenLA takes into account condensation/evaporation, nucleation and coagulation. To represent a source of aerosol particles and the sedimentation of our cloud droplets, we have developed a 1D extension to our model. MAD-VenLA is coupled with the 1D version of the IPSL Venus GCM and by extension can also be used within the 3D version of the GCM.

3. Results

The preliminary results of MAD-VenLA in 1D show a good agreement with observations [3] in the calculation of the droplets' weight percent of sulfuric acid (**Figure 1**).

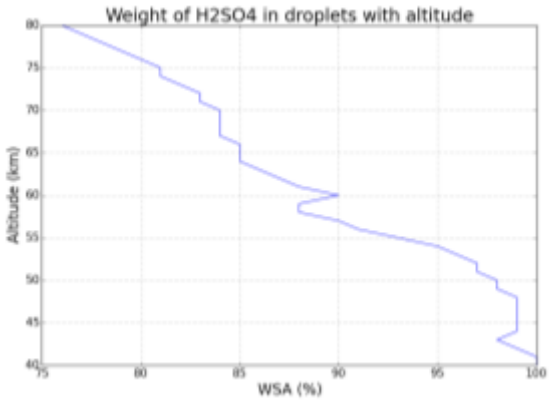

Figure 1. *The Weight percent of sulfuric acid in droplets at different altitudes, at low latitudes (0-30°). The results between 62 and 72 km are more or less 82% like [3].*

We are currently studying the 1D results of IPSL Venus GCM coupled with MAD-VenLA.

First, we will describe MAD-VenLA and the assumptions that we made in the development of this model. Then, we will compare the 1D results with CARMA, a sectional model of Venus [9], and the Pioneer Venus LCPS observations [1]. At last, we will present you the firsts results of the IPSL Venus GCM with a microphysical model.

4. Summary and Conclusions

The development of this model will allow us to have a better understanding of Venusian climate with a complete global climate model. The moment method is already used in the IPSL Mars GCM [11] and the IPSL Titan GCM [12] to describe the cloud microphysics.

Acknowledgements

This work has been supported by the French Planetology program (Programme National de Planétologie, ATMARVEN project)

References

[1] Knollenberg, R. G. and Hunten, D. M. The microphysics of the clouds of Venus - Results of the Pioneer Venus particle size spectrometer experiment. Journal of Geophysical Research, 85:8039 8058, December 1980.

[2] Ohtake, T. Freezing points of h2so4 aqueous solutions and formation of stratospheric ice clouds. Tellus, 45:138 144, April 1993.

[3] Cottini, V., Ignatiev, N., Piccioni, G., Drossart, P., Grassi, D. and Markiewicz, W. Water vapor near the cloud tops of Venus from Venus Express/VIRTIS dayside data. Icarus, 217(2), pp. 561-569, 2012.

[4] Wilson, C. F., Guerlet, S., Irwin, P. G. J., Tsang, C. C. C., Taylor, F. W., Carlson, R. W., Drossart, P., and Piccioni, G. Evidence for anomalous cloud particles at the poles of Venus. Journal of Geophysical Research, 113, 2008.

[5] Toon, O. B., Ragent, B., Colburn, D., Blamont, J. and Cot, C. Large, solid particles in the clouds of Venus: Do they exist? Icarus, 57:143 160, 1984.

[6] Lee, Y. J., Titov, D. V., Tellmann, S., Piccialli, A., Ignatiev, N. I., Patzold, M., Hausler, B., Piccioni, G. and Drossart, P. Vertical structure of the Venus cloud top from the vera and virtis observations onboard Venus Express. Icarus, 217:599 609, 2012.

[7] Lebonnois, S., Sugimoto, N., Gilli, G. Wave analysis in the atmosphere of Venus below 100-km altitude, simulated by the LMD Venus GCM. Icarus 278, pp. 38-51, 2016.

[8] Seigneur, C. et al. Simulation of Aerosol Dynamics: A Comparative Review of Mathematical Models. Aerosol Science and Technology, 5:2, pp. 205-222, 1986.

[9] McGouldrick, K., Toon, O. B., 2007. An investigation of possible causes of the holes in the condensational Venus cloud using a microphysical cloud model with radiative-dynamical feedback. Icarus, Vol. 191, pp. 1-24.

[10] Pruppacher, H. R. and Klett, J. D. Microphysics of Clouds and Precipitation - Second Edition, volume 18, chapter 7, 9, 11, 12, 13, 14, 15. Springer, 2010.

[11] Montmessin, F., Rannou, P. and Cabane, M. New insights into Martian dust distribution and water-ice cloud microphysics. Journal of Geophysical Research, 107, E6, 10.1029/2001JE001520, 2002.

[12] Burgalat, J., Rannou P., Cours T., Rivière, E. Modeling cloud microphysics using a two-moments hybrid bulk/bin scheme for use in Titan climate models: Application to the annual and diurnal cycles. Icarus [serial online]. March 1, 2014;231:310-322. Available from: ScienceDirect, Ipswich, MA. Accessed April 28, 2015.

EPSC Abstracts
Vol. 11, EPSC2017-586-2, 2017
European Planetary Science Congress 2017

Photometry of Venus upper clouds by Venus Monitoring Camera (VEx): spatial and temporal distributions of the retrieved aerosol parameters

O. S. Shalygina[1], E. V. Petrova[2], and W. J. Markiewicz[1]
[1]Max-Planck-Institut für Sonnensystemforschung, Göttingen, Germany (o.s.shalygina@gmail.com), [2]Space Research Institute, Russian Academy of Sciences, Moscow, Russia

1 Introduction

During 2 006 – 2 014 the Venus Monitoring Camera (VMC) onboard Venus Express (VEx) was imaging the Venus clouds in four narrow spectral channels that shared one CCD: UV (0.365 µm), VIS (0.513 µm), NIR1 (0.965 µm), and NIR2 (1.010 µm) [1]. Around 350 000 wide-angle images of the planet were obtained covering almost all the latitudes, which allowed the knowledge on morphology and dynamics of the cloud deck of Venus to be substantially extended [2].

The first images of a full glory in unpolarized light on the upper cloud deck of Venus were obtained with VMC [3] (see fig. 1). Glory is an optical phenomenon observed near opposition that poses constraints on the properties of cloud particles: they have to be spherical, and their size distribution has to be rather narrow. Observations of glory are of key importance for the phase function analysis of the Venus upper clouds, composed of H_2SO_4 droplets: the angular positions of maximum and minimum are determined by the size of particles, and the brightness of the first peak depends on their refractive index (especially in NIR, see fig. 2) [3, 4].

In this report we summarise our retrievals from the all VMC dataset [3–7]. From fitting the phase profiles with models, we have obtained the optical properties of the Venusian clouds (*i.e.* effective radius $R_{\rm eff}$ and variance $\nu_{\rm eff}$ of particles' size distribution, refractive index m_r of aerosols, optical thickness of cloud layer τ and haze τ_h), and their spatial (in latitude) and temporal (in local time) variations.

2 VMC data and modelling

To estimate the properties of cloud particles, we modeled the phase dependence of brightness retrieved from the dayside images. We have analysed the whole set of the VMC data and separated them into two types: the data obtained in three channels (NIR1, UV ans VIS) in glory region, *i.e.* at small phase angles ($0° < \alpha < 60°$) [3–5, 7], and the data retrieved only in NIR1 channel at phase angle range $0° < \alpha < 140°$ for the local solar time (LST) interval of 6 – 18 h [6].

The model assumes plane-parallel atmosphere and consists of two layers: an optically thick cloud layer and a thin haze layer above it. For the main cloud layer two versions were considered: (1) only H_2SO_4 droplets of the 1-m mode are in the clouds, and (2) the clouds are composed of 1 micron H_2SO_4 droplets homogeneously mixed with small submicron particles of the same size as those in the above haze. This allowed us to distinguish the influence of the submicron mode, which is always present in the clouds, on the measured phase profile.

To find the intensity of light scattered by the cloud-haze system, the radiative-transfer code solving numerically the invariant embedding equation was used [8]. To calculate the single scattering phase functions of spherical particles in the clouds and the haze, the Mie theory was used, because the particles in Venus clouds are expected to be liquid (*i.e.*, spherical) and the smaller submicron particles presumably present in the haze and everywhere in the clouds are so small for the VMC wavelengths that can be also treated as spherical, even if they are solid. The total number of combinations in the values of varied parameters exceeded 1 500 [see 6]. The best fits were chosen

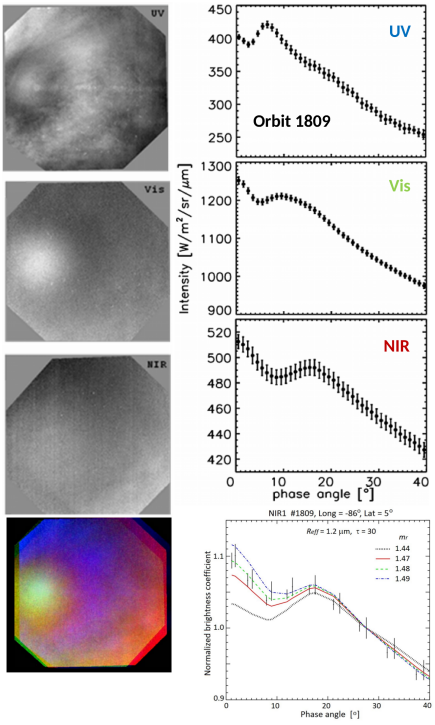

Figure 1: Venus glory as observed by VMC. Left: VMC images and a false-color composite of the glory. Right: the normalized measured values of NIR1 brightness (dots with error bars) as a function of α are compared to the cloud models [3].

automatically by the least square method.

3 Summary

Joint analysis of the whole VMC data set (the glory data obtained in three VMC channels and the full phase dependencies built for NIR1) yielded the maps of temporal (within a local day) and spatial variations in the retrieved parameters of the clouds, and allow us to conclude the following [3–7]:

- The decrease of the particle sizes at high latitudes down to 0.6 μm at 60°S is definitely seen.
- The cases with a relatively high real part of the refractive index (1.45 – 1.49 with sporadic spikes up to 1.52) are very often observed for the 1-micron cloud particles. An additional component (sulfur or ferric chloride) with a high refractive index should be present in the cloud droplets.
- Small submicron particles ($R_{\text{eff}} = 0.23\,\mu\text{m}$) are detected mostly in the morning within the clouds and/or in the haze above the clouds.
- No clear long-term variations of the retrieved parameters were found.

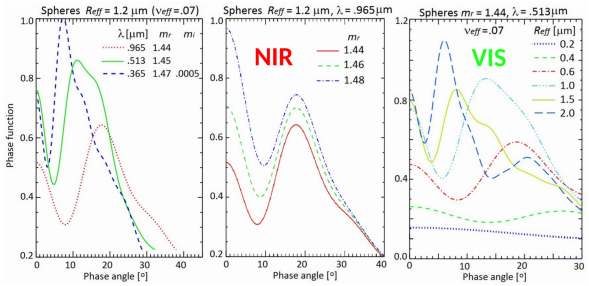

Figure 2: Examples of the single-scattering phase functions calculated for VMC wavelengths and different optical properties of particles.

References

[1] W. J. Markiewicz et al. In: *Planet. Space Sci.* 55.12 (2007), pp. 1701–1711. DOI: 10.1016/j.pss.2007.01.004.

[2] D. V. Titov et al. In: *Icarus* 217.2 (2012), pp. 682–701. DOI: 10.1016/j.icarus.2011.06.020.

[3] W. J. Markiewicz et al. In: *Icarus* 234 (2014), pp. 200–203. DOI: 10.1016/j.icarus.2014.01.030.

[4] E. Petrova, O. Shalygina, and W. J. Markiewicz. In: *Planet. Space Sci.* 113-114 (2015), pp. 120–134. DOI: 10.1016/j.pss.2014.11.013.

[5] E. Petrova, O. Shalygina, and W. J. Markiewicz. In: *Icarus* 260 (2015), pp. 190–204. DOI: 10.1016/j.icarus.2015.07.015.

[6] O. Shalygina et al. In: *Planet. Space Sci.* 113–114 (2015), pp. 135–158. DOI: 10.1016/j.pss.2014.11.012.

[7] W. J. Markiewicz, E. V. Petrova, and O. S. Shalygina. In: *Icarus* (2017). Under review.

[8] M. I. Mishchenko and L. D. Travis. In: *J. Geophys. Res. Atm.* 102.D14 (1997), pp. 16989–17013. DOI: 10.1029/96JD02425.

EPSC Abstracts
Vol. 11, EPSC2017-594, 2017
European Planetary Science Congress 2017

Experimental simulation of aerosols evolution in Titan's ionosphere

A. Chatain (1,2), N. Carrasco (1), O. Guaitella (2)
(1) LATMOS, Université Versailles St-Quentin, CNRS, 11 blvd d'Alembert, 78280 Guyancourt, France
(2) LPP, Ecole Polytechnique, CNRS, 91128 Palaiseau, France
(audrey.chatain@latmos.ipsl.fr)

Abstract

Many recent studies on Titan are concerned with aerosols. In particular, questions are asked on how these complex organic molecules are formed and evolve in Titan's atmosphere. Here for the first time we experimentally study how harsh plasma environment simulating Titan ionosphere can affect these aerosols. Titan tholins are placed in a N_2-H_2 plasma reactor and sample signatures are measured by infrared transmission spectroscopy. First results show an evolution of the absorption bands. Therefore, plasma conditions seem to change tholin chemical structure.

1. Introduction

Observations by Cassini have revealed the formation of complex organic molecules in Titan ionosphere [1]. To better understand this complex chemistry, several experiments were conducted to reproduce analogs of Titan aerosols in laboratories [2,3,4]. These tholins appeared to be polymeric and nitrogenous molecules, and the influence of different parameters on the aerosol formation process has been studied [5,6].

However, a new issue might be addressed. Indeed, aerosols stay many years in Titan upper atmosphere, a dusty plasma where molecules are continuously bombarded by charged molecules. Consequently, tholins are likely to evolve in such an environment. The aim of this study is therefore to address this question by experimental simulation: we will analyze the effect of harsh plasma environment on tholins already formed.

2. Experimental device

2.1 Sample synthesis

Aerosols samples used are first formed in the plasma reactor PAMPRE at LATMOS, under conditions described in [6].

2.2 Plasma reactor

Samples are positioned at the center of a plasma reactor at LPP, where they are exposed to plasma during several hours.

The plasma reactor chosen is a DC glow discharge ignited in a 2 cm inner diameter tube with 23-centimeter length [7]. A 5 sccm flow of N_2-H_2 gaz mixture with 1% of hydrogen goes through the cell, and the pressure can be adjusted from 0.5 to 3.0 torr. The current is kept constant at 20 mA for this work. The effect of pure N_2 gas is also studied. The plasma reactor is adapted to fit inside the sample compartment of the FTIR, allowing for direct in situ measurement through the tholins sample under direct plasma exposure.

2.3 Analysis with IR spectroscopy

The evolution of these samples exposed to N_2-H_2 plasma is observed by infrared absorption spectroscopy, using a FTIR (Bruker V70 with 0.16 cm^{-1} resolution). Tholins are prepared in shape of thin pellets and placed in the middle of the plasma reactor, and centered on the FTIR beam to perform measurements in transmission through the pellet. However, pure tholins being too absorbent in IR to obtain satisfactory spectra, we diluted samples with 98.5% of KBr, transparent in the IR range studied.

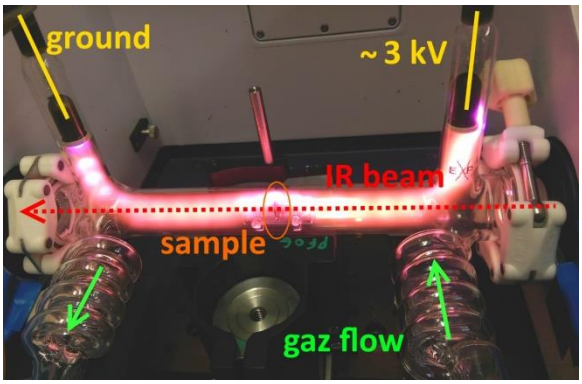

Figure 1: plasma reactor positioned in the FTIR

3. Results

We can observe changes on tholins even with naked eyes. Samples, at first brown, lighten and pellets become rough. Besides, IR spectra of tholin pellets are distorted after exposition to plasma.

3.1 Erosion of pellets

At first, we can note that pellets are eroded by plasma. Absorbance decreases to 40% of its initial value concerning the nitrile 2180 cm^{-1} band after an exposition of two hours at 1.9 torr. This value depends on various parameters, as pressure, exposition time or pellets concentration in tholins.

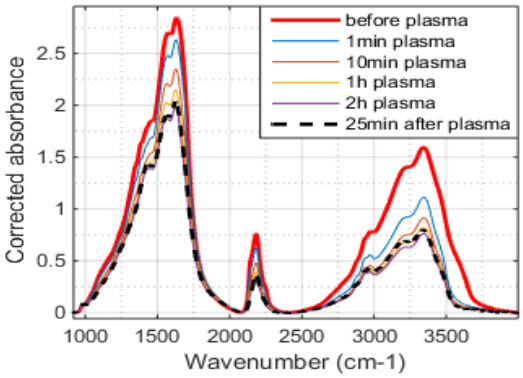

Figure 2: IR absorption spectra obtained by transmission through tholin pellets exposed to plasma at 1.9 torr during different times – with a corrected baseline

3.2 Chemical evolution

The normalization of individual peaks shows that IR absorption bands characteristic of tholins formed in PAMPRE are distorted during exposition to plasma. This witnesses changes in samples chemical structure.

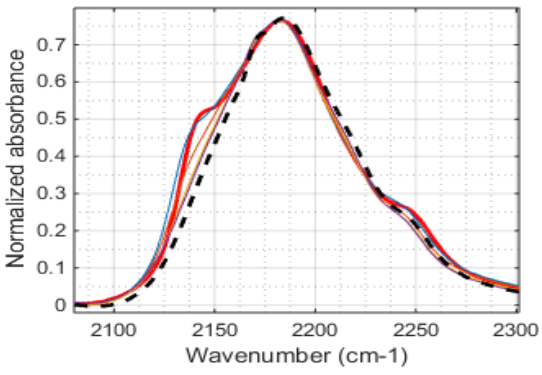

Figure 3: Same absorption spectra as in figure 2, normalized and zoomed on the nitrile band

4. Perspectives

These first results concerning evolution of Titan tholins exposed to N_2-H_2 plasma show that tholins seem sensitive to plasma conditions and structurally changed. An experimental compromise might be done in the choice of parameters to obtain notable structural modifications on tholins without totally eroding the pellets.

Besides, chemical analysis and study of surface state are the next steps to better characterize these changes.

Acknowledgements

AC is grateful to ENS Paris-Saclay for its training and financial support, and to David Yap for its explanations concerning the experimental setup.

NC acknowledges the financial support of the European Research Council (ERC Starting Grant PRIMCHEM, Grant agreement no. 636829).

References

[1] Waite, J. H., Young, D. T., Cravens, T. E., Coates, A. J., Crary, F. J., Magee, B., & Westlake, J. (2007). The process of tholin formation in Titan's upper atmosphere. *Science*, *316*(5826), 870-875.

[2] Imanaka, H., Khare, B. N., Elsila, J. E., Bakes, E. L., McKay, C. P., Cruikshank, D. P., ... & Zare, R. N. (2004). Laboratory experiments of Titan tholin formed in cold plasma at various pressures: implications for nitrogen-containing polycyclic aromatic compounds in Titan haze. *Icarus*, *168*(2), 344-366.

[3] Sebree, J. A., Trainer, M. G., Loeffler, M. J., & Anderson, C. M. (2014). Titan aerosol analog absorption features produced from aromatics in the far infrared. *Icarus*, *236*, 146-152..

[4] Sciamma-O'Brien, E., Ricketts, C. L., & Salama, F. (2014). The Titan Haze Simulation experiment on COSmIC: Probing Titan's atmospheric chemistry at low temperature. *Icarus*, *243*, 325-336.

[5] Gautier, T., Carrasco, N., Schmitz-Afonso, I., Touboul, D., Szopa, C., Buch, A., & Pernot, P. (2014). Nitrogen incorporation in Titan's tholins inferred by high resolution orbitrap mass spectrometry and gas chromatography–mass spectrometry. *Earth and Planetary Science Letters*, *404*, 33-42.

[6] Gautier, T., Schmitz-Afonso, I., Touboul, D., Szopa, C., Buch, A., & Carrasco, N. (2016). Development of HPLC-Orbitrap method for identification of N-bearing molecules in complex organic material relevant to planetary environments. *Icarus*, *275*, 259-266.

[7] D. Marinov, C. Drag, C. Blondel, O. Guaitella, J. Golda, B. Klarenaar, R. Engeln, V. Schulz-von der Gathen, JP. Booth , Pressure broadening of atomic oxygen two-photon absorption laser induced fluorescence, 2016 *Plasma Sources Sci. Technol.* 25 06LT03

EPSC Abstracts
Vol. 11, EPSC2017-599-2, 2017
European Planetary Science Congress 2017

H_2O and CO_2 vapor pressure measurements at temperatures relevant to the middle atmosphere of Earth and Mars

M. Nachbar (1), D. Duft (2) and T. Leisner (1,2)

(1) Institute of Environmental Physics, University of Heidelberg, Heidelberg, Germany
(2) Institute of Meteorology and Climate Research, Karlsruhe Institute of Technology – KIT, Karlsruhe, Germany
(Mario.nachbar@kit.edu)

Abstract

Measurements of the vapor pressure of H_2O and CO_2 at temperatures relevant to the middle atmosphere of Earth and Mars are rare but important in order to describe cloud formation and ice particle growth processes. In this contribution we present a novel technique for measuring the vapor pressure of condensable gases by analyzing the depositional growth rates on free nanoparticles at high supersaturation. The method is applied to measure the vapor pressure of CO_2 between 75K and 85K. By comparison with previous measurements and parameterizations we are able to show the excellent functionality of the method. In addition, the method is used to measure the vapor pressure over H_2O ice between 135K and 160K. We show that the vapor pressure of so called stacking disordered ice I_{sd} deposited at temperatures below 160K is significantly higher compared to hexagonal ice I_h. The consequences for ice cloud formation in the atmosphere of Earth and Mars will be discussed.

1. Introduction

Measurements of the vapor pressure of H_2O and CO_2 at temperatures relevant to the middle atmosphere of Earth and Mars are rare but important in order to predict conditions for H_2O and CO_2 cloud formation and ice particle growth processes. Whereas CO_2 is known to have one phase down to a temperature of about 50K [5], water ice can in addition to the well characterized and stable hexagonal ice I_h freeze in different metastable forms. At temperatures relevant to the middle atmosphere of Earth and Mars, water has been identified to form so called stacking disordered ice I_{sd} [e.g. 7], and below about 120K amorphous ice I_a [e.g. 4]. The vapor pressure of I_a has been determined to be about 3 times larger as compared to I_{sd} [e.g. 10]. Due to heat capacity measurements [e.g. 11] and direct pressure measurements between 180K and 190K [9], the vapor pressure of I_{sd} is believed to be about 10% to 15% higher as compared to I_h [8]. However, high quality vapor pressure measurements of I_{sd} at temperatures below 160K do not exist and are eminent in order to proof the expected difference in the vapor pressures of I_{sd} and I_h.

Recently, we introduced a novel experimental setup [2, 6] specifically designed for the investigation of adsorption, nucleation and subsequent depositional growth of H_2O and CO_2 on nanoparticles at temperatures relevant to the middle atmosphere of Earth and Mars. Analyzing the CO_2 and H_2O ice growth rate of the particles at high saturation (S>1000) allows us to determine the vapor pressure at the investigated temperatures.

2. Experimental Method

Singly charged nanometer size iron oxide and silica particles are produced in a microwave plasma particle source and directly transferred into the TRAPS vacuum system [6]. The particles are size selected and accumulated in the novel supersaturation chamber and ion trap MICE [2]. In MICE, the particles are exposed to realistic mesospheric conditions in terms of background pressure and temperature as well as CO_2 and H_2O vapor concentrations. The vapor pressures of CO_2 and H_2O are adjusted by controlling the temperature and therefore the sublimation speed of molecules from CO_2 or H_2O covered surfaces. From MICE we extract a small amount of the trapped particle population at periodic time steps and analyze their mass distribution with a time-of-flight mass spectrometer. By observing CO_2 and H_2O growth rates on the nanoparticles at high S values (S>1000) we are able to infer the sublimation rate and therefore

the vapor pressure of CO_2 and H_2O at the controlled surface temperature.

3. Results and Discussion

Figure 1 shows an exemplary measurement of H_2O deposition on a 2.5nm silica particle. The particle temperature has been kept to 129.7K. The surfaces supplying the flow of water molecules have been set to 156.7K.

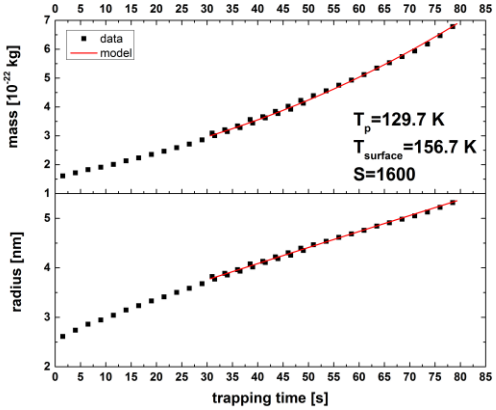

Figure 1: Exemplary measurement of H_2O ice growth on a 2.5nm silica particle at a Saturation of 1600

The H_2O ice growth rate of the nanoparticles can be expressed by the simple equation:

$$\frac{dm}{dt} = [\alpha \cdot j_{in} - j_{out}(t)] \cdot A_c(t) \cdot m_{H_2O} \qquad (1)$$

Here, m_{H_2O} is the mass of one water molecule and $A_c(t)$ is the effective surface area which describes the collision between the particle and a water molecule. The sticking coefficient α has been determined to 1 for CO_2 [3] as well as H_2O [1] at investigated particle temperatures. The outgoing flow j_{out} can be calculated according to the Kelvin effect. However, at S values above 1000, uncertainties in calculating j_{out} become less significant. The red curve in Figure 1 represents a numerical fit of j_{in} in Eq. 1. By knowing the geometry of MICE [2], j_{in} can be used to calculate the vapor pressure at the temperature of the surfaces providing the water molecule flow.

We will present results of the vapor pressure measurements for CO_2 between 75K and 85K. These measurements are compared to existing measurements and CO_2 vapor pressure parameterizations at these temperatures. We conclude that analyzing growth rates on nanoparticles in MICE at high S values is a very sensitive technique to measure the vapor pressure if the sticking coefficient is known. In addition we show determined vapor pressures of I_{sd} between 135K and 160K and conclude that the vapor pressure of I_{sd} might be significantly increased in respect to I_h and discuss its consequences to water ice cloud formation in the atmosphere of Earth and Mars.

Acknowledgements

The authors thank the German Federal Ministry of Education and Research (BMBF, grant number 05K13VH3) and the German Research Foundation (DFG, grant number LE 834/4-1) for financial support of this work.

References

[1] Brown, D.E., George, S. M., Huang, C., et. al.: H2O Condensation Coefficient and Refractive Index for Vapor-Deposited Ice from Molecular beam and Optical Interference Measurements, J. Phys. Chem., Vol. 100, pp. 4988-4995, 1996.

[2] Duft, D., Nachbar, M., Eritt, M. et. al.: A linear ion trap for studying the interaction of nanoparticles with supersaturated vapors. Aerosol. Sci. technol., 2015

[3] Heald, J. H., Brown, Jr. and R.F.: Measurements of condensation and evaporation of carbon dioxide, nitrogen, and argon at gryogenic temperatures using a molecular beam, Report of Aerospace Environmental Facility, 1968

[4] La Spisa, S., Waldheim, M., Lintemoot, J., et. al.: Infrared and vapor flux studies of vapor-deposited amorphous and crystalline water ice films […], Journal of Geophys. Research, Vol. 106(E12), pp. 33,351-33,361, 2001.

[5] Luna, R., Millan, C, Santonja, M.A., et. al.: Triple test under high vacuum conditions to control the reliability of thin ice film accretion and desorption for astrophysical applications, Vacuum, Vol. 83, pp. 942-948, 2009.

[6] Meinen, J., Khasmiskaya, S., Rühl, E., et. al..: The TRAPS Apparatus: Enhancing Target Density of Nanoparticle Beams in Vacuum for X-ray and Optical Spectroscopy, Aerosol. Sci. Technol., Vol. 44(4), pp. 316-328, 2010.

[7] Murray, B. J., Malkin, T.L., Salzmann, C.G.: The crystal structure of ice under mesospheric conditions, Journal of Atmospheric and Solar-Terrestrial Physics, Vol. 127, pp. 78-82, 2015.

[8] Murphy, D. M., Koop, T.: Review of the vapor pressures of ice and supercooled water for atmospheric applications, Q. J. R. Meteorol. Soc., Vol. 131, pp. 1539-1565, 2005.

[9] Shilling, J. E., Tolbert, M. A., Toon, O. B. et. al.: Measurements of the vapor pressure of cubic ice and their implications for atmospheric ice clouds, Geophysical Research Letters, Vol. 33, L17801, 2006.

[10] Speedy, R. J., Debenedetti, P. G., Smith, R. S. et. al.: The evaporation rate, free, energy, and entropy of amorphous water at 150K, J. Chem. Phys., Vol. 105, pp. 240-244, 1996.

[11] Sugisaki, M., Suga, H., Seki, S.: Calorimetric Study of the Glassy State. IV. Heat Capacities of Glassy Water and Cubic Ice, Bulletin of the Chemical Society of Japan, Vol. 41, pp. 2591-2599, 1968.

EPSC Abstracts
Vol. 11, EPSC2017-600-1, 2017
European Planetary Science Congress 2017

Formation of mesospheric clouds on Mars: new model results based on updated parameters

C. Listowski, **A. Määttänen**, J. Audouard and F. Montmessin
(1) LATMOS/IPSL, UVSQ Université Paris-Saclay, UPMC Univ. Paris 06, CNRS, Guyancourt, France
(constantino.listowski@latmos.ipsl.fr, anni.maattanen@latmos.ipsl.fr)

Abstract

Mesospheric clouds have been observed on Mars for about 15 years. Microphysical modeling studies have provided evidence that an exogenous Ice Nucleus (IN) source is needed to form these clouds. These IN are probably Meteor Smoke Particles (MSPs) as in the Earth's mesosphere. Recent studies have provided new information on the properties of the MSPs and of CO_2 ice: we are presenting here updated results using these new parameters.

1. Introduction

Martian mesospheric CO_2 clouds were detected and imaged in 2007 by [1], after first hints of their actual existence from infrared spectroscopy [2]. Several observational datasets on mesospheric clouds have been accumulated over the years (with and without composition retrieval) [3-9] and a long climatology can be established. Global Climate Modeling has shown that the mesospheric clouds form in the temperature minima of migrating and non-migrating tides, but they are not sufficient to cool the atmosphere below the condensation temperature of CO_2 [10]. It was shown [11] that mesospheric cloud observations correlate with the privileged zones of gravity wave propagation to the mesosphere, giving strong evidence of a link between the two phenomena. Subsequent microphysical modeling [12-13] in one dimension showed that using temperature profiles accounting for the effects of thermal tides and gravity waves resulted in observed-like clouds, if the profiles were cooled by some degrees and if a mesospheric IN source was added in the simulation.

1.1 The microphysical model

The microphysical model is based on the work by [14] and was adapted to Martian CO_2 ice clouds by [12-13]. This sectional cloud model describes the processes of cloud crystal formation by heterogeneous (deposition mode) nucleation onto IN, their condensational growth or evaporation, and sedimentation and vertical mixing by eddy diffusion.

1.2 New parameters

Recently published experimental results [15] show that the contact parameter (m) of CO_2 ice that was previously used in the models is too favorable for nucleation of CO_2 ice on dust. The previously measured value for this parameter (m=0.952) came from [16], who studied CO_2 ice nucleation on a flat water ice substrate. When [15] used nanometer-size MSP and Mars dust analogs as IN in their nucleation experiment, they found a much lower value of m=0.78. They also measured a new value for the desorption energy of CO_2 on the IN. In another study [17] the CO_2 ice density was measured at low temperatures showing a clear dependence on temperature. In this work, we are applying the updated values of the aforementioned parameters in our microphysical model [13] to quantify their effect on cloud formation.

2. Results

The new contact parameter has a large influence on the supersaturation necessary to activate the IN. Figure 1 shows the nucleation probability (giving the fraction of the activated IN) for CO_2 ice as a function of saturation ratio and the corresponding temperature deviation below the condensation temperature. The results are shown for four IN radii at the conditions prevailing around 75 km (atmospheric pressure 0.01 Pa). It is clearly seen that the new contact parameter [15] has a profound effect on nucleation: for all studied particle sizes, the saturation ratios required to activate the IN increase by one order of magnitude compared to the contact parameter of [16].

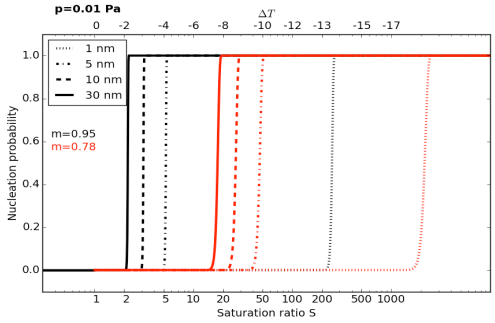

Figure 1: Nucleation probability for four IN radii as a function of the saturation ratio and the corresponding deviation below the condensation temperature. The atmospheric pressure is 0.01 Pa (as around 75 km). The black lines show the results for contact parameter m=0.95 and the red lines for m=0.78.

Figure 2 shows the required temperature deviation below saturation as a function of the IN radius, and includes also the two other parameters, CO_2 ice density and desorption energy of CO_2. For IN of 10 nm radius, the temperatures need to be decreased by 6 K to activate them compared to the old value of m. It can be seen that the other parameters have a minor role on the activation temperature deviation.

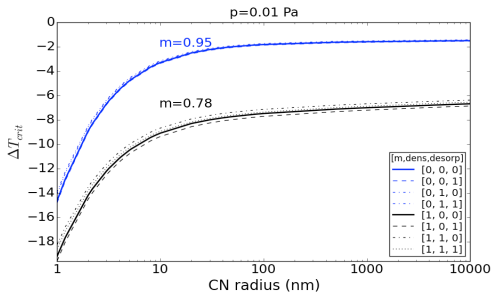

Figure 2: The temperature deviation below saturation required for IN activation as a function of the IN radius. The atmospheric pressure is 0.01 Pa (75 km). The blue lines show the results for contact parameter m=0.95 and the black lines for m=0.78. The legend shows the variation of the different parameters: 0=old value, 1=new value.

We have also looked at the 1D results for the clouds. We chose a good simulation of a daytime cloud from [13] and rerun it with the new parameters. The IN profile of the simulation includes the climatological dust profile and a MSP source in the mesosphere. Figure 3 shows the results of the simulation with the old contact parameter and two simulations with the new one.

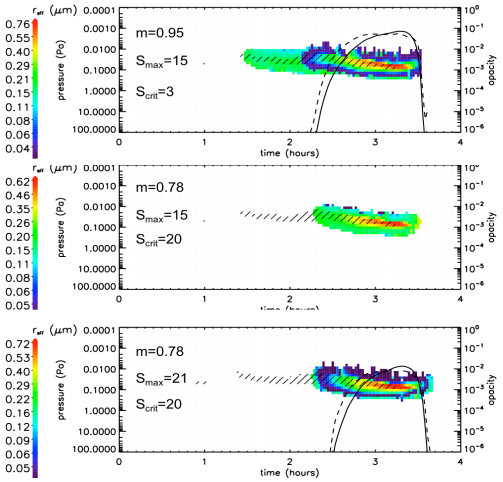

Figure 3: Effective radius (color) and opacity (lines: solid at 1 μm, dashed at 500 nm) of the cloud as a function of pressure and time from the start of the simulation. The IN are injected at the supersaturated region (dashed) and are of 10 nm radius. Upper panel: m=0.95; middle and lower panel: m=0.78. S_{crit} indicates the saturation ratio required for activation of the IN, and S_{max} the maximum supersaturation reached during the simulation.

The upper panel reproduces the results of [13] and shows the formation of a cloud within the supersaturated pocket for a critical saturation ratio of three (S_{crit}=3) with the old value of m. The middle panel shows that for the same saturation conditions (S_{max}=15) the formed cloud is much thinner (opacity<10^{-6}). This indicates that the small IN are actually not activated, since the reached saturation ratios (Smax=15) are only enough to activate the larger particles of the dust lifted from the surface, which is present in very small concentrations (as constrained by the Mars Climate Database [18]). The small number concentration of the activated IN leads to the very small opacity. The lower panel shows that a realistic cloud can be simulated if the cooling is increased (S_{max}=21) so that the new critical saturation ratio (S_{crit}=20) can be reached: in this case, the MSP particles can also be activated as IN (at S_{crit}=20) and the observed cloud opacities are attained.

3. Summary and Conclusions

In the light of new measurements on CO_2 ice properties, modeling results show that the martian mesospheric CO_2 ice clouds are very difficult to form, requiring very high saturation ratios (and thus very low temperatures). The critical saturation ratios increase by an order of magnitude when using the new contact parameter to activate the available IN and to form clouds with observed properties. The first results suggest that the clouds would strongly rely on the maximum saturation ratio reached within the cold pocket, leading to threshold effects making those clouds even more difficult to form. We are currently implementing the microphysics into the LMD GCM [19-20].

Acknowledgements

This work has been supported by the French Planetology program (Programme National de Planétologie, ATMARVEN project). CL thanks CNES for postdoctoral fellowship funding. JA thanks the Labex ESEP for funding.

References

[1] Montmessin F., Gondet B., Bibring J.-P., Langevin Y., Drossart P., Forget F., and Fouchet T. (2007) Hyper-spectral imaging of convective CO2 ice clouds in the equatorial mesosphere of Mars. J. Geophys. Res., 112.

[2] Formisano V., Maturilli A., Giuranna M., D'Aversa E., and López-Valverde M. A. (2006) Observations of non-LTE emission at 4–5 microns with the Planetary Fourier Spectrometer aboard the Mars Express mission. Icarus, 182, 51–67.

[3] Clancy R. T., Wolff M. J., Whitney B. A., Cantor B. A., and Smith M. D. (2007) Mars equatorial mesospheric clouds: Global occurrence and physical properties from Mars Global Surveyor Thermal Emission Spectrometer and Mars Orbiter Camera limb observations. J. Geophys. Res., 112, E04004.

[4] Inada A., Richardson M. I., McConnochie T. H., Strausberg M. J., Wang H., and Bell J. F. III (2007) High-resolution atmospheric observations by the Mars Odyssey Thermal Emission Imaging System. Icarus, 192, 378–395.

[5] Määttänen A., Montmessin F., Gondet B., Scholten F., Hoffmann H., González-Galindo F., Spiga A., Forget F., Hauber E., Neukum G., Bibring J.-P., and Bertaux J.-L. (2010) Mapping the mesospheric CO2 clouds on Mars: MEx/OMEGA and MEx/HRSC observations and challenges for atmospheric models. Icarus, 209, 452–469.

[6] Scholten F., Hoffmann H., Määttänen A., Montmessin F., Gondet B., and Hauber E. (2010) Concatenation of HRSC colour and OMEGA data for the determination and 3D parameterization of high-altitude CO2 clouds in the martian atmosphere. Planet. Space Sci., 58, 1207–1214.

[7] McConnochie T. H., Bell J. F., Savransky D., Wolff M. J., Toigo A. D., Wang H., Richardson M. I., and Christensen P. R. (2010) THEMIS-VIS observations of clouds in the martian mesosphere: Altitudes, wind speeds, and decameter-scale morphology. Icarus, 210, 545–565.

[8] Vincendon M., Pilorget C., Gondet B., Murchie S., and Bibring J.-P. (2011) New near-IR observations of mesospheric CO2 and H2O clouds on Mars. J. Geophys. Res., 116, E00J02.

[9] Sefton-Nash E., Teanby N. A., Montabone L., Irwin P. G. J., Hurley J., and Calcutt S. B. (2013) Climatology and first order composition estimates of mesospheric clouds from Mars Climate Sounder limb spectra. Icarus, 222, 342–356.

[10] González-Galindo F., Määttänen A., Forget F., and Spiga A. (2011) The martian mesosphere as revealed by CO2 cloud observations and general circulation modeling. Icarus, 216, 10–22.

[11] Spiga A., González-Galindo F., López-Valverde M.-A., and Forget F. (2012) Gravity waves, cold pockets and CO2 clouds in the martian mesosphere. Geophys. Res. Lett., 39, L02201.

[12] C. Listowski, A. Määttänen, I. Riipinen, F. Montmessin, F. Lefèvre: Near-pure vapor condensation in the martian atmosphere: CO2 ice crystal growth. J. Geophys. Res. Planets, 118, 2153-2171.

[13] C. Listowski, A. Määttänen, F. Montmessin, A. Spiga, F. Lefèvre, Modeling the microphysics of CO2 ice clouds within wave-induced cold pockets in the Martian mesosphere, Icarus 237, 239-261, 2014.

[14] Montmessin, F., Rannou, P., Cabane, M., 2002. New insights into martian dust disctribution and water-ice cloud microphysics. J. Geophys. Res. 107 (E6), 5037.

[15] Nachbar, M., D. Duft, T. P. Mangan, J. C. G. Martin, J. M. C. Plane, and T. Leisner (2016), Laboratory measurements of heterogeneous CO2 ice nucleation on nanoparticles under conditions relevant to the Martian mesosphere, J. Geophys. Res. Planets, 121, 753–769.

[16] Glandorf, D.L., Colaprete, A., Tolbert, M.A., Toon, O.B., 2002. CO2 snow on Mars and early Earth: Experimental constraints. Icarus 160, 66–72.

[17] T.P. Mangan, C.G. Salzmann, J.M.C. Plane, B.J. Murray, CO2 ice structure and density under Martian atmospheric conditions, Icarus, in press, 2017.

[18] Millour, E. et al., 2008. The latest (version 4.3) Mars Climate Database. LPI Contrib. 1447, 9029–+.

[19] Audouard, J., Määttänen, A., Listowski, C., Millour, E., Forget, F., Spiga, A., 2016: Modeling CO 2 ice clouds with a Mars Global Climate Model. American Astronomical Society, DPS meeting #48, id.220.21.

[20] Audouard, J., Määttänen, A., Listowski, C., Forget, F., Spiga, A., Millour, E., 2017: A Complete CO2 Ice Clouds Model for GCMs and Mesoscale Models. The Sixth International Workshop on the Mars Atmosphere: Modelling and observation, January 17-20 2017, Granada, Spain, p.4106.

EPSC Abstracts
Vol. 11, EPSC2017-621, 2017
European Planetary Science Congress 2017

Stratospheric benzene and hydrocarbon aerosols observed in Saturn's upper atmosphere

S. Guerlet (1), T. Koskinen (2)
(1) Laboratoire de Météorologie Dynamique, Sorbonne Universités, UPMC Univ Paris 06, CNRS, Paris, France (2) LPL, Tucson, Arizona, USA (sandrine.guerlet@lmd.jussieu.fr).

Abstract

Saturn's polar upper atmosphere undergoes significant auroral activity, which could impact Saturn's stratospheric chemistry and in return its radiative budget. Photochemical models including ion chemistry developed for Jupiter predict that benzene is enhanced in the auroral regions due to the precipitation of high-energy electrons and is a precursor for the formation of heavier ring polycyclic aromatic hydrocarbons. Here we review recent observations of benzene in Saturn's middle and upper atmosphere by Cassini/CIRS and Cassini/UVIS that advocate for a strong influence of solar-driven and auroral-driven ion chemistry on Saturn as well. Hydrocarbon aerosols are detected in Saturn's auroral regions by both instruments, supporting a similar aerosol formation scenario than in Jupiter's stratosphere. We then evaluate their radiative impact on Saturn's stratospheric temperatures.

1. Introduction

Saturn's polar regions are characterized by permanent dark polar caps in the ultraviolet, whose latitudinal extent coincides with that of auroral emissions [3]. These dark regions are generally attributed to the presence of polar stratospheric hazes [13, 7], possibly produced by the precipitation of energetic auroral electrons [11]. In the case of Jupiter's polar atmosphere, benzene (C_6H_6) has been proposed as a precursor to the formation of more complex hydrocarbons, such as polyacetylenes and multi-ring compounds, which could condense to form polar aerosols [2, 14]. This formation scenario, in which ion chemistry plays a key role, could also apply to Saturn, but such model has not been applied to Saturn yet. In addition, until recently, only the disk-average benzene column density had been measured from ISO [1]. Such measurements could not shed light on the influence of ion chemistry or aerosol formation in Saturn's atmosphere.

Here we review two recent observational studies that support the importance of ion chemistry in producing benzene and aerosols in Saturn's atmosphere. We then study the radiative impact of stratospheric aerosols on the temperature profile and will present comparisons with seasonal temperature changes observed by Cassini.

2. Benzene observations

The benzene emission band at 673 cm^{-1} has been detected in two sets of spectra acquired by the Composite Infrared Spectrometer (CIRS) in limb viewing geometry: at 80S in 2007 (mid-summer) and at 77N in 2015 (late spring). These measurements probes the neutral, middle stratosphere (3–0.01 mbar). Using a radiative transfer model coupled to an inversion algorithm, its partial column abundance has been retrieved. Upper limits on its column abundance have been derived from other CIRS limb spectra acquired at 40N, 35S and the equator. The partial column of C_6H_6 derived at 80S, of $4.1 \pm 1 \times 10^{13}$ cm^{-1}, is of the same order of magnitude that the upper limits derived at mid and low latitudes [5]. However, photochemical (neutral) models predict 50 times less benzene at 80S than at the equator [10]. Furthermore, at 77N in 2015, we find that the benzene mixing ratio profile must increase with altitude up to at least the 0.01 mbar pressure level to match the radiances measured by CIRS at different tangent altitudes [6], which is also at odds with the neutral photochemical model prediction of a peak abundance at ∼0.5 mbar.

In parallel, absorption by benzene has been detected in 18 Cassini/UVIS stellar occultations, including three pronounced absorptions at latitudes of 48.9S in April 2005, 74.3N in September 2012, and 72.7S in January 2015 [9]. UVIS data uniquely probe the photochemical production region at the 1 μbar pressure level. Hydrocarbon number densities are retrieved as a function of radial distance from Saturn's center and are then converted to volume mixing ratios as a function of pressure. The resulting peak mixing ratios of ben-

zene at 0.1–10 μbar range from about 2×10^{-8} (72.7S) to 5×10^{-7} (74.3N), which is much larger than predictions based on solar UV-driven neutral photochemistry that produces a peak benzene mixing ratio of 2×10^{-10} at 0.4 mbar [10]. The detection of benzene at lower latitudes and near the equator could be explained by solar-driven ion chemistry, with enhanced production from the aurora at high latitudes.

Altogether, these two studies advocate for the inclusion of both solar-driven ion chemistry and auroral-driven ion chemistry in current Saturn photochemical models to explain the observed benzene abundances.

3. Aerosol observations

Three Cassini/CIRS limb spectra, acquired at 80S in 2007, 77S and 77N in 2015 also exhibited residual signatures that were attributed to aerosol signatures. We retrieved their opacity profiles in the range 3–0.1 mbar in distinct spectral bands centered at 700, 750, 780, 1390 and 1450 cm^{-1} [5]. Interestingly, similar spectral features are also observed in Titan's stratosphere [12] which have been assigned to vibration modes of aliphatic and aromatic hydrocarbons. We find that the aerosol scale height is about twice the pressure scale height, which suggests that these aerosols are produced at high altitudes and sediment in the lower stratosphere, where they accumulate. We also estimate the aerosol mass loading in Saturn's polar stratosphere, which is found to be one order of magnitude lower than on Jupiter, consistent with their respective auroral intensities.

Absorption by haze is also detected in one UVIS occultation, at 72.7S in January 2015 [9]. This absorption feature in the 180–190 nm wavelength window is also similar to extinction by haze on Titan [8]. This unique detection occurs during the polar night where the mesospheric temperatures are low (125K, as derived from CIRS limb measurements) and favor the condensation of benzene and hydrocarbon aerosols.

In summary, haze signatures are detected at high latitudes both in CIRS and UVIS datasets. This supports the link between the precipitation of energetic electrons and the production of benzene and aerosols, as suggested by previous Voyager and HST observations and by photochemical models including ion chemistry developed for Jupiter.

4. Radiative impact

We evaluate the radiative impact of this polar haze on the thermal structure using a seasonal radiative-convective model of Saturn's atmosphere [4]. We assume that aerosols are spherical aggregates with a radius of 0.1 μm and use Mie scattering theory to compute their extinction coefficient. We find that the polar haze induces a net stratospheric heating during summer reaching +6 K at the 10-mbar pressure level, and a net stratospheric cooling during winter reaching -5 K at and above the 0.1-mbar pressure level [5]. We will discuss the possibility that Saturn's warm polar hood observed in the middle stratosphere during summer could be partly due to radiative heating by aerosols.

Acknowledgements

SG is supported by the CNES. This work is based on observations with the UVIS and CIRS instruments onboard Cassini.

References

[1] Bézard, B. et al., Icarus Vol. 154, p. 492-500, 2001.

[2] Friedson, A.J. et al., Icarus Vol. 158, p. 389-400, 2002.

[3] Gerard, J.C. et al., Geophys. Res. Let. Vol. 22, p. 2685-2688, 1995.

[4] Guerlet, S. et al., Icarus Vol. 238, p. 110-124, 2014.

[5] Guerlet, S. et al., Astron. & Astrophys. Vol. 580, 2015.

[6] Guerlet, S. et al., *47th DPS meeting*, 2015.

[7] Karkoschka, E. & Tomasko, M. G., Icarus Vol. 106, p. 428, 1993.

[8] Koskinen, T. et al., Icarus Vol. 216, p. 507-534, 2011.

[9] Koskinen, T. et al., Geophys. Res. Let. Vol. 43, p. 7895-7901, 2016.

[10] Moses, J. and Greathouse, T., J. Geophys. Res. Vol. 110, p. 9007, 2005.

[11] Pryor, W. R. & Hord, C. W., Icarus Vol. 91, p. 161-172, 1991.

[12] Vinatier, S. et al., Icarus Vol. 219, p. 5-12, 2012.

[13] West, R. A. et al., Advances in Space Research Vol. 3, p.45-48, 1983.

[14] Wong, A.-S., Yung, Y. L., & Friedson, A. J., Geophys. Res. Let. Vol. 30, p. 1447, 2003.

EPSC Abstracts
Vol. 11, EPSC2017-657, 2017
European Planetary Science Congress 2017

Photochemistry of HCN Ice on Tholins Simulated in Titan's Lower Atmosphere Conditions

D. Dubois (1,2), M. Gudipati (1), B. Henderson (1) N. Carrasco (2,3), B. Fleury (1) and I. Couturier-Tamburelli (4)
(1) Jet Propulsion Laboratory, California Institute of Technology, Pasadena, CA 91109, USA (2) LATMOS, Université de Versailles St-Quentin, Guyancourt, France (3) Institut Universitaire de France, Paris, France (4) Laboratoire Physique des interactions ioniques et moléculaires, Aix-Marseille Université, Marseille, France

Abstract

Titan's organic atmospheric chemistry is unique in the Solar System. Revealed by the Voyager and ongoing Cassini Missions, a variety of latitudinal and altitudinal-changing trace species broken down from the initial $N_2 - CH_4$ $(98 - 2\%)$ composition, are found in Titan's atmosphere in the gas phase [1] and as ices (e.g. C_4N_2, HCN) above the poles [2]. Hydrogen cyanide (HCN) is the most common nitrile trace volatile [1,2] and is known to reach condensation point at stratospheric altitudes [3]. Furthermore, high-energy irradiation in the upper atmosphere (≈1400 km) initiates gas phase reactions known to produce the thick aerosol layers [4]. These aerosols precipitate down to the surface while interacting with the gas medium and are subject to potential condensation of trace species such as HCN onto their surface [5]. The reactivity of HCN is still quite unknown and its potential for prebiotic chemistry pertains to Titan conditions [6,7,8]. Thus, we investigate whether the irradiation reaching Titan's lower atmosphere and near-surface conditions be reactive enough to induce photochemical reactions of condensed HCN ice. To do tackle question, we turn to laboratory simulations of HCN ice deposits on tholins irradiated at wavelengths relevant to low-altitude and near-surface conditions. Ice analysis is performed with *in situ* Fourier-Transform Infrared and UV-VIS spectroscopy.

1. Introduction

1.1 Gas and solid phase chemistry

Saturn's moon Titan displays a unique atmospheric chemistry that is both initiated in the upper atmosphere and further complexified in the vertical column [4]. Direct monitoring of seasonal clouds from Earth-based observations helped us infer their transient locations [9], or compositional characteristics as in the case of hydrogen cyanide HCN [10,11,12] with the rise of ground-based observation techniques such as ALMA. Atmospheric studies with the Voyager 1 mission were able to identify several organic molecules [13,14,15]. Later, the Cassini-Huygens (NASA/ESA) mission provided us with a more precise atmospheric characterization of the composition, winds and temperatures, while the Huygens lander was able to determine the composition of the aerosol particles *in situ*. Further, the presence of organic ice condensation in Titan's atmosphere has been well established since Voyager, but its formation mechanism and potential for chemical reactivity still unknown, especially in the lower altitudes.

1.2 Stratospheric condensation

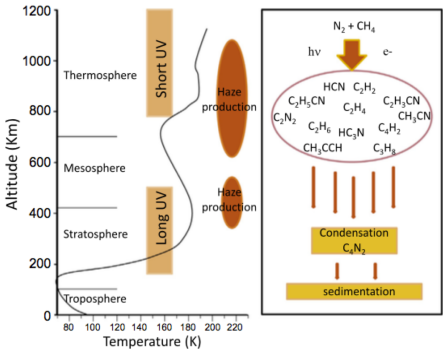

Figure 1: Titan's temperature profile against some important nitrile and hydrocarbon species detected in the atmosphere, from [17]. As also shown in [3], most species reach their condensation point in the lower stratosphere and high troposphere, which can then precipitate to the surface.

C_4N_2 and HCN ices for example were detected above Titan's northern pole, while the presence of HCN clouds [16] seems to be non trivial. [3] have developed a 1D microphysics model pertaining to the condensation of Titan's most abundant hydrocarbon and nitrile species. These ices can have relatively long timescales as they precipitate down to the surface. Hydrogen cyanide HCN is thought to start condensating at low-stratosphere and high-troposphere altitudes, where particles could coat aerosols or form condensed ice particles. [5] reported these condensation mechanisms of photo-produced tholins from C_4N_2 ice photolysis, whereby articles can either exist in an isolated state, as a molecular aggregate, or condensed onto the surface of larger aerosols.

2. Experimental modeling

We use the Titan Organic Aerosol Spectroscopy and chemisTry (TOAST) setup of JPL's Ice Spectroscopy Laboratory (ISL). Tholins were produced with the PAMPRE setup at LATMOS, using different CH_4 concentrations, to see their influence on any potential HCN ice chemical interaction. HCN is produced using stearic acid and KCN, heated and kept at low-controlled pressure. The ice deposition is done at low temperatures ($< 80K$) on $[CH_4]_0 = 1\%$, $[CH_4]_0 = 5\%$ and $[CH_4]_0 = 10\%$ samples. The tholins are then irradiated using long-UV irradiation and analyzed *in situ* with IR (covering 1 micron to 20 microns) and UV-VIS spectroscopy.

3. Summary and Conclusions

Using our laboratory simulations relevant to Titan's lower atmosphere and surface conditions, the role of HCN condensates seems to be important. HCN ice deposited on $[CH_4]_0 = 10\%$ tholins seems to go through a photo-depletion stage, while infrared spectra may hint at a possible production at 2250-2200 cm^{-1} (4.4 - 4.5 μm). UV-VIS-NIR spectroscopy displays uncharacterized production features after just a 1h irradiation ($\approx 10mW$).

Acknowledgements

We are grateful to NASA's Jet Propulsion Laboratory (JPL) and the JPL Visiting Student Research Program; JPL's Ice Spectroscopy Laboratory (ISL) and the Titan Organic Aerosol Spectroscopy and chemisTry (TOAST) laboratory; The European Research Council Starting Grant PRIMCHEM

References

[1] Vinatier et al., 2007, Analysis of Cassini/CIRS limb spectra of Titan acquired during the nominal mission

[2] Loison et al., 2015, The neutral photochemistry of nitriles, amines and imines in the atmosphere of Titan

[3] Barth, 2015, EPSC Abstract, EPSC2015-414

[4] Waite et al., 2007, The process of tholin formation in Titan's upper atmosphere

[5] Gudipati, M. S. et al., 2013, Photochemical activity of Titan's low-altitude condensed haze

[6] Gerakines et al., 2004, Ultraviolet photolysis and proton irradiation of astrophysical ice analogs containing hydrogen cyanide

[7] Rahm et al., 2016, Polymorphism and electronic structure of polyimine and its potential significance for prebiotic chemistry on Titan

[8] Oro J, 1961, Mechanism of synthesis of adenine from hydrogen cyanide under possible primitive earth conditions

[9] Brown et al. 2002, Direct detection of variable tropospheric clouds near Titan's south pole.

[10] Tanguy et al., 1990, Stratospheric Profile of HCN on Titan from Millimeter Observations

[11] Hidayat et al., Millimeter and Submillimeter Heterodyne Observations of Titan: Retrieval of the Vertical Profile of HCN and the ^{12}C / ^{13}C Ratio

[12] Molter et al., 2016, ALMA Observations of HCN and its Isotopologues on Titan

[13] Hanel et al., 1981, Infrared Observations of the Saturnian System from Voyager 1

[14] Kunde et al., 1981, C_4H_2, HC_3N and C_2N_2 in Titan's atmosphere

[15] Maguire et al., 1981, C_3H_8 and C_3H_4 in Titan's atmosphere

[16] de Kok et al., 2014, HCN ice in Titan's high-altitude southern polar cloud

[17] Couturier-Tamburelli et al., 2014, Spectroscopic studies of non-volatile residue formed by photochemistry of solid C4N2: A model of condensed aerosol formation on Titan

EPSC Abstracts
Vol. 11, EPSC2017-728, 2017
European Planetary Science Congress 2017

What Titan's phase curves can teach us about exoplanet atmospheres

A. García Muñoz (1)

(1) Technische Universität Berlin, Berlin, Germany

Abstract

The recent years have seen rapid progress in the characterization of exoplanet atmospheres, a progress that will soon accelerate as new facilities in space and on the ground become available. Because the detection and interpretation of atmospheric features is challenging, it is natural to turn our view towards solar system objects for training our remote sensing techniques but also for inspiration on what to look for. In this context, and using imagery collected by the Cassini Imaging Science Subsystem camera, we have investigated how Titan's disk-integrated brightness varies with the Sun-Titan-observer phase angle at 15 colors covering the spectrum from 300 to 940 nm [1]. Interestingly, Titan's brightness increases very rapidly as the moon approaches back-illumination, and Titan's twilight often outshines the dayside at the largest available angles (166 deg). Closer to back-illumination, it is predicted that the twilight-to-daylight contrast will be in the range of 10-200. This brightness surge is unique to Titan in the solar system, and is caused by the combined effects of an extended atmosphere and abundant haze that scatters efficiently in the forward direction. Hazy and extended atmospheres may be common at exoplanets [2], and thus it is worth asking whether some of them might experience similar brightness surges. The question is relevant because a positive detection will give us insight into the scale height and the optical properties of the prevailing aerosols, and this information is difficult to extract by other means. The presentation will summarize the recent findings on the Titan phase curves, will explore how feasible it is to detect this optical phenomenon with space-based photometry of exoplanets, and will comment on other implications for exoplanet characterization.

1. Titan phase curves

The phase curves were prepared with photometrically calibrated images of Titan obtained with the Cassini Imaging Science Subsystem Narrow Angle Camera. About 6,000 images obtained between 2004 and 2015 were used. The effective wavelengths of the filters range from 300 to 940 nm. Some of the images were captured at phase angles as large as 166 deg, which expands on previous phase angle coverage by the Pioneer 11 and Voyager 2 spacecraft (see Fig. 1).

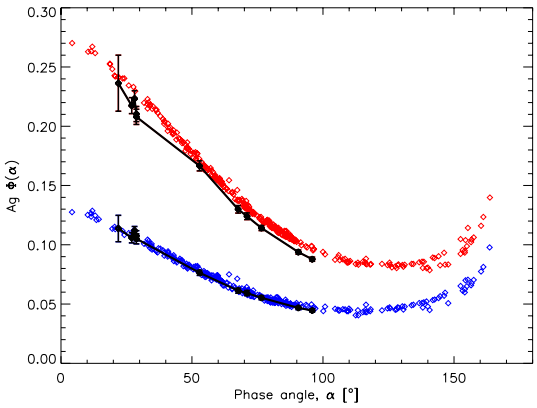

Figure 1. Cassini/ISS (color symbols) and Pioneer 11 (black symbols; [3]) phase curves at comparable blue and red wavelengths.

The brightness surge is attributed to forward scattering by Titan's haze from a ring around the moon's terminator (Fig. 2). The vertical extent of the ring, and thus the strength of the brightness surge, are enhanced by the extended nature of Titan's atmosphere.

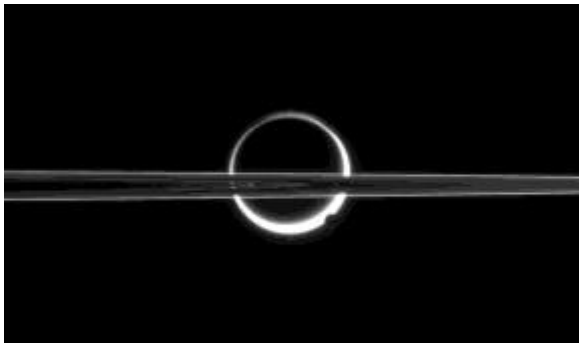

Figure 2. The brightness surge arises from the atmospheric ring that surrounds Titan when it is being back-illuminated.

2. Exoplanet phase curves

The key conditions for such an optical phenomenon to occur at an exoplanet are: 1) it must have an extended atmosphere, 2) abundant aerosols must occur at the optical radius level, 3) the aerosol particles must be efficient at forward scattering. Regarding conditions 1) and 2), it is known that there are numerous exoplanets with inflated atmospheres (Fig. 3, *paper under preparation*), and that haze is a common finding in atmospheric characterization efforts [2]. Assessing condition 3) requires detailed modeling of the aerosol microphysics [4].

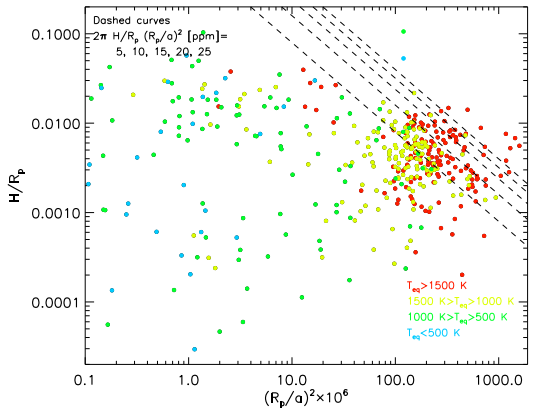

Figure 3. Known exoplanets arranged according to ratio of scale height and planetary radius (H/Rp), and planetary radius and orbital distance (Rp/a). Best conditions for a brightness surge occur towards the right/top of the diagram.

Photometric observations at large phase angles may therefore provide insight into the above conditions. For a few select planets, the brightness surge might reach up to a few tens of ppms (Fig. 3), which is within reach for a few past and future space telescopes such as Kepler, CHEOPS and PLATO. This information is complementary to the information that can be extracted from transits and occultations.

Summary and Conclusions

Motivated by recent findings on Titan, it is proposed that brightness measurements at large phase angles encode key insight into the optical properties and stratification of aerosols in exoplanet atmospheres. Future observational efforts should therefore try to constrain the occurrence of a brightness surge at the larger phase angles of the best exoplanet candidates.

Acknowledgements

A. García Muñoz thanks Panayotis Lavvas and Bob West for their valuable contribution to the Titan work described here.

References

[1] García Muñoz, A., Lavvas, P. & West, R.A. Titan brighter at twilight tan in daylight. Nature Astronomy, Vol 1, Article number: 0114, 2017.

[2] Sing, D.K. et al., A continuum from clear to cloudy hot-Jupiter exoplanets without primordial water depletion. Nature, 529, 59-62, 2016.

[3] Tomasko, M.G. & Smith, P.H. Photometry and polarimetry of titan: Pioneer 11 observations and their implications for aerosol properties. Icarus, 51, 65-95, 1982.

[4] Lee, G., Dobbs-Dixon, I., Helling, Ch., Bognar, K. & Woitke, P. Dynamic mineral clouds on HD 189733b. I. 3D RHD with kinetic, non-equilibrium cloud formation. Astronomy & Astrophysics, 594, A48, 2016.

EPSC Abstracts
Vol. 11, EPSC2017-879, 2017
European Planetary Science Congress 2017

Martian cloud coverage and diurnal cloud life cycle derived from gridded Mars/Express OMEGA data

A. Szantai (1), J. Audouard (2), F. Forget (1), J.-B. Madeleine (1), A. Pottier (1,2), E. Millour (1), B. Gondet (3), Y. Langevin (3), J.-P. Bibring (3)

(1) *Laboratoire de Météorologie Dynamique, (CNRS/UPMC/Ecole Polytechnique/ENS/IPSL), Paris, France (szantai@lmd.polytechnique.fr / Fax : +33/1.69.33.51.08),* (2) *Laboratoire Atmosphères, Milieux, Observations spatiales, (CNRS/UVSQ/IPSL), Guyancourt, France, (3) Institut d'Astrophysique Spatiale, (CNRS, Université Paris 11), Orsay, France.*

Abstract

The ice cloud index (ICI) and the percentage of cloudy pixels (PCP) in a given region are derived from a long series of OMEGA images covering 7 Martian years. The pixels are binned onto a 4D regular grid (longitude, latitude, solar longitude Ls and local time LT). The resulting gridded ICI enables the (partial) climatological reconstruction of the diurnal cloud life cycle by aggregating values from large regions, covering several degrees of longitude and latitude during specific seasons. Clouds are more frequent around summer solstice (Ls=45-135°) early in the morning and in middle and late afternoon than around noon (12 h LT) in the tropics and northern low to mid-latitude regions (lat < 40°N). In the mid-latitude regions closer to the poles, (lat = 40-55° N or S), fewer clouds are present in the afternoon, and more clouds closer to the equinox period (Ls=0-45° and 135-180°).

We also investigated areas partially covered with clouds by determining the percentage of cloudy pixels in the area. During the examined period, partially cloud-covered areas basically overlap with fully cloud-covered areas. Exceptions are the volcanoes (on Tharsis, and Olympus and Elysium Mons), with very few partially cloud-covered areas. Hellas is also a particular case: the basin is covered by a continuous cloud cover surrounded by a thin ring of partially cloud-covered grid-points.

1. Introduction

Water ice clouds have been first observed from space in the 1970-80's (by Mariner and Viking spacecrafts), and more intensively in the 1990's, starting with the MGS mission. But due to their heliosynchronous orbits, most past and current Martian satellites have observed the planet only at a specific local time (LT) during the day (typically at 2-3 p.m. and 2-3 a.m. LT) over most regions, and therefore cannot provide information about the diurnal cloud life cycle. Recently launched satellites MAVEN and MOM / Mangalaayan) move along non-heliosynchronous orbits, but have only provided images over a short period (~2 years). The OMEGA spectrometer onboard the (non-heliosynchronous) Mars Express satellite has been providing spectral images at various times of the day over ~7 Martian years (MY 26-33, i.e. 2003-2016). For each valid pixel from this abundant spectral image data, we derived parameters representative of the presence and abundance of clouds and used them to construct a daily and annual climatology on a regular spatial grid.

2. Methodology

The detection of clouds is based on the measure of the depth of a water ice absorption band, initially applied at 1.5 μm [1]. In practice, we now use the slope of an absorption band around 3.4 μm to define the original ice cloud index (ICIo) and the normalized ice cloud index (ICI = 1 – ICIo) [2]. After comparison with a threshold value, this ICI indicates if the pixel is cloudy or not.

In a second step a cloud climatology is constructed. The pixels are binned into two 4D arrays (cloudy and cloudy+non-cloudy) according to their longitude, latitude, Ls and LT, and counted. The bins have sizes of 1° in latitude and longitude, 5° in Ls and 1 (Martian) hour in LT. ICI values are also binned and averaged on the same 4D grid.

The cloud coverage, i.e. the percentage of cloudy pixels (PCP) of each bin is obtained by dividing the number of cloudy pixels in the first array by the number of all pixels in the corresponding bin in the second array.

In a third step, several 4D bins covering larger spatial areas and longer time periods are assembled (averaged) in order to form 2D subsets showing temporal evolutions of clouds.

Comparisons of the ICI with the integrated water ice column of the Martian Climate Database (derived from the Martian GCM of the LMD) show that both datasets have a good correlation and show the same cloudy areas [2].

3. Cloud cover

Figure 1 shows the average cloud cover of for all values (0-100%) for Ls=[45°-135°] and LT=[7-17h]. The main cloud structures can be identified: the Aphelion Belt, around the Tharsis, Olympus and Elysium volcanoes, Arabia Terra, Syrtis Major, the edges of polar hoods. The areas with partial cloud coverage (fig. 2) are basically the same but less dense. Partial cloud cover is almost absent on Arsia, Olympus, and reduced over most cloudy areas. The Hellas basin is covered by a dense cloud cover, surrounded by a narrow ring with partial cloud coverage.

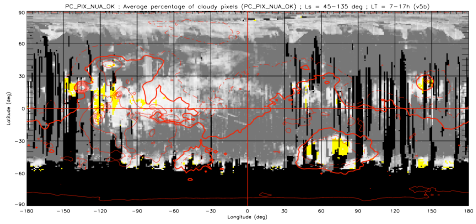

Figure 1: cloud cover (PCP). Highest values in yellow.

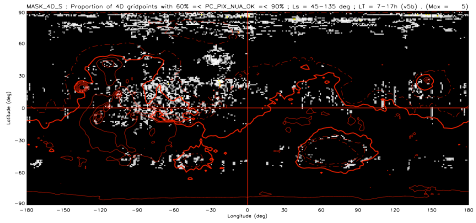

Figure 2: Where are the non-continuous clouds ? Ratio of non-continuously cloud-covered grid-points (60<PCP<90%) to the number of all cloud-covered grid-points (0.01<PCP<100%).

4. Diurnal cloud life cycle

The 4D gridded ICI has been aggregated and averaged over 17 large regions, covering several degrees of longitude and latitude during specific seasons. Although data coverage is sometimes sparse, clouds are more frequent around summer solstice (Ls=45-135°) early in the morning and in middle and late afternoon than around noon (12 h LT) in the tropics and northern temperate regions (lat < 40°N). Fig. 3 shows a different cloud life cycle configuration observed in the Tempe Terra region (30-50°N). In the temperate regions closer to the poles, (lat=35-55° N or S), fewer clouds are present in the afternoon, and more clouds closer to the equinox periods (Ls=0-45° and 135-180°). This may be related to the presence or motion of the edge of the polar hoods.

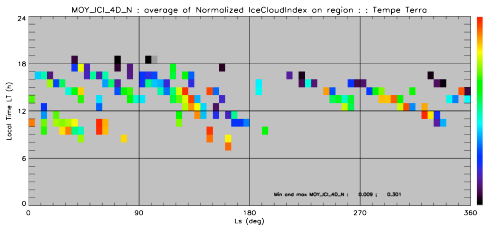

Figure 3: Normalized Ice Cloud Index (ICI) over the Tempe Terra region (30-50°N ; 90°W-55°W). Color scale : black: no cloud ; from purple (low ICI, thin clouds) to red (high ICI, thick clouds) ; gray: no data.

5. Conclusions

Although the spatial and temporal coverage by OMEGA data is sparse (~1-2 % of all 4D grid-points), the derived ICI and PCP are valuable indicators for detecting and characterizing Martian water ice clouds when they are aggregated or averaged over larger regions or longer periods. They may be useful for the validation of results produced by high-resolution Martian GCMs [3].

Acknowledgements

This study was realized partly in the frame of the European project UPWARDS.

References

[1] Y. Langevin et al.: Observations of the south seasonal cap of Mars during recession in 2004–2006 by the OMEGA visible/near-infrared imaging spectrometer on board Mars Express, *JGR*, 112, E08S12, 2007.
[2] A. Szantai et al.: Construction of a 4D water ice cloud database from Mars Express/OMEGA observations - Derivation of the diurnal Martian cloud life cycle, 6th MAMO workshop, 17-20 January 2017, Granada, Spain.
[3] A. Pottier et al.: Unraveling the Martian water cycle with high-resolution global climate simulations, *Icarus* (accepted), 2017.